Summer 2014

Improving the oxidation resistance of diboride-based ceramics

Maryam Kazemzadeh Dehdashti

Department: Materials Science and Engineering

IMPROVING THE OXIDATION RESISTANCE OF DIBORIDE-BASED CERAMICS

by

MARYAM KAZEMZADEH DEHDASHTI

A DISSERTATION

Presented to the Faculty of the Graduate School of the

MISSOURI UNIVERSITY OF SCIENCE AND TECHNOLOGY

In Partial Fulfillment of the Requirements for the Degree

DOCTOR OF PHILOSOPHY

in

MATERIALS SCIENCE AND ENGINEERING

2014

Approved by

William G. Fahrenholtz, Advisor
Greg E. Hilmas
Richard K. Brow
Jeremy L. Watts
Jay Switzer

PUBLICATION DISSERTATION OPTION

This dissertation was prepared in the style for publication in the *Journal of the European Ceramic Society* and *Corrosion Science*. The manuscript entitled "Oxidation of Zirconium Diboride with Niobium Additions" was published in the *Journal of the European Ceramic Society* in volume 33, issue 10 in 2013. The manuscript entitled "Effects of W Additions and Temperature on the Oxidation Behavior of ZrB_2 Ceramics" was accepted for publication in *Corrosion Science* in March 2014. The manuscripts entitled "Effect of Transition Metal Oxide Additions on the Structure of B_2O_3 Glasses" and "Effects of Transition Metals on the Oxidation Behavior of ZrB_2 Ceramics" will be submitted to *Corrosion Science* following revisions based on the suggestions of the dissertation committee.

ABSTRACT

Oxidation behavior has restricted the development of ZrB_2-based ceramics for aerospace and hypersonic flight vehicles applications. The research presented in this dissertation focuses on the effect of transition metal (TM) additives on oxidation behavior of ZrB_2 ceramics. In the first stage of the research, the effect of Nb additions on the morphology of the oxide particles and stability of the protective B_2O_3 glassy layer, which formed on the top surface during oxidation, was investigated. Addition of Nb increased the thickness of the glassy layer and, as a result, improved the oxidation resistance of ZrB_2 after oxidation at 1500°C. Next, the oxidation behavior of nominally pure ZrB_2 and $(Zr,W)B_2$ after oxidation at temperatures ranging from 800 to 1600°C was studied. Two oxidation stages before and after significant evaporation of B_2O_3 at about 1100°C were recognized for nominally pure ZrB_2. Higher stability for the WO_3-B_2O_3 glassy layer compared to pure B_2O_3 resulted in a shift in the onset of the second oxidation regime toward higher temperatures for $(Zr,W)B_2$ specimens and resulted in higher oxidation resistance for $(Zr,W)B_2$ compared to nominally pure ZrB_2. In the third stage of the research, the effects of TM-oxides such as WO_3, Nb_2O_5, or ZrO_2 on weight loss and structure of B_2O_3 glasses was studied. Thermogravimetric analysis performed on (TM-oxide)-B_2O_3 glasses indicated that TM-oxide additions reduced the evaporation of B_2O_3. Since no change in the structure of the glasses was detected, it was concluded that the increased stability of (TM-oxide)-B_2O_3 glasses compared to pure B_2O_3 was due to the lower activity of B_2O_3 in (TM-oxide)-B_2O_3 glasses. Finally, comparison of the effects of W, Mo, or Nb on oxidation behavior of ZrB_2 at 1600°C showed that Mo and Nb were the most effective additives for improving the oxidation resistance of ZrB_2.

ACKNOWLEDGMENT

Firstly, and foremost, I am grateful to my advisor Dr. Bill Fahrenholtz for his advice, encouragement and guidance through the course of this study. His endless support, effort and patience were invaluable during my graduate career. He gave me a great deal of freedom in my research and taught me how to be direct and stay on the point. I would also like to thank my co-advisor Dr. Greg Hilmas for providing continuous insight and support.

I must of course thank the rest of my committee, Dr. Richard Brow, Dr. Jeremy Watts, and Dr. Jay Switzer for their useful and constructive comments about my doctoral research. Special thanks to Dr. Wayne Huebner for his understanding and support.

I should also acknowledge that my research was funded through the National Hypersonic Science Center for Materials and Structures (Grant FA9550-09-1-0477) with Dr. Ali Sayir (AFOSR) and Dr. Anthony Calomino (NASA) as program managers. I also wish to thank project principal investigator Dr. David Marshall of Teledyne Scientific and Imaging for his support and guidance.

I would like to thank my friends and colleagues in the UHTC and glass group at Missouri S&T. I was very fortunate to have them beside me in those four years and learned a great deal from them.

Special thanks goes to my parents and my brother whose love, support, and belief in me inspired me to keep moving forward. Final thanks go to my life partner Hesam for his endless love. I would have never been able to graduate without his support and guidance throughout those years.

TABLE OF CONTENTS

LIST OF ILLUSTRATIONS

Page

SECTION

PAPER I

PAPER II

PAPER III

PAPER IV

LIST OF TABLES

Page

SECTION

1. INTRODUCTION

Ultra high temperature ceramics (UHTCs) are known as a class of materials with the potential to withstand extreme heating environments. Several borides, carbides and nitrides of the group IVB and VB transition metals (TM) such as ZrB_2, ZrC, HfB_2 and HfC are considered UHTCs based on melting temperatures in excess of 3000°C and other properties. The performance advantages of the diboride-based UHTCs come from their high-temperature stability and the capability to transfer and redistribute heat at elevated temperatures. These characteristics are attractive for sharp leading edges for hypersonic aerospace vehicles, which must not only be capable of operating in oxidizing atmospheres at high temperatures and high flow rates, but also transfer heat away from the hottest areas and redistribute it to cooler areas.[1, 2]

Among UHTCs, HfB_2 and ZrB_2 have an exceptional combination of metallic, covalent and ionic types of bonding. Strong covalent bonding gives them extremely high melting temperatures (> 3200°C), high hardnesses and high elastic moduli, while the metallic bonding character gives them high thermal and electrical conductivities.

This combination of properties, along with resistance to erosion/corrosion at high temperatures, makes them suitable for the extreme chemical and thermal environments associated with hypersonic flight, atmospheric re-entry, and rocket propulsion systems.[2-9] Other applications that take advantage of these properties include refractory linings, molten metal crucibles, plasma arc electrodes, and cutting tools.[3, 10] Since ZrB_2 has a lower theoretical density (6.1 g/cm^3) compared to HfB_2 (11.2 g/cm^3) and is also less

expensive, it is often preferred over HfB_2. However, oxidation behavior is a restriction to the development of ZrB_2-based ceramics for rocket propulsion and hypersonic flight applications.

Previous studies have shown that additives that are introduced intentionally or unintentionally during processing, such as SiC, C, B_4C, and WC, improve the densification, mechanical properties, and oxidation resistance of ZrB_2 ceramics.[11-14] The most effective additive for improving the oxidation resistance of ZrB_2, along with other desirable effects at relatively low temperatures (800-1200°C), was SiC and other Si-containing additives. Formation of a protective liquid/glassy borosilicate layer reduced the transport of oxygen toward the unoxidized matrix and improved the oxidation resistance of ZrB_2-SiC ceramics. Although many studies have investigated the effect of Si-containing compounds on the oxidation behavior of ZrB_2,[11, 15] fundamental mechanisms of oxidation of ZrB_2 with TM additives have not been studied yet.

This study is focused on the effects of TM additives such as W, Nb, and Mo on the oxidation behavior of ZrB_2-based ceramics. Parameters including the type and concentration of TM additives and oxidation temperature were examined in the present study. This research addresses several questions including:

1. How do the TM additives affect the oxide scale growth on ZrB_2?
2. What are the effects of W additives on the thickness of the porous oxide scale and the protective B_2O_3 layer in different regimes of oxidation behavior?
3. How do TM additions affect the evaporation and structural properties of B_2O_3 glass?

4. What are the differences between the effects of different TM additives such as W, Mo, or Nb on oxidation of ZrB_2?

Gaining knowledge on how TM additives affect the oxidation behavior of ZrB_2 at different oxidation temperatures can enable the design of ZrB_2 ceramics with improved oxidation resistance at high temperatures for advanced aerospace applications. Improving the oxidation resistance of ZrB_2 ceramics would allow the aerospace industry to improve the efficiency of the thermal protection systems and reduce the need to frequently replace parts of the leading edges in hypersonic flight vehicles.

2. LITERATURE SURVEY

2.1. ZIRCONIUM DIBORIDE

Metal diborides such as ZrB_2, HfB_2, TiB_2, TaB_2, and NbB_2 are composed of alternating layers of 2D graphite like sheets of boron atoms and closed packed metal layers in the hexagonal AlB_2 crystal structure (C32, P6/mmm space group),[16] as shown in Figure 2.1. Each metal atom is surrounded by six metal atoms in plane and 12 nearest boron atoms in adjacent planes. Each boron atom has three equidistant boron neighbors in plane, and six metal atom neighbors, three in each plane above and below.[17, 18] The AlB_2 type crystal structures have an unusual combination of M-M, B-B, and M-B types of bonding in the structure that controls bonding and thermal stability. Strong covalent bonds in the ZrB_2 structure results in high melting temperature, hardness, strength, and chemical stability. The M-B bonds determine the cohesive forces in the c-direction, while the stronger B-B bonds control the behavior in the a-direction.[3] The M-M bonding in the zirconium planes results in high electrical and thermal conductivity.[19, 20] High thermal conductivity reduces thermal stresses under a temperature gradient and increases thermal shock resistance.[12, 21] Some physical properties of ZrB_2 are summarized in Table 2.1.

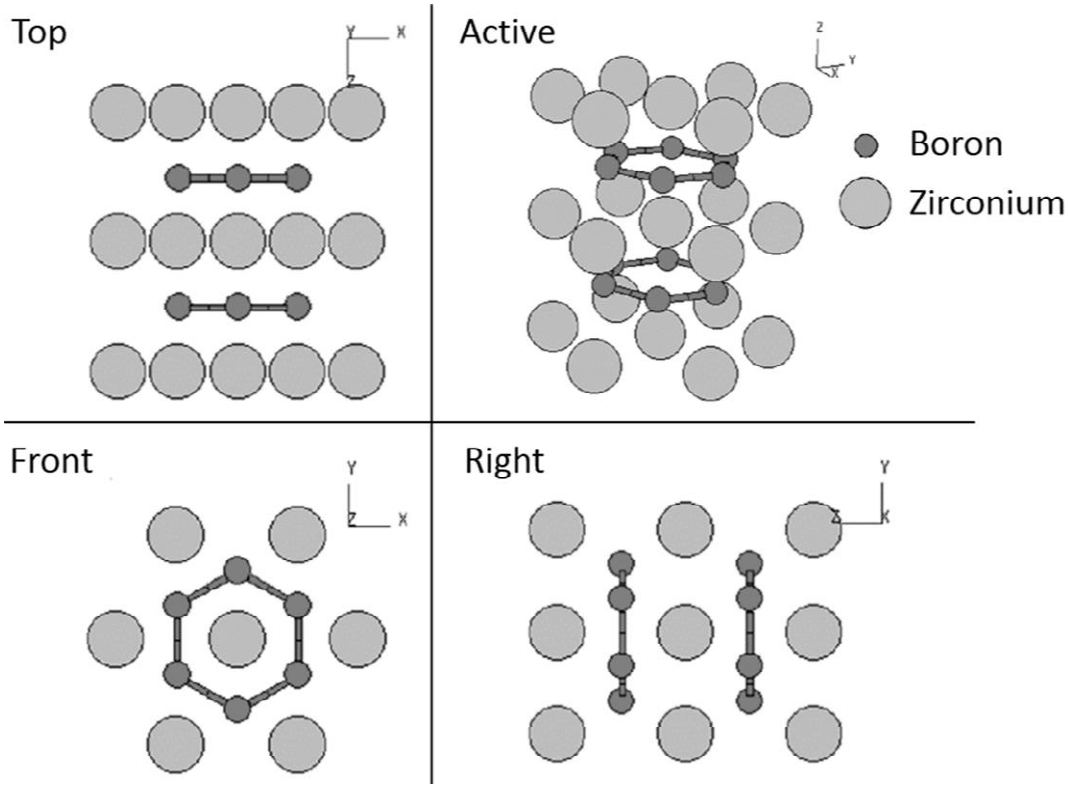

Figure 2.1. Projection of AlB_2 crystal structure showing the symmetry of P6/mmm.[3]

Table 2.1. Physical properties of ZrB_2.

Property	Unit	ZrB_2	Reference
Crystal structure	Space group	P6/mmm AlB_2 (Hexagonal)	4
Lattice constant, a	Å	3.17	4
Lattice constant, c	Å	3.53	4
Density	g/cm^3	6.119	4
Melting temperature	°C	3245	4
Young's modulus	GPa	489	4
Bulk modulus	GPa	215	4
Hardness	GPa	23	4
Coefficient of thermal expansion	K^{-1}	5.9×10^{-6}	9
Heat capacity at 25°C	$J \bullet (mol \bullet K)^{-1}$	48.2	2
Electrical conductivity	S/m	1.48×10^7	10
Thermal conductivity	$W \bullet (m \bullet K)^{-1}$	108	10

Hot pressing is the most common densification method for ZrB_2 due to the strong covalent bonding and low self-diffusion coefficient of the elements in the compound. However, oxygen impurities present on the surface of individual powders hinder the sinterability of ZrB_2 ceramics.[22, 23] Reactive additives such as C[14, 24] and B_4C[14, 22, 25] can be used to react with the oxide impurities and, consequently, increase densification rate, decrease grain coarsening, and improve the oxidation resistance.[14, 24] Equation 1 shows the possible carbothermal reduction reactions for the ZrO_2 and B_2O_3 impurities on ZrB_2. However, B_2O_3 can also evaporate at elevated temperatures, followed by reaction of

carbon with ZrO_2 to form ZrC by Equation 2. Using B_4C as the reducing additive can provide extra boron and reduce the formation of ZrC by promoting formation of ZrB_2.

$$ZrO_2 + B_2O_3 + C \rightarrow ZrB_2 + 5CO_{(g)} \quad (1)$$

$$ZrO_2 + 3C \rightarrow ZrC + 2CO_{(g)} \quad (2)$$

2.2. OXIDATION OF ZrB_2

Assuming stoichiometric oxidation, exposure of ZrB_2 to air at temperatures of 800°C and above results in formation of B_2O_3 and ZrO_2, which leads to measurable mass gain according to the following equation[26]

$$ZrB_{2\,(cr)} + 5/2\ O_{2\,(g)} \rightarrow ZrO_{2\,(cr)} + B_2O_{3\,(l)} \quad (3)$$

The oxidation reaction is favorable at all temperatures with $\Delta G°_{rxn} = -1977 + 0.361T$ (kJ).[3] Two distinct layers covered the surface of the oxidized ZrB_2 ceramics: (1) an outer glassy layer mainly consisting of B_2O_3, and (2) an inner layer mainly consisting of zirconia.[27, 28] The formation of two-layer scales are believed to be due to limited mutual solubility of ZrO_2 and B_2O_3 [29] along with the large volume expansion (~300% based on density calculations) associated with oxidation of ZrB_2 to ZrO_2 and B_2O_3.[26] Thermal gravimetric analysis showed three oxidation regimes.[3] The mass gain was negligible below 700°C. Between 700 and ~1100°C, B_2O_3 forms a continuous oxide layer that provides passive oxidation protection.[3, 30-32] Analysis concluded that the transport of oxygen through B_2O_3 was the rate limiting step for oxidation, which results

in parabolic (diffusion-limited growth) kinetics for mass gain and the oxide layer thickness.[3, 33, 34] The upper limit of the first stage of oxidation is considered to be between 1100 and 1200°C, depending on several parameters such as external pressure, oxygen partial pressure and gas flow rate.[28, 35] Between 1000 and 1400°C, paralinear kinetics are observed due to the fact that the weight change reflects a combination of mass gain resulting from the formation of ZrO_2 and B_2O_3, and mass loss due to the evaporation of B_2O_3.[30, 34, 36] Specimens continue to gain mass as the mass of ZrO_2 plus B_2O_3 formed is greater than the mass of diboride reacted plus the mass of B_2O_3 lost. As B_2O_3 evaporates, a porous ZrO_2 layer is left behind, although a small amount of B_2O_3 may be retained. At temperatures above 1400°C, mass gain kinetics is linear due to the non-protective nature of the ZrO_2 layer.[3, 33]

At low and intermediate temperatures, the pores in the zirconia are filled with boria. In addition, the microstructure of the ZrO_2 appears to change from equiaxed grains at temperatures below 1000°C, to columnar grains with a glassy B_2O_3 in between them at higher temperatures. Parthasarathy et al.[27] summarized the changes in the oxide scale in three oxidation regimes as illustrated in Figure 2.2. They proposed a model to describe the oxidation behavior and final oxidized microstructure for ZrB_2, TiB_2, and HfB_2 as shown in Figure 2.3. It was assumed that the oxygen diffusion through the TM oxide was not significant due to a low oxygen vacancy concentration and to a lack of sufficient electronic conductivity. The dependence of the parabolic rate constant as a function of temperature on the oxygen partial pressure in O_2/N_2 gas mixture of 1 atm total pressure was linear at 1000°C and became negligible at 1600°C.[27] This was consistent with the previous experimental observations.[35, 37]

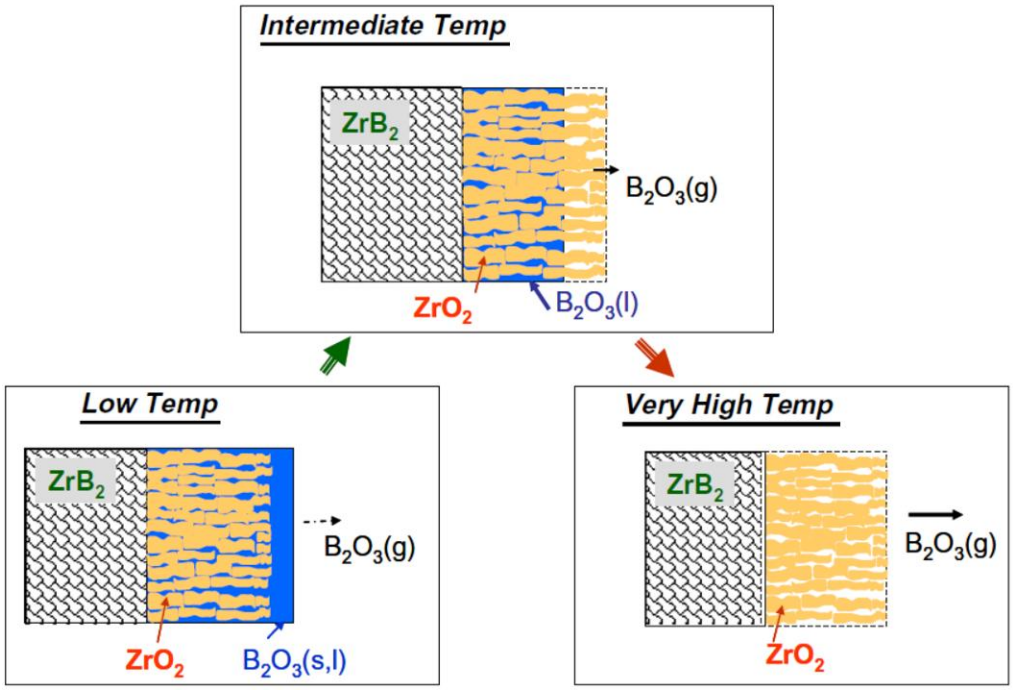

Figure 2.2. The oxidation products formed during oxidation of ZrB_2 in three temperature regimes.[27]

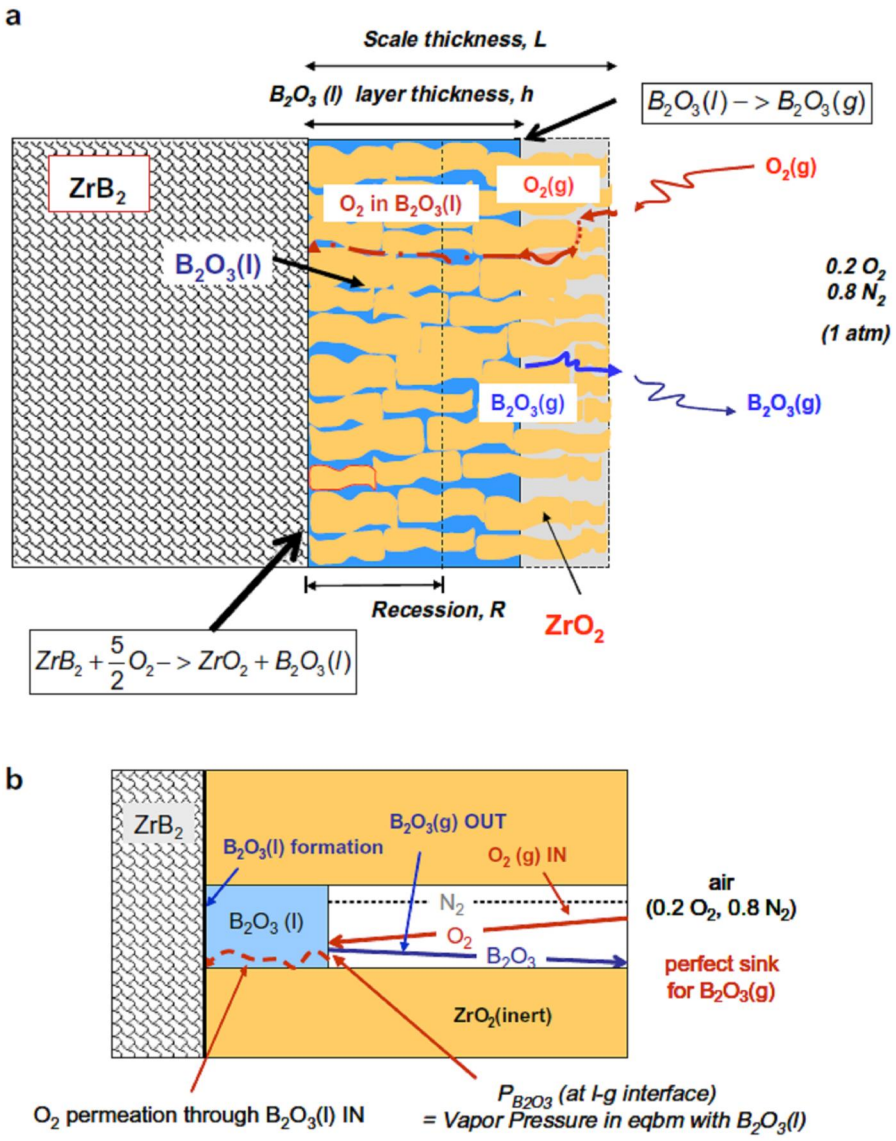

Figure 2.3. (a) Schematic sketch of mechanisms involved in the oxidation of ZrB_2 in air, in the intermediate temperature regime (1000-1800°C). (b) Schematic of the mechanistic steps considered in the model.[27]

2.3. EFFECT OF ADDITIVES ON OXIDATION BEHAVIOR OF ZrB_2 CERAMICS

The relatively severe oxidation of nominally pure ZrB_2 at temperatures above ~1200°C, at which the protective B_2O_3 layer is evaporated, motivated the researchers to

improve the oxidation resistance by approaches such as solid solution additions, synthesizing ternary diboride compositions, and adding second phases.[28]

Addition of SiC as a second phase was found to reduce the thickness of the oxide scale compared to nominally pure ZrB_2 and this is one of the most promising approaches for increasing the oxidation resistance.[6, 8, 15, 35, 38-61] It was reported that below ~1100°C, ZrB_2 oxidized preferentially, leaving SiC unoxidized. Hence, oxidation behavior of ZrB_2-SiC ceramics was not affected by SiC additions at temperatures below ~1100°C.[26, 62] The evaporation of B_2O_3 becomes significant above 1100°C and oxidation of SiC begins, resulting in formation of a protective borosilicate layer on the surface, which results in parabolic mass gain kinetics.[63, 64]

Figure 2.4 shows isothermal oxidation curves for ZrB_2 and ZrB_2-SiC ceramics at 1200 and 1400°C.[65] The weight gain of nominally pure ZrB_2 increased significantly when the temperature increased from 1200°C to 1400°C due to loss of the protective B_2O_3 layer at the higher temperature. Nominally pure ZrB_2 and ZrB_2-SiC had similar weight gains at 1200°C. However, the weight gain of ZrB_2-SiC at 1400°C was ~13% less than ZrB_2 and almost similar to its weight gain at 1200°C.[65] For ZrB_2-SiC, the borosilicate glassy layer that formed on the surface had higher stability compared to pure B_2O_3 formed on ZrB_2. The stable borosilicate glassy layer acted as a barrier to oxygen diffusion and resulted in higher oxidation resistance for ZrB_2-SiC ceramics compared to nominally pure ZrB_2.[26]

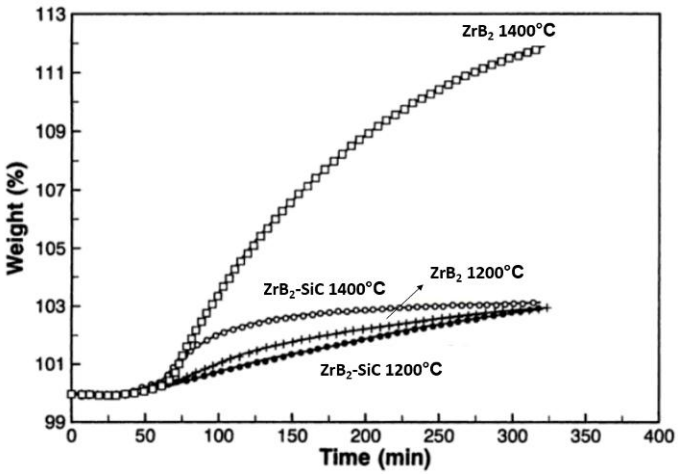

Figure 2.4. Thermal gravimetric analysis oxidation curves for ZrB_2 and ZrB_2-SiC ceramics at 1200 and 1400°C.[65]

Figure 2.5 shows the structure of the oxide layers that form on ZrB_2 containing 30 vol% SiC after oxidation at 1500°C for 30 min.[26] The oxide scale consisted of three layers: (1) a SiO_2 rich liquid/glassy layer, (2) a thin layer of ZrO_2-SiO_2, and (3) a SiC depleted ZrO_2 and/or ZrB_2 layer covering the unoxidized ZrB_2-SiC matrix.[26] Boron is difficult to detect by energy dispersive spectroscopy (EDS), and since the borosilicate phase is amorphous, it is not detected by x-ray diffraction (XRD), so the authors were not able to quantitatively analyze boron content in the SiO_2 glassy phase. However, they concluded that some B_2O_3 probably remained dissolved in the SiO_2 glassy phase. The rate limiting step for oxidation when the glassy layer is present is believed to be diffusion of oxygen molecules through the SiO_2 and ZrO_2-SiO_2 layers. The morphology of the ZrO_2-ZrB_2 layer beneath the ZrO_2-SiO_2 layer was similar to the original ZrB_2-SiC structure before oxidation, except that SiC was partially or entirely removed. Formation of the ZrO_2-ZrB_2 layer indicated existence of an oxygen partial pressure gradient across

the SiC depleted layer.[62] Addition of other Si-containing compounds such as $MoSi_2$[66-71] and $TaSi_2$[49, 72-74] can also be beneficial due to the formation of borosilicate glass layer.

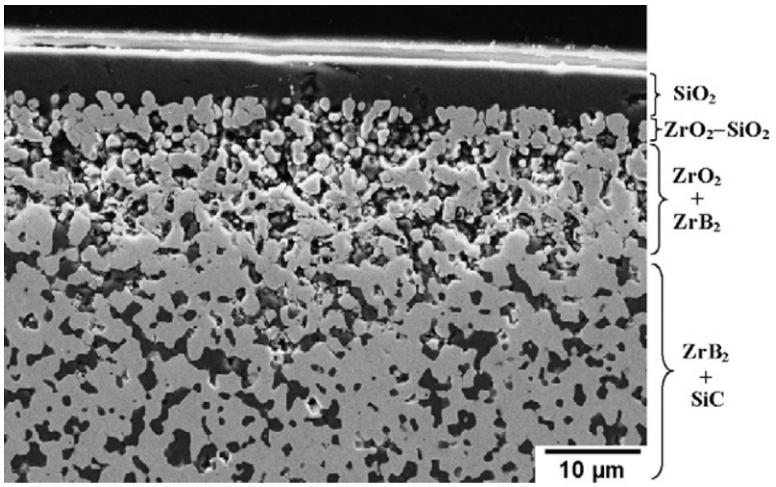

Figure 2.5. Scanning electron micrograph of the layered structure of ZrB_2–SiC after oxidation at 1500°C for 30 min in flowing air.[26]

Karlsdottir et al. observed island-in-lagoon patterns on oxide scales formed by oxidation of a ZrB_2–SiC composite exposed to air at 1550°C, consisting of a central zirconia ‘‘island’’ in a silica-rich ‘‘lagoon’’ surrounding a pattern of B_2O_3 rich lobes, arranged like flower petals (Figure 2.6).[29, 75] These features were interpreted as convection cells transporting a fluid liquid boria-rich borosilicate oxidation product to the surface where B_2O_3 was lost by evaporation, depositing zirconia in a viscous silica-rich liquid, forming the island-in-lagoon pattern. It was proposed that the ZrO_2 in the center of the cells formed by precipitating from a liquid containing B_2O_3, SiO_2, and ZrO_2 (i.e., a BSZ liquid) as B_2O_3 evaporated. The process of convective transport of liquid oxide solution, with evaporation of B_2O_3 and deposition of ZrO_2 in viscous silica liquid, was

suggested as the mechanism of formation of the external zirconia scales observed on ZrB_2–SiC composites.[76] Formation of a more stable liquid/glassy layer on the top surface, along with increased oxidation resistance, supports the idea that the rate limiting step for this stage of oxidation is transport of oxygen through the glassy layer.[27]

Sciti et al. observed similar characteristics of the oxide scales after oxidizing HfB_2-15 vol% $TaSi_2$ at 1600°C.[77] On the surface of the sample, the dominant phase was a complex oxide with platelet morphology that had the stoichiometry $Hf_6Ta_2O_{17}$. The complex oxide was embedded in a borosilicate phase, which also contained Ta and Hf, under which a porous layer containing Ta-doped hafnia grains was generated. It was suggested that by oxidation of HfB_2 and $TaSi_2$, the surface borosilicate liquid layer underwent Ta enrichment due to oxidation of $TaSi_2$. They believed that large convective fluxes were responsible for movement of liquids from the subsurface layer up to the surface, where B_2O_3 evaporation created bubbles and craters. Since the surface liquid was rich in Ta, the preferential crystalline phase, which would crystallize either upon cooling or when the liquid viscosity reached a solubility limit, was the intermediate oxide $Hf_6Ta_2O_{17}$. At the same time, when a continuous Ta-borosilicate layer was formed on the surface, a porous layer was generated underneath.[77]

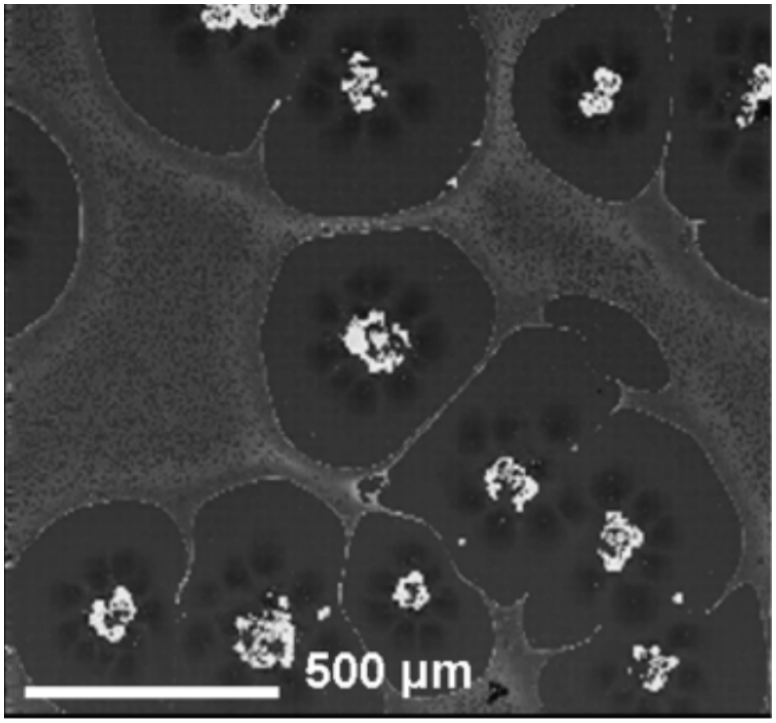

Figure 2.6. SEM image of the features on the surface of ZrB_2-SiC after oxidation at 1550°C for 2 hours.[75]

Peng et al. reported that small (3.32 mol%) additions of TaB_2 to ZrB_2-27.91 mol% SiC were beneficial in improving oxidation resistance at 1500°C. This was attributed to the oxidation and breakup of TaB_2-ZrB_2 solid solution grains into fine scale ZrO_2 and TaC particles, which better retained an encapsulating liquid phase. Increasing TaB_2 content beyond 3.32 mol% improved oxidation resistance at 1200 and 1400°C; however, oxidation resistance was degraded at 1500°C. The presence of higher concentrations of tantalum in some way facilitated the solution and precipitation of zirconia dendrites. After some period of time, these dendrites permitted the acceleration of oxidation by providing a fast diffusion path either through the dendrites or along the glass/ crystal interfaces of these dendrites.[49]

Talmy et al. studied the effect of 2-20 mol% Cr-, Ti-, Nb-, V-, and Ta-borides addition to ZrB_2-25 vol% SiC. They reported that all additions formed solid solutions with ZrB_2 after sintering and improved the oxidation resistance of the ZrB_2-SiC composites.[65] Figure 2.7 shows the results of isothermal (5 hours) thermal gravimetric analysis at 1300°C for ZrB_2-SiC ceramics with 10 mol% CrB_2, NbB_2, TaB_2, TiB_2, and VB_2. The lowest weight gain was observed for ZrB_2-SiC with TaB_2 addition. Addition of TaB_2 resulted in formation of oxide scale with half the thickness of the scale for the baseline material. SEM images obtained from the surface of the ZrB_2-SiC specimen with TaB_2 additions showed the presence of large (>100 μm) droplet-shaped immiscibility regions distributed in the matrix of the glassy layer enriched with Zr and Ta.[65]

One possible effect of TM additions could be lowering the evaporation rate of the borosilicate layer due to reducing the activity of SiO_2 and/or B_2O_3 in the liquid phase. However, the effect of TM additives on evaporation rate of the borosilicate layer was not studied. Also, the effect of the TM additives on the oxidation behavior at high temperatures, at which the borosilicate layer, is removed was not studied. Besides, the effect of the TM additives on the oxidation behavior of ZrB_2 was shadowed by the presence of SiC. Research on the effect of TM additives on the oxidation behavior of nominally pure ZrB_2 can help provide insight into the mechanisms by which the TM additives improve the oxidation resistance of ZrB_2.

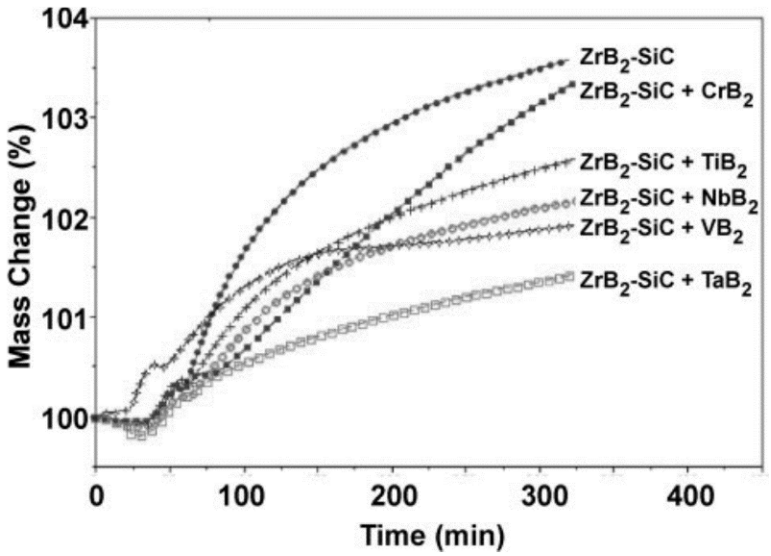

Figure 2.7. Comparison of mass gains for nominally pure ZrB_2-SiC and ZrB_2-SiC ceramics with Cr, Ti, Nb, V, or Ta additions.[65]

Opeka et al. reported that formation of $SiO_{(g)}$ as a result of active oxidation of SiC could build up to pressures exceeding ambient, facilitating rupture of the protective glass layer, resulting in a cyclic protective/ non-protective scale-forming sequence.[6] Besides, formation of the SiC-depleted zirconia layer is common for ZrB_2-SiC samples, which results in more rapid transport of oxygen toward the unoxidized matrix. Also, in a flowing environment most of the B_2O_3 and SiO_2 will evaporate at very high temperatures. Thus, the primary protective oxidation barrier for the refractory metal borides is the refractory metal oxide scale plus any residual B_2O_3 and SiO_2.[63, 78] Hence, due to rapid evaporation of SiO_2 at high temperatures, damage to the texture of the oxide scale by rupture, and formation of a porous SiC-depleted layer, SiC does not seem to be a good choice for improving the oxidation resistance of ZrB_2 ceramics at ultra-high temperatures. According to the positive effects of the transition metals on improving the oxidation resistance of ZrB_2-SiC ceramics,[65] addition of transition metals might also

improve the oxidation resistance of ZrB_2 at high temperatures, without the deleterious effects of SiC.

Zhang et al. reported that WC additions improved the oxidation resistance of ZrB_2 ceramics.[36] Figure 2.8 shows cross-section microstructures for nominally pure ZrB_2 and $(Zr,W)B_2$ ceramics containing 4, 5, or 6 mol% WC after oxidation at 1600°C for 6 hours. The addition of WC led to the formation of a two-layer scale structure. The structure consisted of a light porous zirconia outer layer and a dense dark inner layer containing ZrO_2 and WO_3, in contrast with the single, highly porous and columnar ZrO_2 layer formed on nominally pure ZrB_2.[13, 36] While no significant difference was observed between the scale thicknesses of $(Zr,W)B_2$ specimens with different WC contents, the thickness of the light layer decreased and the thickness of the dark layer increased by increasing the amount of WC additions. The total scale thicknesses for nominally pure ZrB_2 and ZrB_2 with 4, 5, and 6 mol% WC additions after oxidation at 1600°C for 1–6 h are compared in Figure 2.9. The scale on nominally pure ZrB_2 after oxidation for 6 h was much thicker (~3.2 mm) than the scale on $(Zr,W)B_2$ specimens (~0.75 mm).[13] The oxide scale thickness increased linearly with time for oxidation at 1600°C for nominally pure ZrB_2, which indicated that the scale was not protective.[13]

Figure 2.10 shows the microstructures of the outer oxide scales for nominally pure ZrB_2 and $(Zr,W)B_2$ with 4, 5, or 6 mol% WC after oxidation at 1600°C for 3 hours. The densification and grain size of the oxide scale increased with increasing WC content.[13] It was suggested that during oxidation, the presence of WO_3 in the oxide scale resulted in liquid phase sintering of ZrO_2, which modified the microstructure of the scale and increased its relative density, resulting in improvement of the oxidation resistance of

ZrB_2.[13] Hence, additions of WC offer improved oxidation resistance to ZrB_2 ceramics by increasing the densification of the oxide scale, without the deleterious effects of silica formers. However, the effect of the transition metal oxide on the densification of the oxide scale may not be the only reason of higher oxidation resistance of (Zr,TM)B_2 ceramics compared to nominally pure ZrB_2. As mentioned above, the liquid/glassy B_2O_3 layer acts as a barrier against transport of oxygen from the atmosphere towards the unoxidized matrix. The effect of TM additives on the stability of the liquid/glassy layer, which might play an important role on improving the oxidation resistance of ZrB_2, was not investigated in previous studies. Also, the effect of various TM additives on the oxidation behavior of ZrB_2 might be different in different temperature regimes. Comparing the effects of TM additives on the thickness and morphology of the oxide layers could enable design of (Zr,TM)B_2 ceramics with a more stable liquid/glassy B_2O_3 layer, more dense oxide scales, and, consequently, higher oxidation resistance.

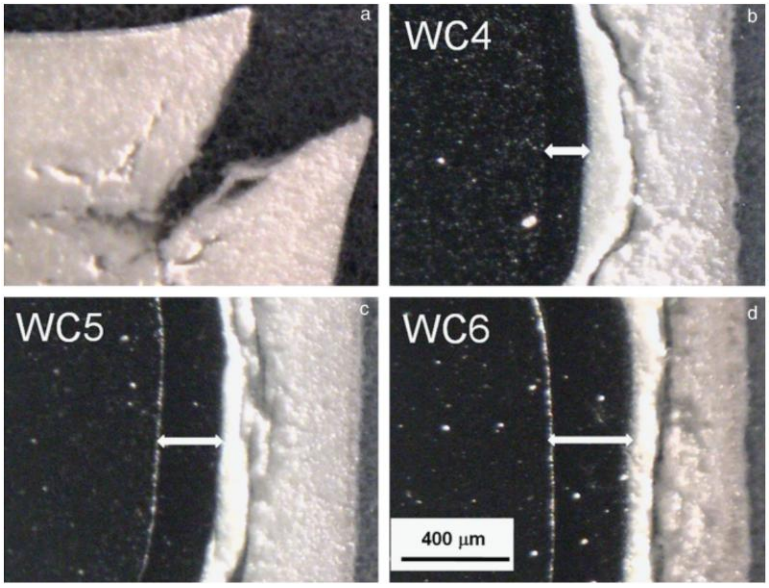

Figure 2.8. Comparison of cross-section microstructures for nominally pure ZrB_2 and (Zr,W)B_2 with 4, 5, or 6 mol% WC after oxidation at 1600°C for 6 hours.[13]

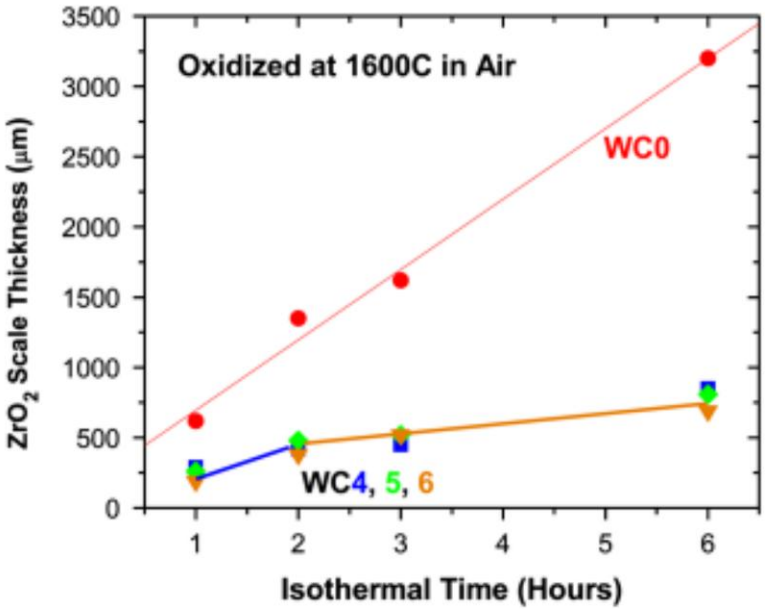

Figure 2.9. Measured scale thicknesses vs. oxidation time for nominally pure ZrB_2 and $(Zr,W)B_2$ with 4, 5, or 6 mol% WC after oxidation at 1600°C.[13]

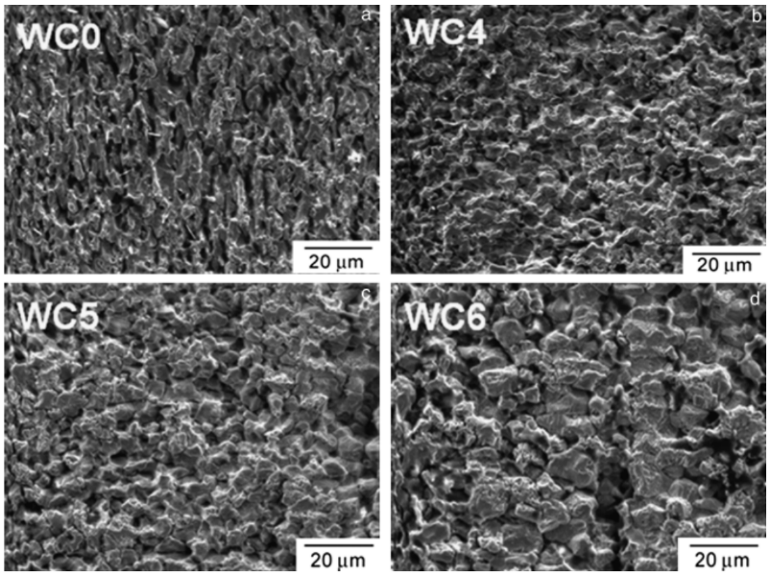

Figure 2.10. Comparison of microstructures of the outer oxide scales for nominally pure ZrB_2 and $(Zr,W)B_2$ with 4, 5, or 6 mol% WC after oxidation at 1600°C for 3 hours.[13]

REFERENCES

1. K. Upadhya, J. M. Yang, and W. P. Hoffman, "Materials for Ultrahigh Temperature Structural Applications," *American Ceramic Society Bulletin,* 76[12] 51-56 (1997).
2. D. M. Van Wie, D. G. Drewry, Jr., D. E. King, and C. M. Hudson, "The Hypersonic Environment: Required Operating Conditions and Design Challenges," *Journal of Materials Science,* 39[19] 5915-24 (2004).
3. W. Fahrenholtz, G. Hilmas, G. Talmy, and J. Zaykoski, "Refractory Diborides of Zirconium and Hafnium," *Journal of the American Ceramic Society,* 90[5] 1347-64 (2007).
4. J. W. Lawson, C. W. Bauschlicher, and M. S. Daw, "Ab Initio Computations of Electronic, Mechanical, and Thermal Properties of ZrB_2 and HfB_2," *Journal of the American Ceramic Society,* 94[10] 3494-99 (2011).
5. S. Q. Guo, "Densification of ZrB_2-based Composites and their Mechanical and Physical Properties: A Review," *Journal of the European Ceramic Society,* 29[6] 995-1011 (2009).
6. M. M. Opeka, I. G. Talmy, E. J. Wuchina, J. A. Zaykoski, and S. J. Causey, "Mechanical, Thermal, and Oxidation Properties of Refractory Hafnium and Zirconium Compounds," *Journal of the European Ceramic Society,* 19[13-14] 2405-14 (1999).
7. R. Monti and D. M. Paterna, "A Low Risk Reentry: Looking Backward to Step Forward," *Aerospace Science and Technology,* 10[2] 156-67 (2006).
8. S. R. Levine, E. J. Opila, M. C. Halbig, J. D. Kiser, M. Singh, and J. A. Salem, "Evaluation of Ultra-high Temperature Ceramics for Aeropropulsion Use," *Journal of the European Ceramic Society,* 22[14-15] 2757-67 (2002).
9. Y.-z. Yang, J.-l. Yang, and D.-n. Fang, "Research Progress on Thermal Protection Materials and Structures of Hypersonic Vehicles," *Applied Mathematics and Mechanics,* 29[1] 51-60 (2008).
10. I. G. Talmy, J. A. Zaykoski, and M. A. Opeka, "Properties of Ceramics in the ZrB_2/ZrC/SiC System Prepared by Reactive Processing," pp. 105-12. in 22nd Annual Conference on Composites, Advanced Ceramics, Materials, and Structures: A: Ceramic Engineering and Science Proceedings**.** John Wiley & Sons, Inc., 2008.
11. S. C. Zhang, G. E. Hilmas, and W. G. Fahrenholtz, "Mechanical Properties of Sintered ZrB_2–SiC Ceramics," *Journal of the European Ceramic Society,* 31[5] 893-901 (2011).
12. J. W. Zimmermann, G. E. Hilmas, and W. G. Fahrenholtz, "Thermal Shock Resistance of ZrB_2 and ZrB_2–30% SiC," *Materials Chemistry and Physics,* 112[1] 140-45 (2008).
13. S. C. Zhang, G. E. Hilmas, and W. G. Fahrenholtz, "Oxidation of Zirconium Diboride with Tungsten Carbide Additions," *Journal of the American Ceramic Society,* 94[4] 1198-205 (2011).

14. W. G. Fahrenholtz, G. E. Hilmas, S. C. Zhang, and S. Zhu, "Pressureless Sintering of Zirconium Diboride: Particle Size and Additive Effects," *Journal of the American Ceramic Society,* 91[5] 1398-404 (2008).
15. W. M. Guo and G. J. Zhang, "Oxidation Resistance and Strength Retention of ZrB_2-SiC Ceramics," *Journal of the European Ceramic Society,* 30[11] 2387-95 (2010).
16. G. P. Shveikin and A. L. Ivanovskii, "The Chemical Bonding and Electronic Properties of Metal Borides," *Russian Chemical Reviews,* 63[9] 711-34 (1994).
17. P. Vajeeston, P. Ravindran, C. Ravi, and R. Asokamani, "Electronic Structure, Bonding, and Ground-state Properties of AlB_2-type Transition-metal Diborides," *Physical Review B,* 63[4] 045115 (2001).
18. J. K. Burdett, E. Canadell, and G. J. Miller, "Electronic Structure of Transition-Metal Borides with the AlB_2 Structure," *Journal of the American Chemical Society,* 108[21] 6561-68 (1986).
19. M. Rahman, C. C. Wang, W. Chen, S. A. Akbar, and C. Mroz, "Electrical Resistivity of Titanium Diboride and Zirconium Diboride," *Journal of the American Ceramic Society,* 78[5] 1380-82 (1995).
20. X. Zhang, X. Luo, J. Han, J. Li, and W. Han, "Electronic Structure, Elasticity and Hardness of Diborides of Zirconium and Hafnium: First Principles Calculations," *Computational Materials Science,* 44[2] 411-21 (2008).
21. M. Gasch, S. Johnson, and J. Marschall, "Thermal Conductivity Characterization of Hafnium Diboride-Based Ultra-High-Temperature Ceramics," *Journal of the American Ceramic Society,* 91[5] 1423-32 (2008).
22. S. C. Zhang, G. E. Hilmas, and W. G. Fahrenholtz, "Pressureless Densification of Zirconium Diboride with Boron Carbide Additions," *Journal of the American Ceramic Society,* 89[5] 1544-50 (2006).
23. M. Thompson, W. G. Fahrenholtz, and G. Hilmas, "Effect of Starting Particle Size and Oxygen Content on Densification of ZrB_2," *Journal of the American Ceramic Society,* 94[2] 429-35 (2011).
24. S. Zhu, W. G. Fahrenholtz, G. E. Hilmas, and S. C. Zhang, "Pressureless Sintering of Carbon-Coated Zirconium Diboride Powders," *Materials Science and Engineering: A,* 459[1–2] 167-71 (2007).
25. G. J. K. Harrington, G. E. Hilmas, and W. G. Fahrenholtz, "Effect of Carbon and Oxygen on the Densification and Microstructure of Hot Pressed Zirconium Diboride," *Journal of the American Ceramic Society,* 96[11] 3622-30 (2013).
26. A. Rezaie, W. G. Fahrenholtz, and G. E. Hilmas, "Evolution of Structure during the Oxidation of Zirconium Diboride-Silicon Carbide in Air up to 1500°C," *Journal of the European Ceramic Society,* 27[6] 2495-501 (2007).
27. T. A. Parthasarathy, R. A. Rapp, M. Opeka, and R. J. Kerans, "A Model for the Oxidation of ZrB_2, HfB_2 and TiB_2," *Acta Materialia,* 55[17] 5999-6010 (2007).
28. W. G. Fahrenholtz and G. E. Hilmas, "Oxidation of Ultra-high Temperature Transition Metal Diboride Ceramics," *International Materials Reviews,* 57[1] 61-72 (2012).
29. S. N. Karlsdottir, J. W. Halloran, and A. N. Grundy, "Zirconia Transport by Liquid Convection during Oxidation of Zirconium Diboride-Silicon Carbide," *Journal of the American Ceramic Society,* 91[1] 272-77 (2008).

30. A. K. Kuriakose and J. L. Margrave, "The Oxidation Kinetics of Zirconium Diboride and Zirconium Carbide at High Temperatures," *Journal of The Electrochemical Society,* 111[7] 827-31 (1964).
31. F. Monteverde and A. Bellosi, "Oxidation of ZrB_2-based Ceramics in Dry Air," *Journal of The Electrochemical Society,* 150[11] B552-B59 (2003).
32. J. B. Berkowitz-Mattuck, "High-Temperature Oxidation III. Zirconium and Hafnium Diborides," *Journal of The Electrochemical Society,* 113[9] 908-14 (1966).
33. W. C. Tripp and H. C. Graham, "Thermogravimetric Study of the Oxidation of ZrB_2 in the Temperature Range of 800° to 1500°C," *Journal of The Electrochemical Society,* 118[7] 1195-99 (1971).
34. R. J. Irving and I. G. Worsley, "The Oxidation of Titanium Diboride and Zirconium Diboride at High Temperatures," *Journal of the Less Common Metals,* 16[2] 103-12 (1968).
35. A. Rezaie, W. G. Fahrenholtz, and G. E. Hilmas, "Oxidation of Zirconium Diboride-Silicon Carbide at 1500°C in a Low Partial Pressure of Oxygen," *Journal of the American Ceramic Society,* 89[10] 3240-45 (2006).
36. S. C. Zhang, G. E. Hilmas, and W. G. Fahrenholtz, "Improved Oxidation Resistance of Zirconium Diboride by Tungsten Carbide Additions," *Journal of the American Ceramic Society,* 91[11] 3530-35 (2008).
37. M. M. Opeka, I. G. Talmy, and J. A. Zaykoski, "Oxidation-Based Materials Selection for 2000°C + Hypersonic Aerosurfaces: Theoretical Considerations and Historical Experience," *Journal of Materials Science,* 39[19] 5887-904 (2004).
38. C. M. Carney, P. Mogilvesky, and T. A. Parthasarathy, "Oxidation Behavior of Zirconium Diboride Silicon Carbide Produced by the Spark Plasma Sintering Method," *Journal of the American Ceramic Society,* 92[9] 2046-52 (2009).
39. S. N. Karlsdottir and J. W. Halloran, "Oxidation of ZrB_2-SiC: Influence of SiC Content on Solid and Liquid Oxide Phase Formation," *Journal of the American Ceramic Society,* 92[2] 481-86 (2009).
40. M. Mallik, K. K. Ray, and R. Mitra, "Oxidation behavior of hot pressed ZrB2-SiC and HfB2-SiC composites," *Journal of the European Ceramic Society,* 31[1-2] 199-215 (2011).
41. F. Monteverde, R. Savino, M. D. S. Fumo, and A. Di Maso, "Plasma Wind Tunnel Testing of Ultra-High Temperature ZrB_2–SiC Composites under Hypersonic Re-entry Conditions," *Journal of the European Ceramic Society,* 30[11] 2313-21 (2010).
42. F. Monteverde, R. Savino, and M. D. S. Fumo, "Dynamic Oxidation of Ultra-high Temperature ZrB_2-SiC under High Enthalpy Supersonic Flows," *Corrosion Science,* 53[3] 922-29 (2011).
43. X. Zhang, P. Hu, J. Han, and S. Meng, "Ablation Behavior of ZrB_2-SiC Ultra High Temperature Ceramics under Simulated Atmospheric Re-entry Conditions," *Composites Science and Technology,* 68[7-8] 1718-26 (2008).
44. S. Zhou, W. Li, P. Hu, C. Hong, and L. Weng, "Ablation Behavior of ZrB_2-SiC-ZrO_2 Ceramic Composites by Means of the Oxyacetylene Torch," *Corrosion Science,* 51[9] 2071-79 (2009).

45. D. Gao, Y. Zhang, C. Xu, Y. Song, and X. Shi, "Atomic Oxygen Adsorption and its Effect on the Oxidation Behaviour of ZrB_2-ZrC-SiC in Air," *Materials Chemistry and Physics,* 126[1-2] 156-61 (2011).
46. A. L. Chamberlain, W. G. Fahrenholtz, G. E. Hilmas, and D. T. Ellerby, "Characterization of Zirconium Diboride for Thermal Protection Systems," pp. 493-96. in 8th Conference and Exhibition of the European Ceramic Society, Vol. 264-268. Istanbul, Turkey, 2004.
47. X. Li, X. Zhang, J. Han, C. Hong, and W. Han, "A Technique for Ultrahigh Temperature Oxidation Studies of ZrB_2-SiC," *Materials Letters,* 62[17-18] 2848-50 (2008).
48. W. M. Guo, X. J. Zhou, G. J. Zhang, Y. M. Kan, Y. G. Li, and P. L. Wang, "Effect of Si and Zr Additions on Oxidation Resistance of Hot-pressed ZrB_2-SiC Composites with Polycarbosilane as a Precursor at 1500 °C," *Journal of Alloys and Compounds,* 471[1-2] 153-56 (2009).
49. F. Peng, Y. Berta, and R. F. Speyer, "Effect of SiC, TaB_2 and $TaSi_2$ Additives on the Isothermal Oxidation Resistance of Fully Dense Zirconium Diboride," *Journal of Materials Science,* 24 [5] 1855-67. (2009).
50. D. Gao, Y. Zhang, C. Xu, Y. Song, and X. Shi, "Effect of Ozone Adsorption on the Oxidation Behaviour of ZrB_2-SiC Ceramic Composites," *Corrosion Science,* 53[2] 840-44 (2011).
51. S. N. Karlsdottir and J. W. Halloran, "Formation of Oxide Scales on Zirconium Diboride–Silicon Carbide Composites During Oxidation: Relation of Subscale Recession to Liquid Oxide Flow," *Journal of the American Ceramic Society,* 91[11] 3652-58 (2008).
52. S. N. Karlsdottir and J. W. Halloran, "Formation of Oxide Films on ZrB_2–15 vol% SiC Composites during Oxidation: Evolution with Time and Temperature," *Journal of the American Ceramic Society,* 92[6] 1328-32 (2009).
53. S. S. Hwang, A. L. Vasiliev, and N. P. Padture, "Improved Processing and Oxidation-resistance of ZrB_2 Ultra-high Temperature Ceramics Containing SiC Nanodispersoids," *Materials Science and Engineering A,* 464[1-2] 216-24 (2007).
54. S. Gangireddy, S. N. Karlsdottir, S. J. Norton, J. C. Tucker, and J. W. Halloran, "In situ Microscopy Observation of Liquid Flow, Zirconia Growth, and CO Bubble Formation During High Temperature Oxidation of Zirconium Diboride-silicon Carbide," *Journal of the European Ceramic Society,* 30[11] 2365-74 (2010).
55. P. Sarin, P. E. Driemeyer, R. P. Haggerty, D. K. Kim, J. L. Bell, Z. D. Apostolov, and W. M. Kriven, "In situ Studies of Oxidation of ZrB_2 and ZrB_2-SiC Composites at High Temperatures," *Journal of the European Ceramic Society,* 30[11] 2375-86 (2010).
56. S. Gangireddy, S. N. Karlsdottir, and J. W. Halloran, "Liquid Oxide Flow during Oxidation of Zirconium Diboride-Silicon Carbide Ultra High Temperature Ceramics," *Key Engineering Materials,* 434-435 144-48 (2010).
57. D. Alfano, L. Scatteia, F. Monteverde, E. Bêche, and M. Balat-Pichelin, "Microstructural Characterization of ZrB_2-SiC Based UHTC Tested in the MESOX Plasma Facility," *Journal of the European Ceramic Society,* 30[11] 2345-55 (2010).

58. I. Akin, F. Cinar Sahin, O. Yucel, and G. Goller, "Oxidation Behavior of Zirconium Diboride-Silicon Carbide Composites," pp. 105-11. in 34th International Conference on Advanced Ceramics and Composites, Vol. 31. Daytona Beach, FL, 2010.
59. T. Zhu, W. Li, X. Zhang, P. Hu, C. Hong, and L. Weng, "Oxidation Behavior of ZrB_2-SiC-ZrO_2 Ceramic Composites in the Temperature Range of 800-1200°C," *Materials Chemistry and Physics,* 116[2-3] 593-98 (2009).
60. P. Hu, W. Guolin, and Z. Wang, "Oxidation Mechanism and Resistance of ZrB_2-SiC Composites," *Corrosion Science,* 51[11] 2724-32 (2009).
61. W. Zhanjun, W. Zhi, Q. Qiang, and S. Guodong, "Oxidation Mechanism of a ZrB_2-SiC-ZrC Ceramic Heated through High Frequency Induction at 1600°C," *Corrosion Science,* 53[6] 2344-49 (2011).
62. A. L. Chamberlain, W. G. Fahrenholtz, G. E. Hilmas, and D. T. Ellerby, "Oxidation of ZrB_2-SiC Ceramics Under Atmospheric and Reentry Conditions," *Refractories Applications Transactions,* 1[2] 1-8 (2005).
63. E. J. Opila and M. C. Halbig, "Oxidation of ZrB_2-Based Ultra-High Temperature Ceramics," *Ceramic Engineering and Science Proceedings,* 22[3] 221-28 (2001).
64. O. N. Grigoriev, B. A. Galanov, V. A. Lavrenko, A. D. Panasyuk, S. M. Ivanov, A. V. Koroteev, and K. G. Nickel, "Oxidation of ZrB_2-SiC-$ZrSi_2$ Ceramics in Oxygen," *Journal of the European Ceramic Society,* 30[11] 2397-405 (2010).
65. I. G. Talmy, J. A. Zaykoski, M. M. Opeka, and S. Dallek, "Oxidation of ZrB_2 Ceramics Modified with SiC and Group IV-VI Transition Metal Diborides," *Electrochemical Society Proceedings,* 12 144-58 (2001).
66. D. Sciti, M. Brach, and A. Bellosi, "Oxidation behavior of a pressureless sintered ZrB2-MoSi2 ceramic composite," *Journal of materials research,* 20[4] 922-30 (2005).
67. S. Guo, T. Mizuguchi, M. Ikegami, and Y. Kagawa, "Oxidation Behavior of ZrB_2-$MoSi_2$-SiC Composites in Air at 1500°C," *Ceramics International,* 37[2] 585-91 (2011).
68. A. L. Chamberlain, W. G. Fahrenholtz, G. E. Hilmas, and D. T. Ellerby, "Characterization of zirconium diboride for thermal protection systems," pp. 493-96. in, Vol. 264-268. 2004.
69. M. A. Kuzenkova and P. S. Kislyi, "Investigation Of Scale Stability Of Alloys Of Zirconium Boride With Molybdenum Disilicide," *Porosh. Met., Akad. Nauk Ukr. SSR,* 10 75-79 (1965).
70. D. Sciti, M. Brach, and A. Bellosi, "Long-term Oxidation Behavior and Mechanical Strength Degradation of a Pressurelessly Sintered ZrB_2–$MoSi_2$ Ceramic," *Scripta Materialia,* 53[11] 1297-302 (2005).
71. D. Sciti, M. Brach, and A. Bellosi, "Oxidation Behavior of a Pressureless Sintered ZrB_2–$MoSi_2$ Ceramic Composite," *Journal of Materials Research,* 20[4] 922-30 (2005).
72. I. G. Talmy, J. A. Zaykoski, and M. M. Opeka, "High-Temperature Chemistry and Oxidation of ZrB_2 Ceramics Containing SiC, Si_3N_4, Ta_5Si_3, and $TaSi_2$," *Journal of the American Ceramic Society,* 91[7] 2250-57 (2008).

73. P. Hu, X. H. Zhang, J. C. Han, X. G. Luo, and S. Y. Du, "Effect of Various Additives on the Oxidation Behavior of ZrB_2-Based Ultra-High-Temperature Ceramics at 1800°C," *Journal of the American Ceramic Society,* 93[2] 345-49 (2010).
74. E. Opila, S. Levine, and J. Lorincz, "Oxidation of ZrB_2- and HfB_2-based Ultra-high Temperature Ceramics: Effect of Ta Additions," *Journal of Materials Science,* 39[19] 5969-77 (2004).
75. S. N. Karlsdottir, J. W. Halloran, and C. E. Henderson, "Convection Patterns in Liquid Oxide Films on ZrB_2-SiC Composites Oxidized at a High Temperature," *Journal of the American Ceramic Society,* 90[9] 2863-67 (2007).
76. S. N. Karlsdottir, J. W. Halloran, and C. E. Henderson, "Convection Patterns in Liquid Oxide Films on ZrB2–SiC Composites Oxidized at a High Temperature," *Journal of the American Ceramic Society,* 90[9] 2863-67 (2007).
77. D. Sciti, V. Medri, and L. Silvestroni, "Oxidation Behaviour of HfB_2-15 vol.% $TaSi_2$ at Low, Intermediate and High Temperatures," *Scripta Materialia,* 63[6] 601-04 (2010).
78. S. R. Levine and E. J. Opila, "Tantalum Addition to Zirconium Diboride for Improved Oxidation Resistance." in. NASA/TM-2003-212483, 2003.

PAPER

1. Oxidation of Zirconium Diboride with Niobium Additions

Maryam Kazemzadeh Dehdashti, William G. Fahrenholtz and Greg E. Hilmas

Department of Materials Science and Engineering

Missouri University of Science and Technology, Rolla, MO 65401

Abstract

Oxidation of ZrB_2 ceramics containing Nb additions at 1500 °C resulted in the formation of a two-layer oxide scale. The outer surface was partially covered by a glassy layer containing B_2O_3 with smaller amounts of Nb and Zr oxides dissolved into it. With increasing exposure time, evaporation of B_2O_3 from the outer layer resulted in precipitation of oxide particles in the receding glassy phase. Between the outer layer and the unoxidized $(Zr,Nb)B_2$ was a porous layer that consisted of particles containing Zr, Nb, and O. The formation of $Nb_2Zr_6O_{17}$ was observed in the porous oxide layer. Since this compound is solid at the oxidation temperature, liquid phase sintering of the ZrO_2 scale was not possible. However, dissolution of Nb into B_2O_3 increased the stability of the liquid/glassy layer, which acted as a barrier to the transport of oxygen at higher temperatures compared to the scale formed on nominally pure ZrB_2.

Key Words: ZrB_2; Nb; Oxidation; ZrO_2; Composites.

1.1. Introduction

Ultra high temperature ceramics (UHTCs) are a group of materials that includes ZrB_2, ZrC, HfB_2 and HfC. These materials are candidates for applications that require

exposure to extreme thermal and chemical environments. The performance advantages of the diboride-based UHTCs come not only from their high-temperature stability but also from the capability to transfer and redistribute heat at elevated temperatures. This characteristic is attractive for sharp leading edges for hypersonic aerospace vehicles, which must transfer heat away from the hottest areas and redistribute it to cooler areas. [1] Among UHTCs, ZrB_2 has the lowest theoretical density combined with reported thermal conductivity values as high as ~100 W/m•K at room temperature, which is an advantage over other candidates for aerospace applications.[2]

Oxidation behavior is a restriction to the development of ZrB_2-based ceramics for rocket propulsion and hypersonic flight applications. Assuming stoichiometric oxidation according to Reaction 1, exposure of ZrB_2 to air at temperatures of 800°C and above results in formation of B_2O_3 and ZrO_2, which leads to measurable mass gain.[3]

$$ZrB_{2\,(cr)} + 5/2\ O_{2\,(g)} \rightarrow ZrO_{2\,(cr)} + B_2O_{3\,(l)} \qquad (1)$$

Evaporation of B_2O_3 is considerable at temperatures above ~1200 °C. The loss of $B_2O_{3\,(l)}$ leaves behind a porous ZrO_2 layer with a columnar microstructure, which offers channels for rapid oxygen transport to the reaction interface and results in significant mass gain at temperatures above 1200°C.[4] The conventional approach to improving the oxidation resistance of diboride ceramics is to add Si-containing compounds such as SiC [1, 5-13], $MoSi_2$ [14-16], or $TaSi_2$. [17, 18] The formation of a borosilicate layer on the surface of the diborides provides improved oxidation resistance in air compared to the borate glass on nominally pure ZrB_2 due to the increased stability of the borosilicate glass compared to the borate material. [3, 19] At elevated temperatures, $SiO_{(g)}$ forms beneath the borosilicate

glass as a result of active oxidation of SiC. When the pressure of $SiO_{(g)}$ exceeds ambient, the resulting pressure can rupture the protective glassy layer, which can result in a cyclic protective/ non-protective scale-forming sequence.[20] Further, some authors have noted the formation of the SiC-depleted layer in ZrB_2-SiC samples, which facilitates the transport of oxygen through the oxide scale to the unoxidized matrix.[21, 22] Hence, SiC may not be the best choice for improving the oxidation resistance of ZrB_2 ceramics at ultra high temperatures.

Several studies showed that additions of Cr-, Ti-, Nb-, V-, and Ta-borides improved the oxidation resistance of ZrB_2-SiC composites. [22-26] Hence, additions of transition metals offer improved oxidation resistance to ZrB_2 ceramics without the deleterious effects of silica formers. Similarly, Zhang et al. reported that WC additions improved the oxidation resistance of ZrB_2 ceramics. The addition of WC led to the formation of a two-layer scale structure, which consisted of a porous zirconia outer layer and a dense inner layer containing ZrO_2 and WO_3, in contrast with the single, highly porous and columnar ZrO_2 layer formed on nominally pure ZrB_2. [27, 28] It was suggested that during oxidation, the presence of WO_3 in the oxide scale resulted in liquid phase sintering of ZrO_2, which increased the relative density of the scale, resulting in improved oxidation resistance. [28] Other transition metal additives, such as Nb, may offer similar beneficial effects on the oxidation behavior of zirconium diboride. Unlike the presence of WO_3, the formation of Nb_2O_5 during oxidation is not expected to result in the formation of a liquid phase. Examination of the Nb_2O_5-ZrO_2 phase diagram shows that at 1500°C, the presence of small (less than 10 mol%) concentrations of Nb should lead to the formation of solid compounds such as Nb-doped ZrO_2 or $Nb_2Zr_6O_{17}$ rather than a

liquid phase, such as the WO_3-ZrO_2 solution predicted for the presence of small amounts of W with ZrO_2. [29, 30] The purpose of this paper was to examine the effect of niobium additions on the oxidation behavior of ZrB_2 at elevated temperatures to gain insight into the mechanism by which transition metal additions improve oxidation resistance.

1.2. Experimental procedure

High purity (>99%) ZrB_2 powder (Grade B, H.C. Starck, Newton, MA) with an average particle size of ~2 μm was used to prepare the specimens for this study. To enhance densification, 2 wt% B_4C (~0.8 μm, Grade HS, H.C Starck) was added to all batches to react with and remove oxide impurities from the powder particle surfaces. For some batches, 6 mol% niobium was added in form of Nb powder (Johnson Matthey, MA), which had an average particle size of ~1 μm. To reduce particle size and promote intimate mixing, the as-received ZrB_2, B_4C, and Nb (for Nb containing batches) were dispersed in methyl ethyl ketone (MEK) by ball milling with zirconia media for 24 hr. An organic dispersant (DISPERBYK-110, BYK-Chemie Co., Wesel, Germany) was added at a level of 0.54 mg of dispersant per m^2 of ZrB_2 surface area. The amount of zirconia contamination added to the batches as a result of ball milling was determined to be less than 1 wt% based on the mass of ZrB_2 powder by measuring the mass of the media before and after milling. After mixing, the solvent was removed using rotary evaporation, and then the powder was ground and sieved to -80 mesh.

Powders were densified by hot pressing (Model HP-3060, Thermal Technology, Santa Rosa, CA) at 2100°C for 45 min at a pressure of 32 MPa. Powders were loaded into a graphite die lined with graphite foil that was coated with BN spray. Billets with a diameter of ~25 mm and a thickness of ~5 mm were produced. Specimens with

dimensions of 10 mm by 4 mm by 4 mm were diced from the billets and polished on all sides to a 15 μm finish for testing and characterization. Images obtained by scanning electron microscopy (SEM; S-4700, Hitachi, Japan) from the polished surfaces of as processed $(Zr,Nb)B_2$ and ZrB_2 were used to study the microstructure of the specimens. The amount of B_4C remaining after densification was calculated using image analysis software (ImageJ, U. S. National Institutes of Health, Bethesda, MD). The bulk densities of the hot pressed billets were measured using the Archimedes technique with water as the immersing medium.

Oxidation studies were performed in a $MoSi_2$ resistance-heated horizontal tube furnace (Model 0000543 Rapid Temperature Furnace, CM Inc., Bloomfield, NJ) equipped with a high-purity alumina tube with a diameter of 6.35 cm. Specimens were cleaned in acetone in an ultrasonic bath and then placed on a zirconia foam setter that was on an alumina D-tube. The specimen assembly was inserted into the center of the furnace and leveled. The ends of the tube were sealed using gas-tight end caps. Specimens were heated at ~5 °C/min to 1500 °C or 1600 °C and held for up to 3 hours in air with a flow rate of 0.2 cm/s (linear flow rate was calculated according to the volumetric flow rate and the size of the tube). To minimize changes such as further oxidation that may occur during cooling, specimens were air quenched to room temperature by removing them from the furnace after the desired oxidation time.

The thicknesses of the resulting oxidation layers were measured from fracture surfaces that were observed in SEM. In addition, the microstructures of the oxide scales were observed using SEM and chemical compositions were analyzed using energy dispersive spectroscopy (EDS; EDAX, Mahwah, NJ). X-ray diffraction (XRD; Philips X-

Pert Pro diffractometer, Westborough, MA) analysis was used to identify major crystalline phases present in both the pre-oxidized and the post-oxidized composites and the data were analyzed *using X'Pert High Score* software.

1.3. Results and discussion

1.3.1. Densification, Microstructure, and Phase Analysis

A microstructure typical of the $(Zr,Nb)B_2$ specimens used in this investigation is presented in Figure 1. The darker phase is B_4C and it appears to be uniformly dispersed in the lighter $(Zr,Nb)B_2$ matrix. Based on image analysis, the amount of B_4C remaining after densification was 1.4 wt%. The average bulk density of bars cut from hot-pressed $(Zr,Nb)B_2$ billets was 6.03 g/cm^3. Using a volumetric rule of mixtures calculation, and assuming true densities of 6.09 g/cm^3 for ZrB_2, 2.52 g/cm^3 for B_4C, and 8.57 g/cm^3 for Nb, the theoretical density of ZrB_2 containing 6 mol% Nb was calculated to be 6.05 g/cm^3. Using this true density, the hot-pressed bars had relative densities of >99%. The calculated relative density is consistent with the minimal amount of porosity revealed by SEM analysis. Also, Archimedes' measurements showed the amount of open porosity to be insignificant. Thus, porosity was not considered to have a significant effect on the oxidation behavior. Microstructure and phase analysis using SEM and XRD were consistent with the dissolution of Nb into the matrix to form a $(Zr,Nb)B_2$ solution, which was identified as hexagonal by indexing to ZrB_2 (PDF card number 34-0423).

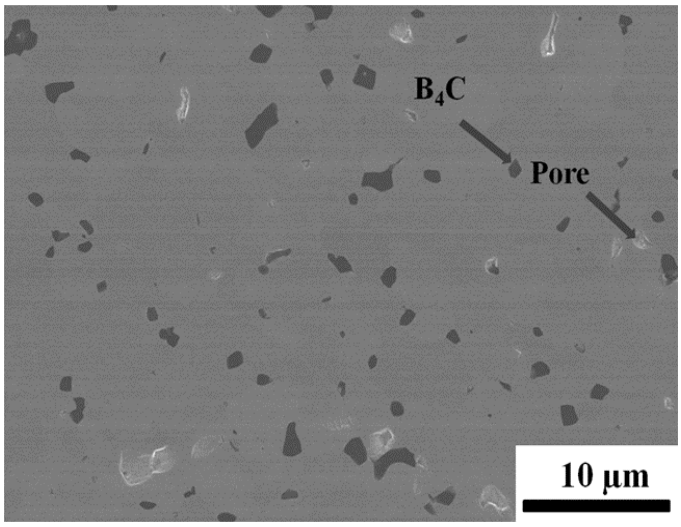

Figure 1. SEM image of a polished cross section showing the microstructure of ZrB_2 containing 1.5 vol% B_4C and 6 mol% Nb.

1.3.2. Surface Morphology and Composition

Assuming that the oxidation of $(Zr_{1-x}Nb_x)B_2$ proceeds stoichiometrically, reaction at temperatures of 800 °C and above should produce molten B_2O_3 (melting temperature ~450 °C), solid ZrO_2, and solid Nb_2O_5 in the molar ratios shown in Reaction 2. In this case, the addition of 6 mol% Nb to ZrB_2 is equivalent to x = 0.06, which produces an oxide scale with a molar ratio of Nb_2O_5 to ZrO_2 of 1 to 33 or 93.5 wt% ZrO_2 plus 6.5 wt% Nb_2O_5. According to the ZrO_2-Nb_2O_5 phase diagram[29, 30], the primary crystalline phases that should form are a monoclinic solid solution based on ZrO_2 that contains dissolved Nb and an orthorhombic compound, $Nb_2Zr_6O_{17}$. By increasing the temperature, the solubility limit of Nb_2O_5 into ZrO_2 increases and the ratio of $Nb_2Zr_6O_{17}$ to the ZrO_2 solid solution decreases. The melting temperature of $Nb_2Zr_6O_{17}$ is 1670 °C and the solubility limit of Nb_2O_5 in ZrO_2 at 1500 °C is about 7 mol% (14 mol% Nb). Due to the formation of solid $Nb_2Zr_6O_{17}$, no liquid phase is predicted for the composition of the oxide scale, which should be ZrO_2 containing 6 mol% of dissolved Nb at 1500 °C. Upon

cooling to room temperature, the solubility limit of Nb_2O_5 in ZrO_2 decreases and some $Nb_2Zr_6O_{17}$ should precipitate from the ZrO_2 solid solution. At room temperature, $Nb_2Zr_6O_{17}$ comprises about 18 mol% of the oxide phase along with an amorphous phase that is mainly B_2O_3.

$$(Zr_{1-x}Nb_x)B_{2\,(cr)} + (5/2+x/4)\,O_{2\,(g)} \rightarrow (1-x)\,ZrO_{2\,(cr)} + x/2\,Nb_2O_{5\,(cr)} + B_2O_{3\,(l)} \qquad (2)$$

The surface of $(Zr,Nb)B_2$ oxidized at 1500 °C for 0 hours (i.e., quenched as soon as it reached 1500°C) is shown in Figure 2a. A majority of the surface of the specimen was covered by a dark phase that had a glassy appearance (~90% of the surface area) with a small fraction of the surface composed of oxide particles (~10% of the surface area). After 3 hours at 1500 °C (Figure 2b), the area fraction of the glassy phase had decreased to ~60% and the glassy phase was concentrated in several pools that were surrounded by oxide particles.

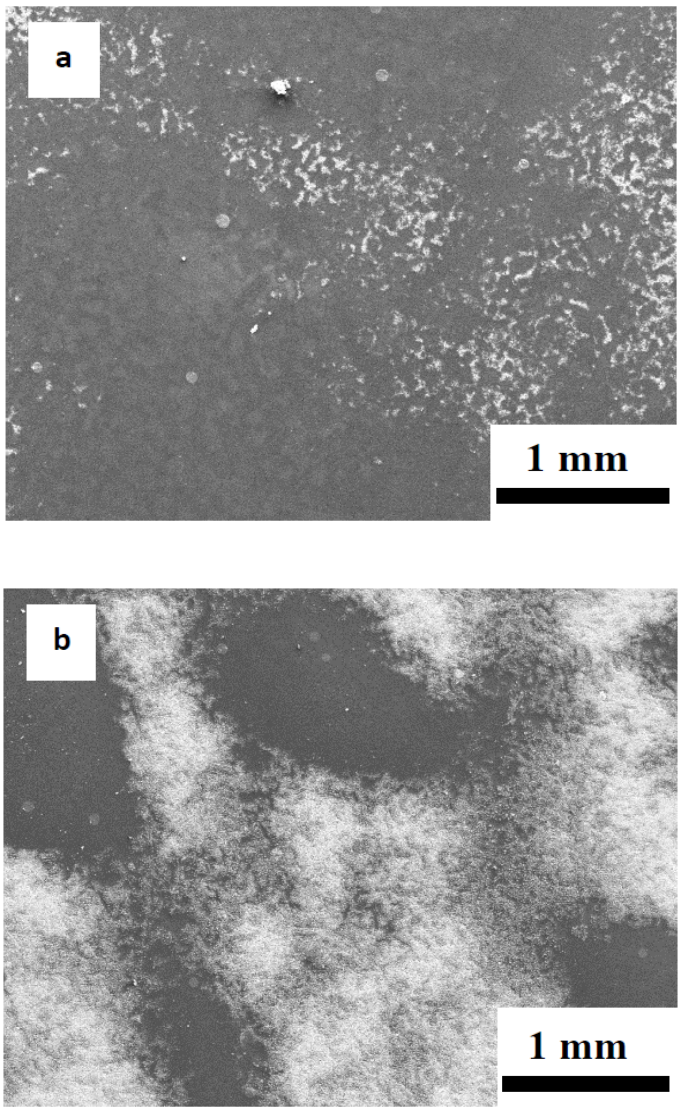

Figure 2. Surface of (Zr,Nb)B_2 oxidized at 1500°C for (a) 0 hours, (b) 3 hours, showing the presence of a glassy oxide (dark phase) and crystalline oxide particles (light phase).

Due to low sensitivity of EDS to light elements, quantification of the boron content in the glassy phase was not possible. However, EDS results indicated that the matrix of the glassy phase contained O and Nb along with a small amount of Zr, presumably all dissolved in B_2O_3. Small particles that contained both Zr and Nb (Figure 3a) were also observed in the glassy phase. According to the ZrO_2-B_2O_3 [31] and Nb_2O_5-

B_2O_3 [32] phase diagrams, approximately 12 mol% ZrO_2 can dissolve into B_2O_3 at 1500°C while both Nb_2O_5 and B_2O_3 are liquids at that temperature. Hence, the particles observed at room temperature could be ZrO_2, Nb_2O_5, or an oxide containing Zr and Nb. The particles could have formed either during oxidation or during cooling. They could form during oxidation due to evaporation of B_2O_3 that would result in supersaturation of the remaining B_2O_3 with ZrO_2, which could result in precipitation. Conversely, the particles could precipitate from the glassy phase when the specimen was cooled from the processing temperature due to the change in solubility of ZrO_2 in B_2O_3 with temperature. According to the ZrO_2-Nb_2O_5 phase diagram[29], two different crystalline phases could form when ZrO_2 and Nb_2O_5 precipitate from the B_2O_3 melt. For Nb_2O_5 contents less than about 5 mol%, a $(Zr_{1-x}Nb_x)O_{2+0.5x}$ solid solution is the stable phase. If the Nb_2O_5 concentration in the glassy phase is higher, then the crystalline phase $Nb_2Zr_6O_{17}$ (also designated $6ZrO_2 \cdot Nb_2O_5$) could form in addition to the ZrO_2 solid solution. X-ray diffraction was used to characterize the phases present on the surface of oxidized $(Zr,Nb)B_2$. The major phases detected were triclinic H_3BO_3, monoclinic ZrO_2 and orthorhombic $Nb_2Zr_6O_{17}$ (PDF card numbers 30-0199, 83-0944 and 72-1745, respectively). Boric acid formed after cooling the specimen to room temperature due to the instability of B_2O_3 in the humid ambient air.

With increasing exposure time, more B_2O_3 should evaporate from the surface, which would increase precipitation of Zr- and Nb-rich oxide particles from the liquid phase. Near the edges of the pools, spherical particles precipitated as the B_2O_3 liquid evaporated. Figure 3a shows that the particles were uniformly distributed in the glassy phase and that they had an average diameter of about 0.5 μm. Closer to the centers of the

glassy pools, elongated precipitates appeared to grow from the spherical particles (Figure 3b). The elongated precipitates were typically about 3 μm long.

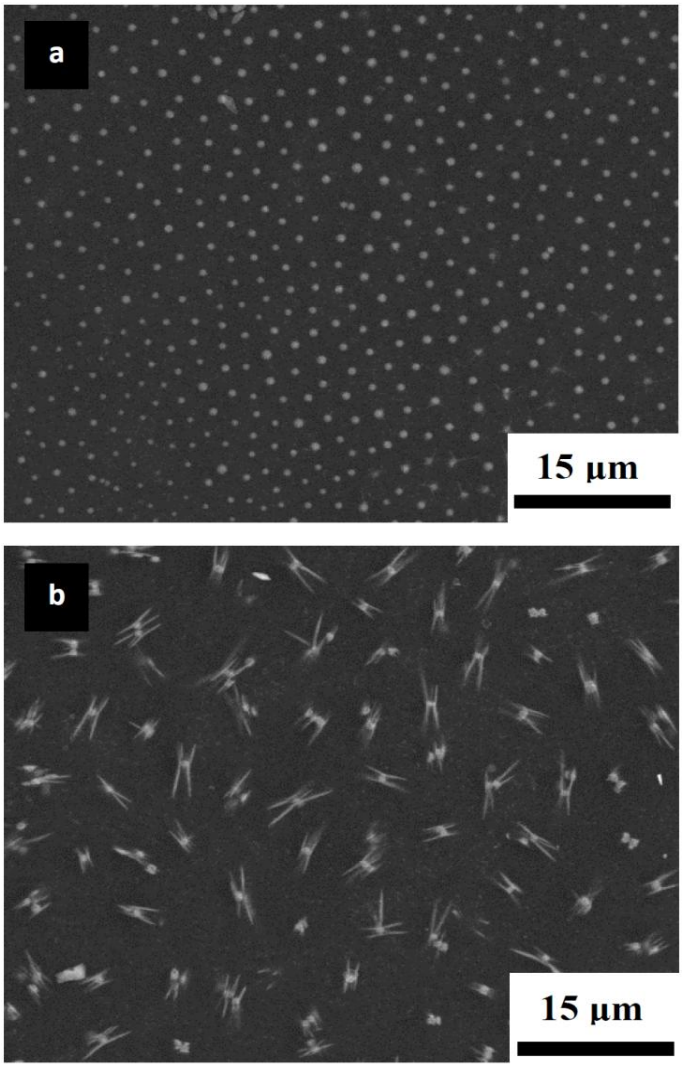

Figure 3. SEM images of the surface of a $(Zr,Nb)B_2$ specimen oxidized at 1500°C for 3 hours that were (a) close to the edge of the liquid pool, and (b) in the middle of the liquid pool. The images show a homogeneous distribution of oxide particles containing Zr and Nb and formation of elongated particles.

As the glassy phase receded during extended exposure at 1500 °C, the underlying oxide particles were revealed (Figure 4a and b). As the liquid receded, the small spherical particles that were observed in the glassy phase appeared to attach to the larger particles that were exposed. Some smaller particles were visible between the larger ones. In areas where the glassy phase remained, particularly in the middle of the glassy pools, the precipitated particles became more concentrated. As can be seen in Figure 5, clusters of elongated particles formed in the areas where the last of the glassy pools were present.

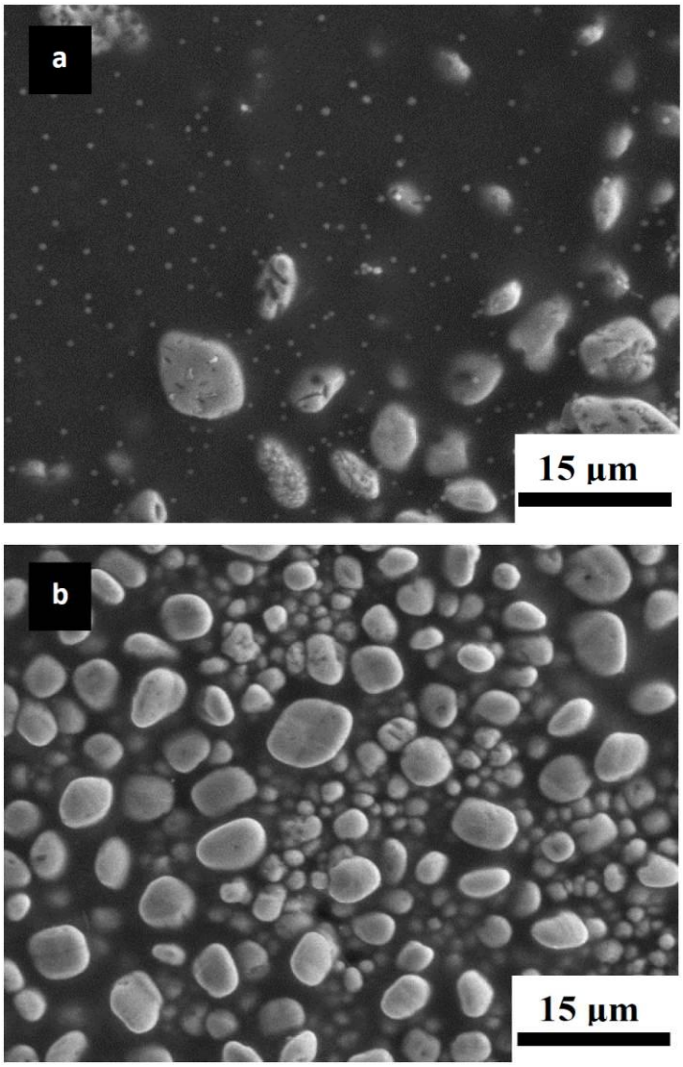

Figure 4. SEM images of a $(Zr,Nb)B_2$ specimen oxidized at 1500 °C for 3 hours (a) at the edge of the liquid pool, (b) in the crystalline oxide region close to the liquid pool, showing the growth of the oxide particles by joining the small precipitated particles.

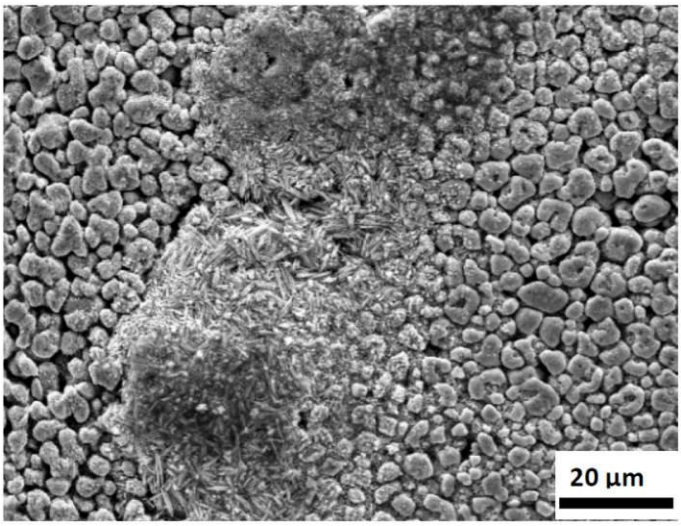

Figure 5. SEM image of the $(Zr,Nb)B_2$ specimen oxidized at 1500°C for 3 hours showing the clustering of the equiaxed and elongated particles on the surface of the crystalline oxide particles.

1.3.3. Oxide Scale Morphology and Thickness

Initial attempts to polish cross sections of oxidized samples revealed that the oxide scales were damaged by the preparation process. To produce cross sections that were representative of the oxide scales, fracture surfaces were examined. Figure 6 shows a low magnification SEM image of the fracture surface of a $(Zr,Nb)B_2$ sample oxidized at 1500 °C for 3 hours. Significant differences were observed in the thickness of the glassy layer between the middle and edge of the glassy pool. After oxidation at 1500 °C for 3 hours the thickness of the glassy layer ranged from a maximum of about 0 µm to ~40 µm. In addition, the thickness of the porous oxide layer ranged from about 45 µm to 60 µm. Areas of thick glassy oxide had thinner porous oxide layers while areas with thinner glassy oxide had thicker porous layers.

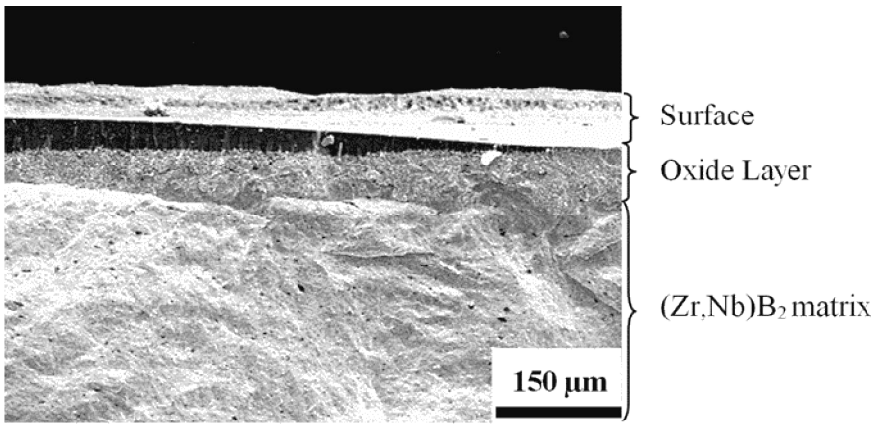

Figure 6. Fracture surface of a $(Zr,Nb)B_2$ specimen oxidized at 1500 °C for 3 hours.

Figure 7 shows cross sectional SEM images of the oxide scales from regions with maximum glassy layer thickness. The scales were formed on the surfaces of the $(Zr,Nb)B_2$ samples after oxidation at 1500 °C for 0, 1.5 and 3 hours. The oxide scales in these regions consisted of two layers: (1) a dense outer glassy layer, and (2) an inner layer that appeared to be porous. The two-layer scale is believed to be formed due to volume expansion upon conversion of ZrB_2 to ZrO_2 and B_2O_3, which is ~300% volume expansion based on density calculations. Oxidation produces two phases because of the immiscibility of the two materials while the large volume expansion associated with formation of B_2O_3 causes it to be forced to the surface of the specimen.[3]

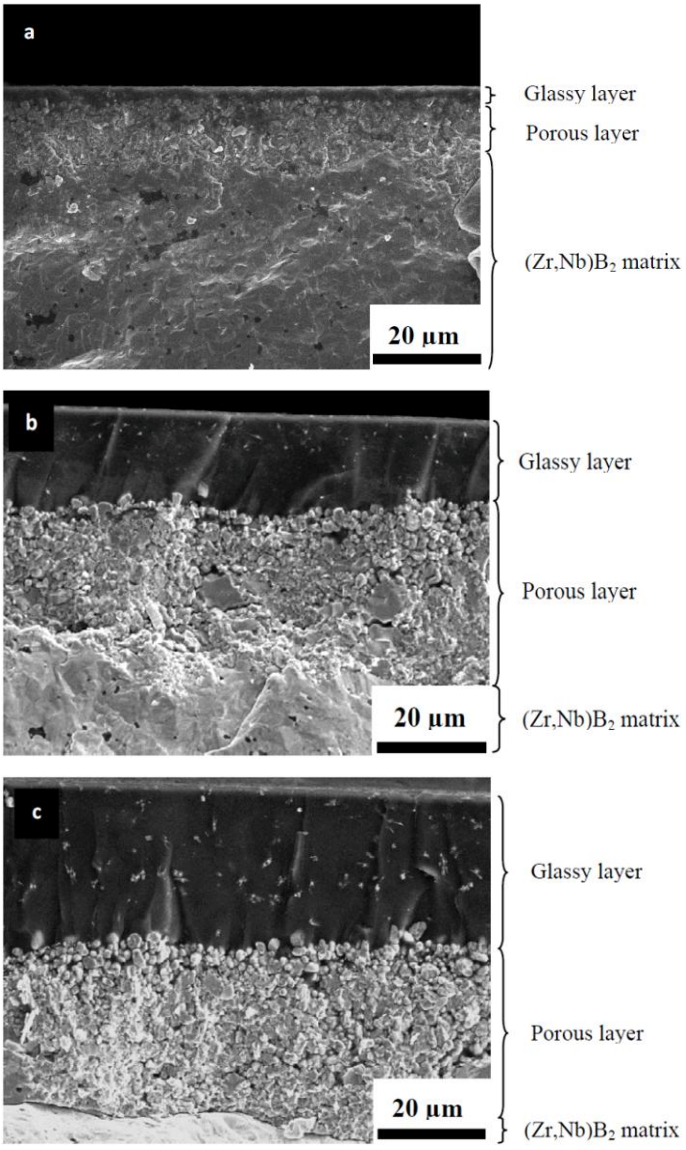

Figure 7. Fracture surfaces of $(Zr,Nb)B_2$ oxidized at 1500°C for: (a) 0 hours, (b) 1.5 hours, and (c) 3 hours.

Several small elongated particles can be observed in the glassy layer in Figure 7a and b. The particles were uniformly distributed through the thickness of the glassy layer. Also, some residual glassy phase was observed between the oxide particles in the porous layer. The oxide particles in the porous layer of oxidized $(Zr,Nb)B_2$ were less than 10 µm in diameter and had equiaxed shapes. For comparison, the scale formed on nominally pure ZrB_2 was composed of larger ZrO_2 particles that had an elongated morphology. [33]

Figure 8 shows the results of the scale thickness measurements for nominally pure ZrB_2 compared to $(Zr,Nb)B_2$ after oxidation at 1500 °C for 0, 1.5 and 3 hours. While the scales formed on nominally pure ZrB_2 were mostly uniform, considerable differences in the thickness of the scales between the middle and edge of the glassy pools were observed in the $(Zr,Nb)B_2$ specimens. Therefore, the measurements were performed on the regions with maximum glassy layer thickness for $(Zr,Nb)B_2$. When nominally pure ZrB_2 and $(Zr,Nb)B_2$ reached 1500 °C, the glassy layers for both materials were ~4 μm thick, while the porous oxide scale was ~26 μm for ZrB_2 and ~18 μm for $(Zr,Nb)B_2$. After 1.5 hours at 1500 °C, the glassy and porous layers on the nominally pure ZrB_2 were ~2 and ~59 μm thick, respectively. For the same oxidation time, $(Zr,Nb)B_2$ had a maximum glassy layer thickness of ~18 μm. The porous layer beneath the glassy layer with the maximum thickness was ~35 μm. No glassy layer was observed on pure ZrB_2 after 3 hours at 1500 °C, while the glassy layer on $(Zr,Nb)B_2$ had a maximum thickness of ~37 μm. The thickness of the porous layer on nominally pure ZrB_2 was ~73 μm compared to ~45 μm for $(Zr,Nb)B_2$ after 3 hours at 1500°C. Although the surface area of the glassy pools on $(Zr,Nb)B_2$ decreased with increasing the exposure time at 1500°C, the thickness of the glassy layer increased with exposure time.

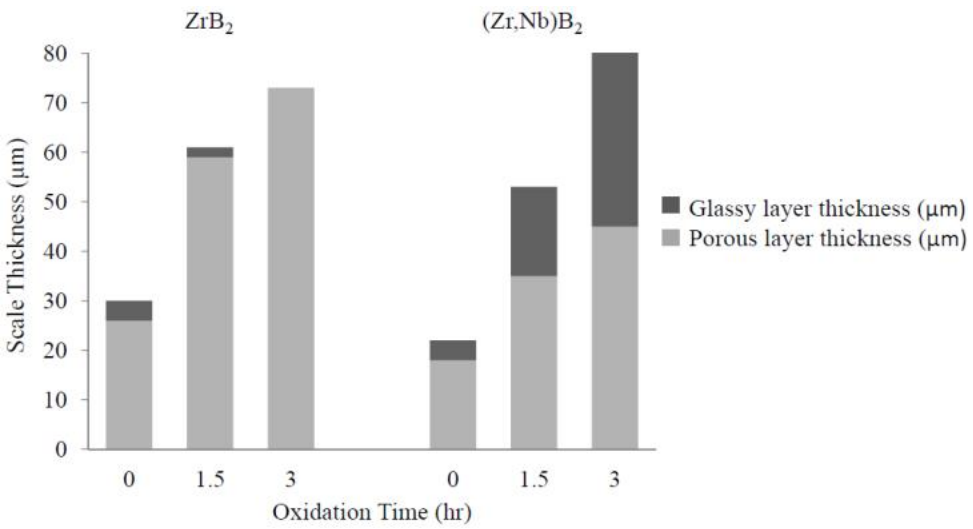

Figure 8. Scale thickness as a function of oxidation time at 1500°C comparing nominally pure ZrB_2 to areas with the maximum glassy thickness for $(Zr,Nb)B_2$.

For nominally pure ZrB_2, the thickness of the glassy layer decreased with increasing oxidation time at 1500 °C due to evaporation of B_2O_3. Previous studies have reported that evaporation of B_2O_3 is substantial above 1100 °C due to its high vapor pressure. [3] In contrast, increasing the oxidation time at 1500°C for $(Zr,Nb)B_2$ resulted in an increase in the thickness of the glassy layer. The presence of glassy phase after oxidation of $(Zr,Nb)B_2$ at 1500 °C for 3 hours indicated that the addition of Nb increased the stability of the liquid phase at high temperatures. Dissolution of Nb_2O_5 into the liquid phase should decrease the activity of B_2O_3 and, consequently, reduce its vapor pressure and evaporation rate. The presence of a glassy layer should improve the oxidation resistance of the ceramic since borate glasses act as a barrier to oxygen transport. [34]

After oxidation at 1500 °C for 3 hours, the thickness of the porous layer was ~75 μm for nominally pure ZrB_2 compared to ~45 μm for $(Zr,Nb)B_2$. Based on this observation, the stability of the glassy layer resulted in a decreased oxidation rate for

$(Zr,Nb)B_2$. The addition of Nb increased the stability of the liquid phase, providing better protection at high temperatures, which decreased the oxidation rate of the $(Zr,Nb)B_2$ compared with nominally pure ZrB_2. Not only was the initial thickness of the porous oxide layer thinner for $(Zr,Nb)B_2$ (~18 μm compared to ~26 μm for nominally pure ZrB_2), the porous oxide layer was thinner after 3 hours at 1500°C (~45 μm compared to ~75 μm for nominally pure ZrB_2). Based on the calculations performed on the thickness of the porous layers, the oxidation exhibited linear kinetic behavior (R^2>0.94) at 1500°C. Further, the addition of Nb to ZrB_2 resulted in a lower oxidation rate (9 μm/h) compared to nominally pure ZrB_2 (16 μm/h).

1.3.4. Evolution of Structure

Figure 9 is a schematic description of the evolution of the structure of the oxide scale on $(Zr,Nb)B_2$. At the early stages, Zr, Nb, and B oxides form as $(Zr,Nb)B_2$ is oxidized. The Zr-Nb oxide particles form on the $(Zr,Nb)B_2$ surface, but are covered by a liquid phase composed of mainly B_2O_3 with smaller amounts of dissolved Nb and Zr oxides. During oxidation, Nb and Zr oxides dissolve into the liquid borate phase. At higher temperatures, the evaporation rate of B_2O_3 from the outer surface increases, which results in precipitation of particles in the liquid. The particles contain Zr, Nb, and O and join together to form either the equiaxed or elongated grains visible in the glassy phase of the quenched specimens (e.g., Figure 3). As exposure time increases, B_2O_3 evaporation continues and the liquid phase concentrates in pools that are separated by regions of crystalline oxide. As the glass recedes, it exposes the underlying porous oxide scale. Previous studies have shown that the addition of W to ZrB_2 leads to liquid phase sintering of the porous ZrO_2 scale, which improved the oxidation resistance by decreasing oxygen

transport through the scale. In contrast, Nb_2O_5 and ZrO_2 form a solid Zr-Nb-O compound at the oxidation temperature, namely $Nb_2Zr_6O_{17}$, so no liquid phase sintering of ZrO_2 occurred. However, dissolution of Nb_2O_5 into the B_2O_3 liquid phase increased the stability of the liquid phase compared to the nominally pure B_2O_3 that forms when ZrB_2 is oxidized. The improved stability of the glassy layer leads to improved oxidation behavior because the external layer and glassy phase trapped among the particles that make up the porous oxide layer acts as a barrier to the transport of oxygen. Therefore, the addition of Nb to ZrB_2 increased the oxidation resistance, but only as long as the Nb-containing B_2O_3 phase was present.

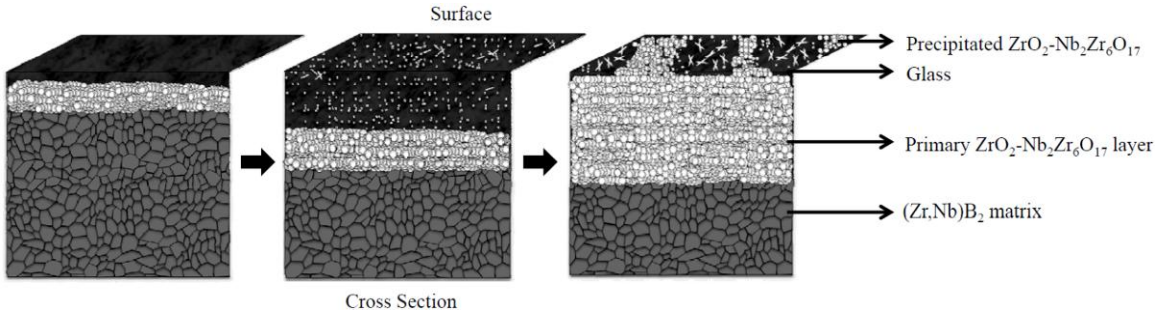

Figure 9. Model of the evolution of the oxide structure of $(Zr,Nb)B_2$.

1.4. Conclusion

The oxidation behavior of $(Zr,Nb)B_2$ ceramics was studied. At 1500 °C, exposure to air resulted in the formation of a two-layer oxide scale structure on $(Zr,Nb)B_2$. The two layers were: (1) an outer layer of a glassy phase containing B_2O_3 with Nb and Zr dissolved in it; and (2) a porous oxide layer composed of oxide particles containing Zr and Nb. Small spherical particles, presumably a ZrO_2 containing dissolved Nb, grew in the glassy phase with increasing exposure time. Some of the particles were spherical

while others were elongated. As the B_2O_3 evaporated, the particles became concentrated and were eventually incorporated into the newly exposed porous oxide layer, which contained both ZrO_2 and $Nb_2Zr_6O_7$. As the glass receded, the small precipitated particles joined the porous oxide layer that was present under the glassy layer. Because of high melting point of $Nb_2Zr_6O_7$ that was formed in the porous oxide layer, liquid phase sintering was not active as has been reported for W-containing ZrB_2. However, dissolution of Nb into the B_2O_3 liquid phase increased the stability of the protective liquid layer by reducing the volatility of B_2O_3 from the liquid phase. Hence, $(Zr,Nb)B_2$ showed improved oxidation resistance compared with pure ZrB_2.

Acknowledgment

This work was supported as part of the National Hypersonic Science Center for Materials and Structures (Grant FA9550-09-1-0477) with Dr. Ali Sayir (AFOSR) and Dr. Anthony Calomino (NASA) as program managers. The authors wish to thank project principal investigator Dr. David Marshall of Teledyne Scientific and Imaging for his support and guidance.

REFERENCES

1. F. Monteverde, R. Savino, M. D. S. Fumo, and A. Di Maso, "Plasma Wind Tunnel Testing of Ultra-High Temperature ZrB_2–SiC Composites under Hypersonic Re-entry Conditions," *Journal of the European Ceramic Society,* 30[11] 2313-21 (2010).
2. S. Q. Guo, "Densification of ZrB_2-Based Composites and Their Mechanical and Physical Properties: A Review," *Journal of the European Ceramic Society,* 29[6] 995-1011 (2009).
3. A. Rezaie, W. G. Fahrenholtz, and G. E. Hilmas, "Evolution of Structure during the Oxidation of Zirconium Diboride-Silicon Carbide in Air up to 1500°C," *Journal of the European Ceramic Society,* 27[6] 2495-501 (2007).
4. T. A. Parthasarathy, R. A. Rapp, M. Opeka, and R. J. Kerans, "Effects of Phase Change and Oxygen Permeability in Oxide Scales on Oxidation Kinetics of ZrB_2 and HfB_2," *Journal of the American Ceramic Society,* 92[5] 1079-86 (2009).
5. A. Rezaie, W. G. Fahrenholtz, and G. E. Hilmas, "Oxidation of Zirconium Diboride-Silicon Carbide at 1500°C in a Low Partial Pressure of Oxygen," *Journal of the American Ceramic Society,* 89[10] 3240-45 (2006).
6. C. M. Carney, P. Mogilvesky, and T. A. Parthasarathy, "Oxidation Behavior of Zirconium Diboride Silicon Carbide Produced by the Spark Plasma Sintering Method," *Journal of the American Ceramic Society,* 92[9] 2046-52 (2009).
7. W. M. Guo and G. J. Zhang, "Oxidation Resistance and Strength Retention of ZrB_2-SiC Ceramics," *Journal of the European Ceramic Society,* 30[11] 2387-95 (2010).
8. F. Monteverde, R. Savino, and M. D. S. Fumo, "Dynamic Oxidation of Ultra-high Temperature ZrB_2-SiC under High Enthalpy Supersonic Flows," *Corrosion Science,* 53[3] 922-29 (2011).
9. X. Zhang, L. Xu, S. Du, W. Han, and J. Han, "Preoxidation and Crack-Healing Behavior of ZrB_2-SiC Ceramic Composite," *Journal of the American Ceramic Society,* 91[12] 4068-73 (2008).
10. S. N. Karlsdottir, J. W. Halloran, and C. E. Henderson, "Convection Patterns in Liquid Oxide Films on ZrB_2-SiC Composites Oxidized at a High Temperature," *Journal of the American Ceramic Society,* 90[9] 2863-67 (2007).
11. I. Akin, F. Cinar Sahin, O. Yucel, and G. Goller, "Oxidation Behavior of Zirconium Diboride-Silicon Carbide Composites," pp. 105-11. in 34th International Conference on Advanced Ceramics and Composites*,* Vol. 31. Daytona Beach, FL, 2010.
12. S. N. Karlsdottir and J. W. Halloran, "Oxidation of ZrB_2-SiC: Influence of SiC Content on Solid and Liquid Oxide Phase Formation," *Journal of the American Ceramic Society,* 92[2] 481-86 (2009).
13. M. Mallik, K. K. Ray, and R. Mitra, "Oxidation Behavior of Hot Pressed ZrB_2-SiC and HfB_2-SiC Composites," *Journal of the European Ceramic Society,* 31[1-2] 199-215 (2011).
14. S. Guo, T. Mizuguchi, M. Ikegami, and Y. Kagawa, "Oxidation Behavior of ZrB_2-$MoSi_2$-SiC Composites in Air at 1500°C," *Ceramics International,* 37[2] 585-91 (2011).

15. A. L. Chamberlain, W. G. Fahrenholtz, G. E. Hilmas, and D. T. Ellerby, "Characterization of Zirconium Diboride for Thermal Protection Systems," pp. 493-96. in 8th Conference and Exhibition of the European Ceramic Society, Vol. 264-268. Istanbul, Turkey, 2004.
16. D. Sciti, M. Brach, and A. Bellosi, "Oxidation Behavior of a Pressureless Sintered ZrB_2–$MoSi_2$ Ceramic Composite," *Journal of Materials Research,* 20[4] 922-30 (2005).
17. I. G. Talmy, J. A. Zaykoski, and M. M. Opeka, "High-Temperature Chemistry and Oxidation of ZrB_2 Ceramics Containing SiC, Si_3N_4, Ta_5Si_3, and $TaSi_2$," *Journal of the American Ceramic Society,* 91[7] 2250-57 (2008).
18. D. Sciti, V. Medri, and L. Silvestroni, "Oxidation Behaviour of HfB_2-15 vol.% $TaSi_2$ at Low, Intermediate and High Temperatures," *Scripta Materialia,* 63[6] 601-04 (2010).
19. E. J. Opila and M. C. Halbig, "Oxidation of ZrB_2-SiC,″ pp. 221-28 in 25th Annual Conference on Composites, Advanced Ceramics, Materials and Structures. Vol. 22. (2001).
20. M. M. Opeka, I. G. Talmy, and J. A. Zaykoski, "Oxidation-Based Materials Selection for 2000°C + Hypersonic Aerosurfaces: Theoretical Considerations and Historical Experience," *Journal of Materials Science,* 39[19] 5887-904 (2004).
21. E. J. Opila and M. C. Halbig, "Oxidation of ZrB_2-Based Ultra-High Temperature Ceramics," *Ceramic Engineering and Science Proceedings,* 22[3] 221-28 (2001).
22. S. R. Levine and E. J. Opila, "Tantalum Addition to Zirconium Diboride for Improved Oxidation Resistance." in. NASA/TM-2003-212483, 2003.
23. F. Peng, Y. Berta, and R. F. Speyer, "Effect of SiC, TaB_2 and $TaSi_2$ Additives on the Isothermal Oxidation Resistance of Fully Dense Zirconium Diboride," *Journal of Materials Science,* 24 [5] 1855-67. (2009).
24. I. G. Talmy, J. A. Zaykoski, M. M. Opeka, and S. Dallek, "Oxidation of ZrB_2 Ceramics Modified with SiC and Group IV-VI Transition Metal Diborides," *Electrochemical Society Proceedings,* 12 144-58 (2001).
25. P. Hu, X. H. Zhang, J. C. Han, X. G. Luo, and S. Y. Du, "Effect of Various Additives on the Oxidation Behavior of ZrB_2-Based Ultra-High-Temperature Ceramics at 1800°C," *Journal of the American Ceramic Society,* 93[2] 345-49 (2010).
26. X. H. Zhang, P. Hu, J. C. Han, L. Xu, and S. H. Meng, "The Addition of Lanthanum Hexaboride to Zirconium Diboride for Improved Oxidation Resistance," *Scripta Materialia,* 57[11] 1036-39 (2007).
27. S. C. Zhang, G. E. Hilmas, and W. G. Fahrenholtz, "Improved Oxidation Resistance of Zirconium Diboride by Tungsten Carbide Additions," *Journal of the American Ceramic Society,* 91[11] 3530-35 (2008).
28. S. C. Zhang, G. E. Hilmas, and W. G. Fahrenholtz, "Oxidation of Zirconium Diboride with Tungsten Carbide Additions," *Journal of the American Ceramic Society,* 94[4] 1198-205 (2011).
29. F. Wang and D. O. Northwood, "Oxides Formed Between ZrO_2 and Nb_2O_5," *Journal of Materials Science,* 30[16] 4003-08 (1995).
30. R. S. Roth and L. W. Coughanour, "Phase Equilibrium Relations in the Systems Titania-Niobia and Zirconia-Niobia," *Journal of Research of the National Bureau of Standards,* 55 209-13 (1955).

31. S. N. Karlsdottir, J. W. Halloran, and A. N. Grundy, "Zirconia Transport by Liquid Convection during Oxidation of Zirconium Diboride-Silicon Carbide," *Journal of the American Ceramic Society,* 91[1] 272-77 (2008).
32. E. M. Levin, "Phase Equilibria in the System Niobium Pentoxide-Boric Acid," *Journal of Research of the National Bureau of Standards,* 70A[1] 11-16 (1966).
33. W. G. Fahrenholtz, "The ZrB_2 Volatility Diagram," *Journal of the American Ceramic Society,* 88[12] 3509-12 (2005).
34. A. K. Kuriakose and J. L. Margrave, "The Oxidation Kinetics of Zirconium Diboride and Zirconium Carbide at High Temperatures," *Journal of The Electrochemical Society,* 111[7] 827-31 (1964).

2. Effects of Temperature and the Incorporation of W on the Oxidation of ZrB_2 Ceramics

M. Kazemzadeh Dehdashti, W.G. Fahrenholtz, G.E. Hilmas

Department of Materials Science and Engineering, Missouri University of Science and Technology, Rolla, MO 65401, United States

Abstract

The effects of tungsten additions and temperature on the oxidation behavior of nominally pure ZrB_2 and ZrB_2 containing 4, 6 or 8 mol% of W after oxidation at temperatures ranging from 800 to 1600°C were investigated. For pure ZrB_2, the protective liquid/glassy layer covering the surface as a result of oxidation was evaporated above 1500°C. For $(Zr,W)B_2$ specimens, the liquid/glassy layer was present after exposure up to 1600°C. The higher stability of the liquid/glassy phase in the W-containing compositions was attributed to the presence of tungsten in the liquid/glassy phase, resulting in improved oxidation resistance for ZrB_2 samples containing W.

Key Words: Zirconium Diboride; Tungsten; Oxidation.

2.1. Introduction

Zirconium diboride has advantages over other candidates for hypersonic aerospace applications due to its high melting point (~3250 °C) and low theoretical density (6.09 g/cm^3) combined with a thermal conductivity as high as 100 W/m•K at room temperature [1, 2]. Ultrahigh-temperature stability and high thermal conductivity provide ZrB_2 with the ability to transfer heat away from the hottest areas of structures and redistribute it to cooler areas, which makes it attractive for sharp leading edges for hypersonic aerospace vehicles [3].

The use of ZrB_2-based ceramics for applications requiring elevated temperatures in air is restricted by its oxidation behavior. Assuming stoichiometric oxidation, exposure of ZrB_2 to air results in the formation of B_2O_3 and ZrO_2, which leads to measurable mass gain (Eq. 1) [4].

$$ZrB_{2\,(s)} + 5/2\ O_{2\,(g)} \rightarrow ZrO_{2\,(s)} + B_2O_{3\,(l)} \quad (1)$$

The oxidation reaction is favorable at all temperatures with $\Delta G°_{rxn} = -1977 + 0.361T$ (kJ) [5]. Previous studies have divided the oxidation behavior of ZrB_2 into three different temperature regimes, although the transition temperatures depend on parameters such as heating rate, gas flow rate, oxygen activity, etc. The low temperature regime occurs below about 1100 °C. At these temperatures, ZrO_2 and B_2O_3 form a continuous oxide layer that provides passive oxidation protection [6-9]. Analysis concluded that the transport of oxygen through B_2O_3 was the rate limiting step for oxidation in this regime, which results in parabolic (diffusion-limited growth) kinetics for mass gain and changes

in the oxide layer thickness [9, 10]. Between ~1100 °C and ~1400 °C, paralinear kinetics have been observed. In this intermediate temperature regime, the weight change reflects a combination of mass gain from formation of ZrO_2 and B_2O_3, and mass loss due to the evaporation of B_2O_3 [6, 10, 11]. Specimens continue to gain mass as the mass of ZrO_2 plus retained B_2O_3 is greater than the mass of diboride reacted plus the mass of volatilized B_2O_3. As B_2O_3 evaporates, a porous ZrO_2 layer is left behind. In the highest temperature regime, ~1500 °C and above, the B_2O_3 is no longer protective and mass gain kinetics become linear due to the non-protective nature of the ZrO_2 layer [9]. Parthasarathy *et al.* [12, 13] presented a physical model to predict the oxidation behavior of refractory diborides in these three different temperature regimes. The model assumed that diffusion of dissolved oxygen through boria, in capillaries between nearly columnar blocks of the ZrO_2 was the rate-limiting step when condensed boria was present. After evaporation of boria, the oxidation rate was limited by Knudsen diffusion of molecular oxygen through the capillaries. The model agreed with experimental results in predicting weight change, recession, oxide scale thickness and the temperature dependence of the parabolic rate constant for ZrB_2.

Addition of Si-containing compounds such as SiC [3, 4, 14-23], $MoSi_2$ [24-26], or $TaSi_2$ [27, 28] is the conventional approach to improving the oxidation resistance of diboride ceramics. Improved oxidation resistance is obtained as a result of formation of a borosilicate glassy layer on the surface of the diboride with higher stability compared to the borate glassy layer which forms on nominally pure ZrB_2 [4, 23]. However, SiC or other Si-containing additives may not be the best choice due to problems, such as rupture of the protective glassy layer as a result of $SiO_{(g)}$ formation [29], or formation of a SiC-depleted

layer. Either of these issues has been shown to result in loss of protection at temperatures above 1600 °C [30, 31].

Transition metal additives can also improve the oxidation behavior of diborides. Led by Talmy *et al.*, several groups have investigated transition metal additions including Cr-, Ti-, Nb-, V-, and Ta-borides, to improve the oxidation resistance of ZrB_2-based composites [31-35]. In addition, Zhang *et al.* [11, 36] reported that WC additions improved the oxidation resistance of ZrB_2 ceramics due to the formation of WO_3 in the oxide scale, which resulted in liquid phase sintering of ZrO_2 and consequently increased the relative density of the scale. The purpose of the present paper was to study the effect of the amount of W added on the oxidation behavior of ZrB_2 at temperatures from 800 to 1600 °C. The initial results indicated the effectiveness of W on increasing the stability of the protective liquid/glassy B_2O_3 scale. Hence, B_2O_3 glasses with 0, 4, 6, or 8 mol% WO_3 were also prepared to investigate the effect of WO_3 on weight loss of B_2O_3 glasses. This study was intended as an initial investigation of oxidation behavior in a controlled furnace oxidation environment with the goal of gaining insight into fundamental oxidation mechanisms prior to testing in more complex environments that are representative of hypersonic flight conditions.

2.2. Experimental procedure

Specimens for this study were prepared from high purity (>99%) ZrB_2 powder (~2 μm, Grade B, H.C. Starck, Newton, MA). 2 wt% B_4C (~0.8 μm, Grade HS, H.C Starck) was added to all batches to remove the oxide impurities from the powder particle surfaces and enhance densification. For some batches, 4, 6, or 8 mol% tungsten was added in form of W powder (~3 μm, Alfa Aesar, Ward Hill, MA) with a reported purity

of 99.9%. Hereafter, ZrB_2 ceramics containing only B_4C are referred to as "nominally pure ZrB_2" while ZrB_2 with B_4C and W additions are referred to as $(Zr,W)B_2$.

The powders were mixed by ball milling in butan-2-one (methyl ethyl ketone) with ZrO_2 media for 24 hrs. Measurement of the mass of media before and after milling indicated that the amount of zirconia contamination added to the batches was less than 1 wt% based on the mass of ZrB_2 powder. After drying and sieving (-80 mesh), the powders were densified by hot pressing (Model HP-3060, Thermal Technology, Santa Rosa, CA) at 2100 °C for 45 min at a pressure of 32 MPa. For oxidation studies and initial characterization of the as processed microstructures, bars with dimensions of 10 mm by 4 mm by 4 mm were diced from the produced billets. Prior to testing, bars were finished by polishing on all sides using successively finer diamond abrasives with a final polishing step using a 15 μm diamond slurry.

The microstructures of the polished surfaces of as processed $(Zr,W)B_2$ and ZrB_2 were studied using images obtained by scanning electron microscopy (SEM; S-4700, Hitachi, Japan). Image analysis software (ImageJ, U. S. National Institutes of Health, Bethesda, MD) was used to calculate the amount of B_4C remaining after densification. The Archimedes technique, with water as the immersing medium, was used to measure the bulk density of the hot pressed billets.

Oxidation studies were performed in a $MoSi_2$ resistance-heated horizontal tube furnace (Model 0000543 Rapid Temperature Furnace, CM Inc., Bloomfield, NJ) equipped with a high-purity alumina tube with a diameter of 6.35 cm. Specimens were placed on a ridged zirconia setter that was on an alumina D-tube in the center of an alumina tube that was sealed with gas-tight end caps. Specimens were heated at ~5

°C/min to temperatures ranging from 800 to 1600 °C in flowing air with a flow rate of 0.2 cm/s (linear flow rate was calculated from the volumetric flow rate and the diameter of the tube). Specimens were air quenched to room temperature by removing them from the furnace after the desired oxidation time to minimize changes such as further oxidation that may occur during cooling.

The weight and surface area of the specimens were measured before and after oxidation to calculate the weight gain as a result of oxidation. The fracture surfaces observed in the SEM were used to study the microstructure and calculate the thicknesses of the resulting oxide layers. In addition, chemical compositions of the scales were analyzed using energy dispersive spectroscopy (EDS; EDAX, Mahwah, NJ).

Borate glasses were prepared from high purity (≥99.5%) boric acid powder (H_3BO_3, ACS reagent, Sigma-Aldrich, Saint Louis, MO) and WO_3 (99.99%, metal basis, Alfa Aesar, Ward Hill, MA). The powders were mixed using dry ball milling followed by grinding with a mortar and pestle. The mixtures were calcined at 500 °C in a platinum crucible until no bubbling was observed. The glasses were then melted at 900 °C for 1 hour followed by quenching onto copper plates. After grinding and sieving (-80 mesh), thermogravimetric analysis (Netzsch Simultaneous TGA/DTA, Selb, Germany) was performed at temperatures up to 1500 °C using a heating rate of 10 °C/min and a flowing nitrogen atmosphere. Before initiating the analysis, the samples were held for 1 hour at 170 °C to eliminate any hydration of the B_2O_3 that may have occurred during preparation or storage.

2.3. Results and discussion

All of the compositions reached nearly full density during hot pressing. The measured bulk densities of the specimens are shown in Table 1. To determine the theoretical densities, the area fraction of B_4C remaining in each composition after densification was estimated by analyzing SEM images and assumed to be equivalent to the B_4C volume fraction. Using true densities of 6.09 g/cm^3 for ZrB_2, 19.25 g/cm^3 for W, and 2.52 g/cm^3 for B_4C, a volumetric rule of mixtures was used to calculate the theoretical density of nominally pure ZrB_2 and $(Zr,W)B_2$ specimens. Combined with the bulk density measurements, all of the specimens had relative densities that were >98%. In addition, the Archimedes' measurements indicated that open porosity was not significant in any of the compositions. Therefore, porosity should not have an effect on the oxidation behavior.

Table 1. Area fraction of B_4C remaining after densification and density data for nominally pure ZrB_2 and $(Zr,W)B_2$ specimens.

Designation	B_4C Area Fraction (%)	Theoretical Density (g/cm^3)	Bulk Density (g/cm^3)	Relative Density (%)
ZrB_2	4.8	5.92	5.87	99.2
ZrB_2+4mol%W	1.6	6.31	6.08	98.7
ZrB_2+6mol%W	1.1	6.47	6.22	98.7
ZrB_2+8mol%W	0.8	6.62	6.41	99.4

Oxidation of $(Zr,W)B_2$ should produce ZrO_2, B_2O_3, and WO_3, assuming that oxidation proceeds stoichiometrically (Eq. 2), although oxidation is minimal below ~800° C. Individually, the stable phases of these compounds in this temperature range are solid ZrO_2 (monoclinic below 1170°C and tetragonal above), liquid B_2O_3 (melting temperature ~450°C), and WO_3. When combined, the scale formed on the surface of $(Zr,W)B_2$ specimens after oxidation at elevated temperature and cooling to room temperature consists of crystalline oxides containing Zr, and/or W, plus an amorphous phase that is mainly B_2O_3. According to the ZrO_2-WO_3 phase diagram [37], the presence of small (less than 5 mol%) concentrations of W should lead to the formation of W-doped ZrO_2. Higher amounts of W result in formation of ZrO_2 and WO_3 (up to 1105 °C) or ZrO_2 and ZrW_2O_8 (from 1105 to 1257 °C).

$$(Zr_{1-x}W_x)B_{2\,(s)} + (x+5)\,O_{2\,(g)} \rightarrow (1-x)\,ZrO_{2\,(s)} + x\,WO_{3\,(s)} + B_2O_{3\,(l)} \qquad (2)$$

Figure 1 and Figure 2 show cross sectional SEM images of the oxide scales of nominally pure ZrB_2 and ZrB_2 containing 4, 6, or 8 mol% W after oxidation at 900 and 1300 °C, respectively. The oxide scales on these specimens consisted of two distinct layers: (1) a dense outer glassy layer, and (2) a porous inner layer. Due to low sensitivity of EDS to light elements, quantification of the boron content in the glassy phase was not possible. However, EDS results indicated that the matrix of the glassy phase contained O and W along with a small amount of Zr, presumably all dissolved in B_2O_3. According to the ZrO_2-B_2O_3 [38] and WO_3-B_2O_3 [39] phase diagrams, approximately 10 mol% WO_3 can dissolve into B_2O_3 at 900 °C, while ZrO_2 is not soluble in pure B_2O_3 at that temperature.

At 1300°C, the solubility of ZrO_2 and WO_3 in B_2O_3 increases to 2 and 45 mol%, respectively. Immiscibility of ZrO_2 and B_2O_3 along with the large volume expansion (~300% based on density calculations) associated with oxidation of ZrB_2 to ZrO_2 and B_2O_3 are believed to result in the formation of two-layer scales [4]. After oxidation at 1600 °C (Figure 3), the scales formed on all of the specimens consisted of a porous layer with only some residual glassy phase observed between the oxide particles.

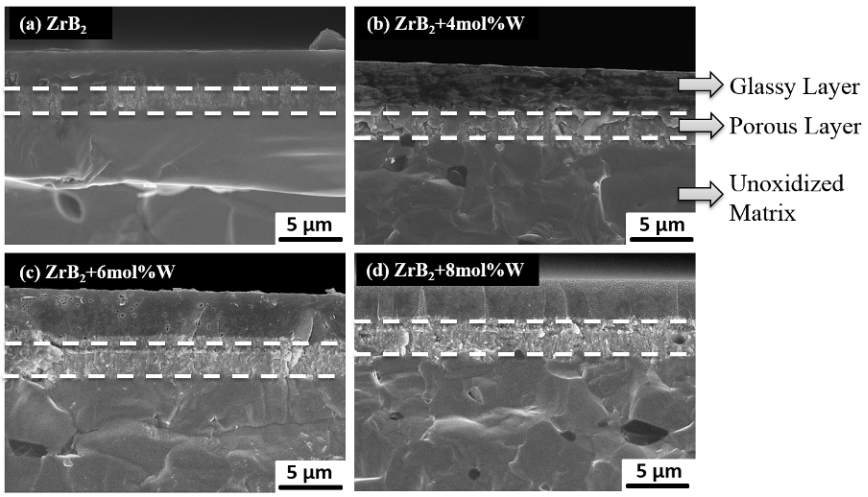

Figure 1. SEM images of the fracture surfaces of nominally pure ZrB_2 (a) and ZrB_2 containing 4 mol% W (b), 6 mol% W (c) , or 8 mol% W (d) after oxidation at 900°C for 0 hours. Note that the images in this figure have a different magnification than those in Figure 2 and 3.

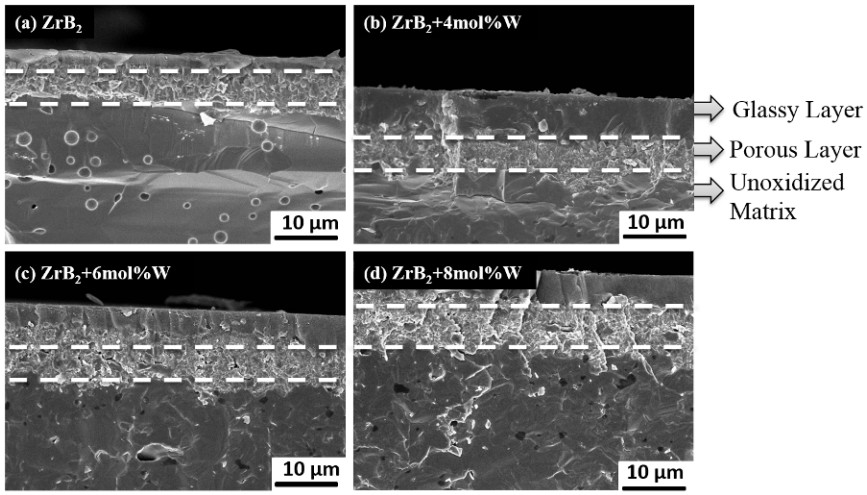

Figure 2. SEM images of the fracture surfaces of nominally pure ZrB_2 (a) and ZrB_2 containing 4 mol% W (b), 6 mol% W (c) , or 8 mol% W (d) after oxidation at 1300°C for 0 hours.

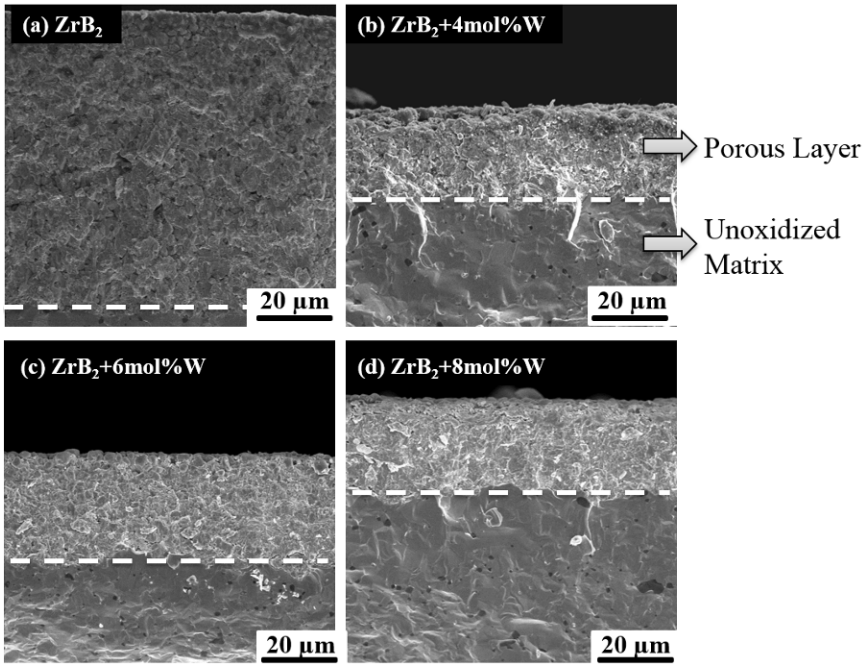

Figure 3. SEM images of the fracture surfaces of nominally pure ZrB_2 (a) and ZrB_2 containing 4 mol% W (b), 6 mol% W (c) , or 8 mol% W (d) after oxidation at 1600 °C for 0 hours.

The thicknesses of the glassy and porous layers after oxidation of nominally pure ZrB_2 and $(Zr,W)B_2$ containing 4, 6, an 8 mol% W at temperatures from 800°C to 1600°C are summarized in Figure 4. Between 800 and 1000 °C, the thickness of the glassy layers increased from ~3 to ~5 μm. The differences in the thickness of the glassy layers for nominally pure ZrB_2 and $(Zr,W)B_2$ specimens were less than 1 μm in this temperature range. Hence, the addition of W did not have a significant effect on the thickness of the glassy layer after oxidation at temperatures below 1000 °C. At temperatures ranging from 1000 to 1200 °C, the increase in the thickness of the glassy layers was less for nominally pure ZrB_2 than $(Zr,W)B_2$ specimens, presumably due to lower evaporation of B_2O_3 from the $(Zr,W)B_2$ compositions. The highest thickness of the glassy layer for nominally pure ZrB_2 was 5 μm at 1200 °C, while the glassy layer was 8 μm thick for $(Zr,W)B_2$ containing 4 mol% W, 11 μm for 6 mol% W, and 7 μm for 8 mol% W at 1300 °C. Even if it has no other effects, the dissolution of WO_3 into B_2O_3 at elevated temperatures should lower the activity of B_2O_3 and, consequently, lower the evaporation of B_2O_3 from the liquid/glassy phase. The thickness of the glassy layers decreased after oxidation at temperatures above 1200 °C or 1300 °C for nominally pure ZrB_2 and $(Zr,W)B_2$ specimens, respectively. However, the differences between the thicknesses of the glassy layers for nominally pure ZrB_2 and $(Zr,W)B_2$ specimens were still significant (up to 14 μm) with W additions promoting the formation of thicker glassy layers compared to nominally pure ZrB_2. No glassy layer was observed on the surface of nominally pure ZrB_2 at 1500 °C or $(Zr,W)B_2$ specimens at 1600 °C.

After oxidation at temperatures up to 1400°C, the thicknesses of the porous layers were almost the same for all of the compositions. Oxidation at 1600 °C produced a

significantly thicker porous oxide layer on nominally pure ZrB_2 (~85 μm) compared to the specimens containing W (~30 μm). No considerable differences were observed between the porous layer thicknesses for specimens with different amounts of W. Based on these measurements, the addition of W shifted the temperature at which the protective liquid/glassy layer evaporated and resulted in higher oxidation resistance of ZrB_2 specimens with W additions compared to nominally pure ZrB_2.

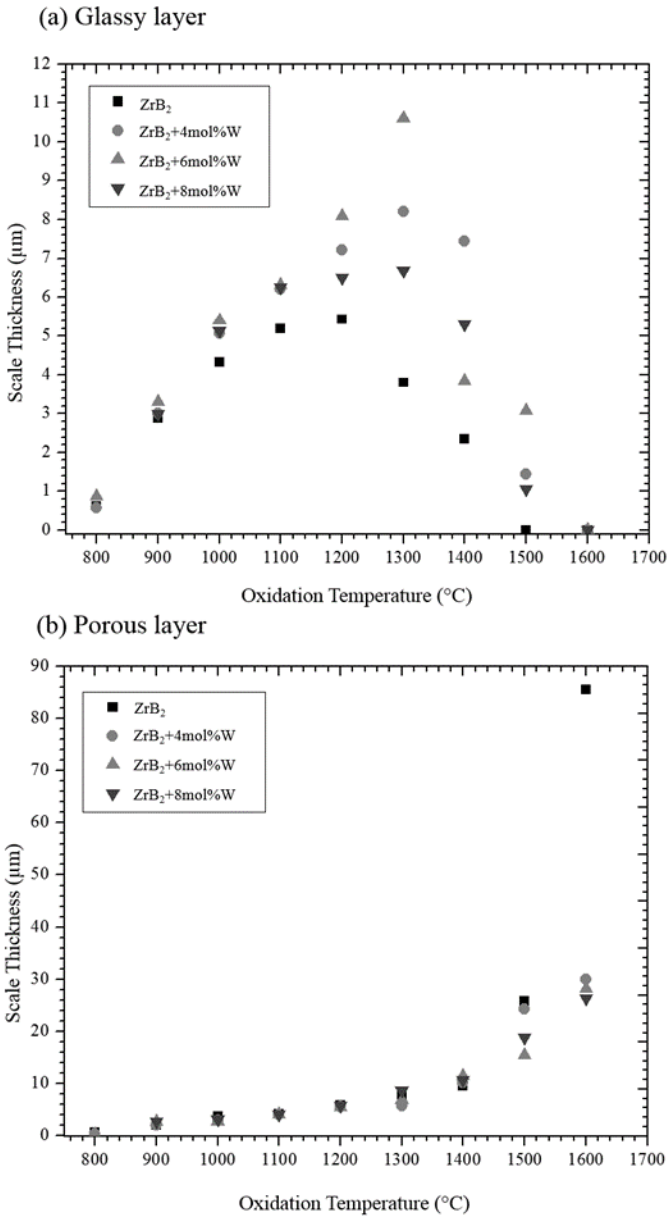

Figure 4. (a) Glassy layer and (b) porous layer scale thicknesses as a function of oxidation temperature comparing nominally pure ZrB_2 to ZrB_2 containing 4, 6, or 8 mol% W after oxidation for 0 hours. Note the difference in the y-axis scale between the two plots.

To compare the evaporation of B_2O_3 from the ZrB_2 and $(Zr,W)B_2$ specimens, Eq. 1 was used to predict the thickness of the glassy scales. For this calculation, oxidation was assumed to be stoichiometric so that equal molar amounts of ZrO_2 and B_2O_3 were formed. Building on that assumption, the glassy scale thickness was estimated from the thickness of the porous oxide scale assuming a relative density of 98% up to 1200 °C (i.e., below the monoclinic to tetragonal phase transition temperature) and 93% at higher temperatures. The results of the predictions are shown in Figure 5. Next, the amount of the glassy scale that evaporated during oxidation was estimated by subtracting the measured thickness from the estimated thickness (Figure 6). Based on this analysis, the onset of evaporation increased from ~900 °C for nominally pure ZrB_2 to ~1300 °C for ZrB_2+4mol%W. The evaporation of B_2O_3 from ZrB_2+4mol%W was significantly lower than for ZrB_2 for temperatures up to ~1500 °C. Hence, the presence of W in ZrB_2 suppressed evaporation of the glassy scale at temperatures below 1500 °C.

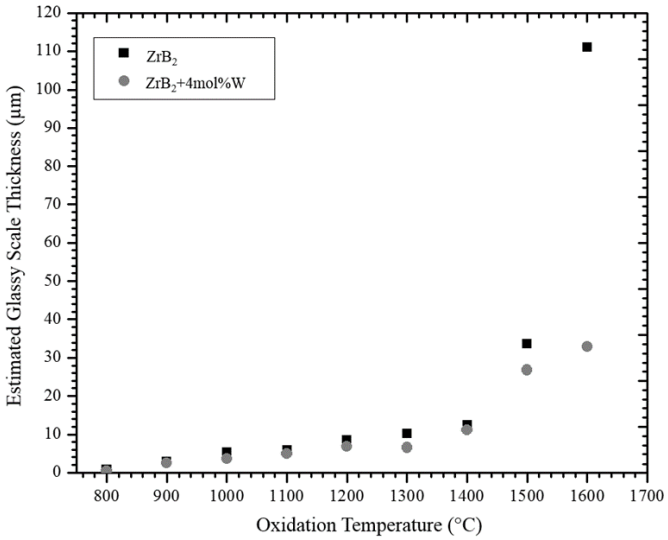

Figure 5. Predicted thicknesses of the glassy scales without evaporation estimated from the thickness of the porous oxide scales, comparing nominally pure ZrB_2 to ZrB_2 containing 4 mol% W after oxidation for 0 hours.

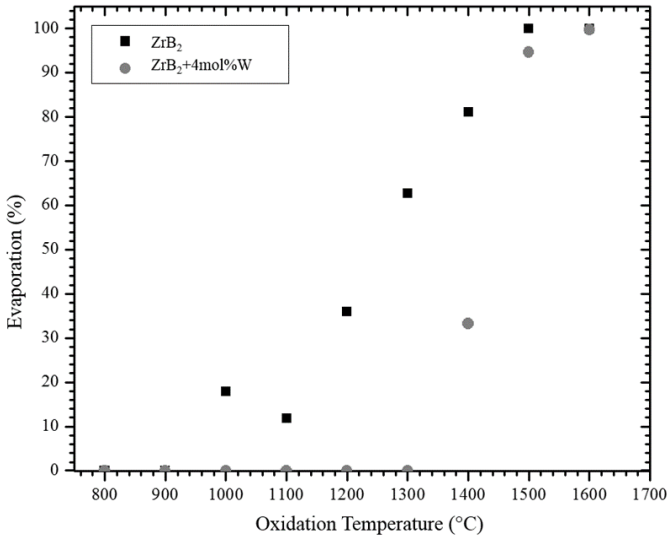

Figure 6. The percentage of the glassy scale lost to evaporation estimated by subtracting the measured thickness values for the glassy scales from the estimated thickness without evaporation, comparing nominally pure ZrB_2 to ZrB_2 containing 4 mol% W after oxidation for 0 hours.

Figure 7 shows the weight gain for nominally pure ZrB_2 and $(Zr,W)B_2$ specimens containing 4, 6, or 8 mol% W after oxidation from 800 to 1600 °C in flowing air. The W content did not have a significant effect on the weight gain of ZrB_2 after oxidation at temperatures below 1000 °C. The weight gains were ~1 mg/cm^2 for ZrB_2 and $(Zr,W)B_2$ specimens at 1000 °C. The weight gains for $(Zr,W)B_2$ specimens were nearly constant between 1000 °C and 1200 °C, while for nominally pure ZrB_2 weight gain increased to ~1.5 mg/cm^2 at 1100 °C and then decreased to ~1 mg/cm^2 at 1300 °C. At 1500 °C, the weight gain of $(Zr,W)B_2$ specimens increased to ~4 mg/cm^2, while it was ~3 mg/cm^2 for nominally pure ZrB_2. The weight gain for $(Zr,W)B_2$ decreased significantly from ~4 mg/cm^2 at 1500 °C to ~2 mg/cm^2 at 1600 °C, while the weight gain of nominally pure ZrB_2 increased from ~3 mg/cm^2 at 1500 °C to ~5 mg/cm^2 at 1600 °C. The measured weight gain values are representative of both the weight of oxygen added to the system due to formation of ZrO_2, B_2O_3, and WO_3 for $(Zr,W)B_2$ and weight loss due to evaporation of B_2O_3 and probably WO_3 for $(Zr,W)B_2$ specimens. The increase in weight gain from 800 to 1000 °C is the result of an increase in oxidation along with insignificant evaporation of B_2O_3. The constant weight gain for the $(Zr,W)B_2$ specimens from 1000 to 1200 °C indicates almost equal weights of oxygen added and B_2O_3 lost from the specimens. Between 1300 and 1500 °C, the evaporation of B_2O_3 from nominally pure ZrB_2 increases from ~65% to 100% of the glassy layer thickness, while it increases from 0% to 95% for $(Zr,W)B_2$ specimens (see Figure 6). On the other hand, the thickness values for the porous oxide layers (Figure 4) are almost the same over this range of temperatures. This results in higher weight gain for $(Zr,W)B_2$ specimens compared to nominally pure ZrB_2. At 1600 °C, the higher weight gain for nominally pure ZrB_2 is due

to its more rapid oxidation due to the nearly complete evaporation of B_2O_3. The thicknesses of the porous layers are lower for (Zr,W)B_2 specimens at 1600 °C, indicating less oxidation of W-containing compositions.

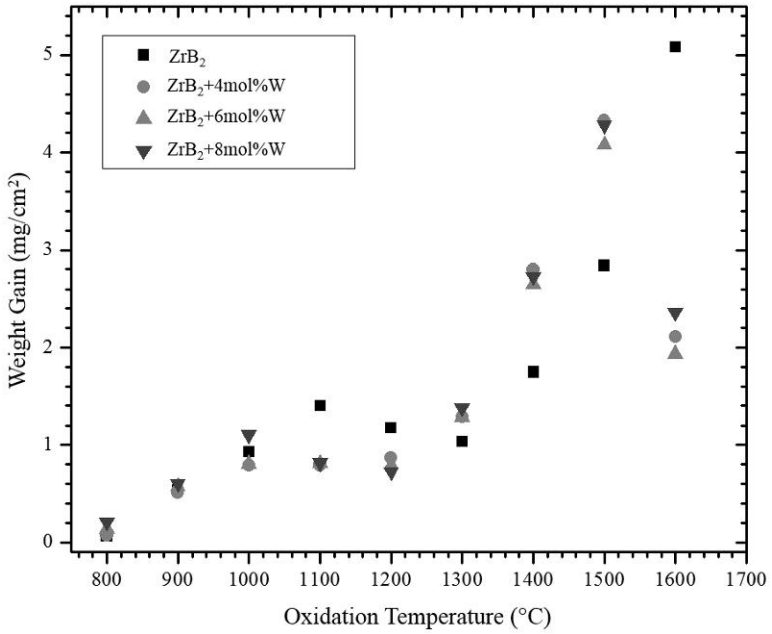

Figure 7. Weight gain as a function of oxidation temperature for nominally pure ZrB_2 and ZrB_2 containing 4, 6, or 8 mol% W after oxidation at 800-1600°C for 0 hours in flowing air.

According to the WO_3-B_2O_3 phase diagram [39], the presence of small concentrations (<10 mol%) of WO_3 with B_2O_3 results in the formation of a liquid phase above 800 °C. Dissolution of WO_3 into the liquid phase should decrease the activity of B_2O_3 and, consequently, reduce its vapor pressure and evaporation rate. Further, the presence of W in the glass may also affect the B coordination state in the B_2O_3 network, which could further decrease the vapor pressure of B_2O_3 for W-containing

compositions[40, 41]. To investigate the effect of WO_3 additions on evaporation of B_2O_3, thermogravimetric analysis (TGA) was performed on pure B_2O_3 and borate glasses containing 4, 6 and 8 mol% WO_3 at temperatures ranging from 25 to 1500 °C. The total weight loss curves as function of temperature are shown in Figure 8. To minimize the influence of different levels of hydration among the different compositions, all of the curves were normalized to the weight at 500 °C, which is above the decomposition temperature for boric acid, but below the temperature at which significant evaporation of B_2O_3 begins. The weight loss for pure B_2O_3 was less than about 0.5% between 500 and 1000 °C. Weight loss increased linearly from ~0.5% at 1000 °C to ~5% at 1400 °C, and showed a sharp increase above 1400 °C. In comparison, the B_2O_3-WO_3 glasses had weight losses of less than 0.6% up to 1300 °C. Above 1300°C, they showed a sharp increase in weight loss. The glasses with higher amounts of WO_3 showed higher weight losses between 1300 and 1500 °C, probably indicating the volatility of WO_3 in this temperature range. Interestingly, B_2O_3 containing 4 mol% WO_3 exhibited the lowest weight loss of any of the compositions. Based on these observations, the presence of WO_3 reduces the volatility of the borate glass up to about 1300 °C.

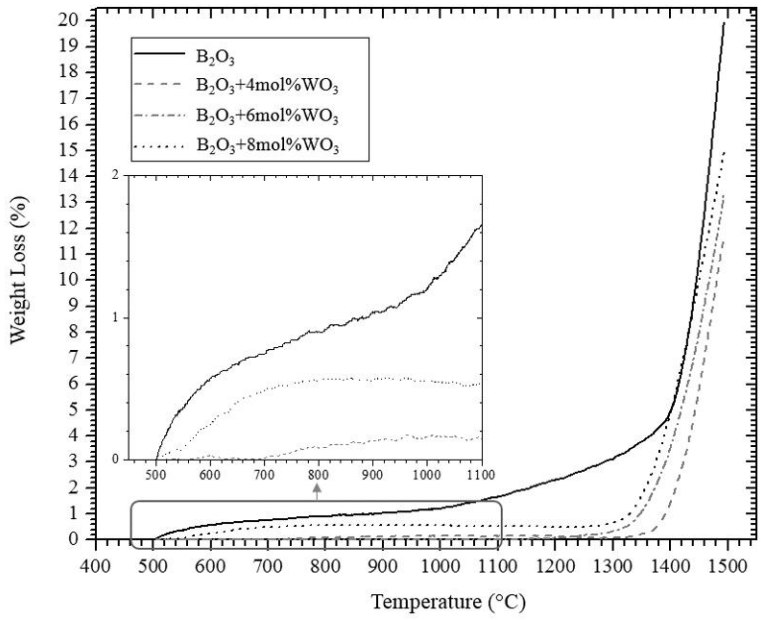

Figure 8. Weight loss as a function of temperature for B_2O_3 and borate glasses containing 4, 6 and 8 mol% WO_3 obtained by thermogravimetric analysis.

Combined with the scale thickness and mass change results, the TGA weight loss measurements reveal several similarities and differences between the oxidation behavior of nominally pure ZrB_2 and $(Zr,W)B_2$. In the low temperature regime, below about 1000 °C, no significant differences were observed. Both ZrB_2 and $(Zr,W)B_2$ have similar scale thickness and mass gain values. Above about 1000 °C, B_2O_3 begins to evaporate. As indicated by TGA weight loss, pure B_2O_3 becomes volatile at these temperatures, which leads to the observed decrease in the thickness of the outer glassy layer on ZrB_2 as shown in Figure 4. In contrast, TGA showed that W-containing B_2O_3 exhibited lower weight losses, with almost no loss of mass below 1300 °C. The presence of W in the outer glassy scale reduced its volatility, which resulted in thicker glassy layers on $(Zr,W)B_2$ up to ~1500 °C (Figure 4). The overall mass change (Figure 7) did not show any significant

differences between ZrB_2 and $(Zr,W)B_2$ up to ~1300 °C, despite the increased stability of the outer glassy layer for W-containing compositions. Between 1300 and 1500 °C, $(Zr,W)B_2$ compositions showed higher mass gains than ZrB_2 (Figure 7), indicating the higher stability of the outer glassy layer. Hence, one impact of W additions to ZrB_2 is to stabilize the outer glassy layer. Based on these results, as shown in Figure 9, the addition of W to ZrB_2 appears to extend the low temperature regime of oxidation behavior, where a layer of W-containing liquid B_2O_3 is stable on the surface of the oxidizing $(Zr,W)B_2$.

The thickness of the porous oxide layers show a sharp increase above 1400 °C due to the increased evaporation rate of B_2O_3 at these temperatures (Figure 8) that results in a lower thickness of the protective liquid/glassy layers. However, the difference between the porous scales on ZrB_2 and $(Zr,W)B_2$ specimens were not significant below 1500 °C. As shown by TGA weight loss curves, at 1500 °C, the weight loss of pure B_2O_3 (~20%) was significantly higher than B_2O_3-WO_3 melts (<15%). The increased stability of the protective liquid/glassy layers formed on the surface of $(Zr,W)B_2$ specimens, to higher temperatures compared to ZrB_2, resulted in significantly lower weight gain and scale thickness for $(Zr,W)B_2$ specimens compared to nominally pure ZrB_2 after oxidation between 1500 and 1600 °C. Above 1500 °C for nominally pure ZrB_2 and 1600 °C for $(Zr,W)B_2$ specimens, no protective glassy layer was present on the surface of the specimens and oxidation was more severe compared to earlier regimes. However, B_2O_3 continues to form at these temperatures and the pores in the porous oxide layers are filled with borate melt. In the highest temperature regime, where the pores are depleted of B_2O_3, oxidation behavior is controlled by the flow (i.e., Knudsen diffusion as described by Parthasarathy [12,13]) of molecular oxygen through the porous ZrO_2 scale.

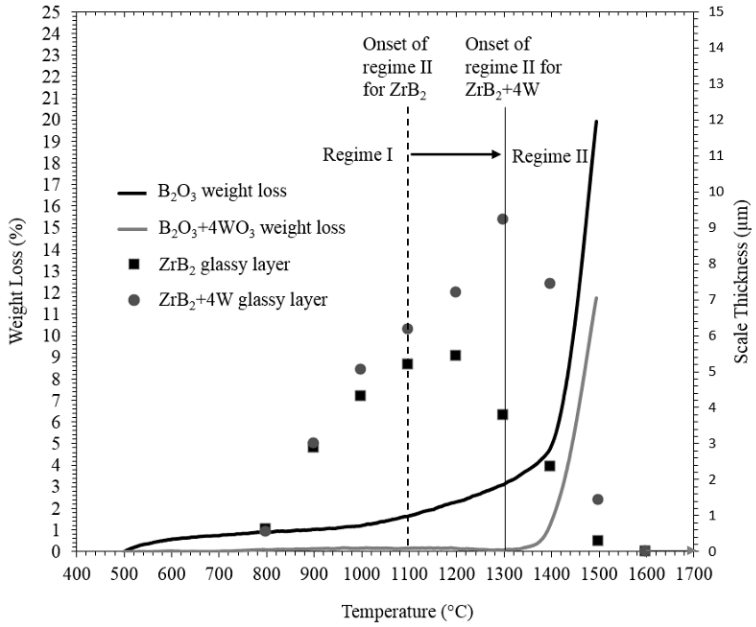

Figure 9. TGA results showing lower weight loss for B_2O_3 + 4 mol% WO_3 compared to B_2O_3 that results in lower glassy thicknesses for ZrB_2 + 4 mol% W compared to ZrB_2 after oxidation at 800-1600 °C for 0 hours. The onset of the second oxidation regime shifts toward higher temperatures for ZrB_2 + 4 mol% W.

Evaluating the reliability of the weight gain measurements versus the weight loss calculated from the TGA results, as a reference for the evaporation of B_2O_3 during oxidation, could be useful for future studies. The thickness of the glassy scales for ZrB_2 and ZrB_2+4mol%W were calculated using the porous scale thickness measurements with evaporation calculated from weight gain (Figure 7) and the TGA data (Figure 8). The results are shown in Figure 10. Again, the porosity of the porous scales were assumed to be 98% up to 1200 °C and 93% at higher temperatures. The weight losses obtained by TGA were multiplied by 6 to compensate for the differences between the air flow rates in the isothermal oxidation and TGA tests. The thickness values calculated from the TGA

results showed to be a good fit to the experimental results at most of the oxidation temperatures. The thickness values calculated from the weight gain results did not fit the experimental data. The calculated results indicate that weight loss obtained by TGA is more reliable than weight loss measurements made on bulk specimens that were oxidized and then cooled with respect to the evaporation of B_2O_3 during oxidation.

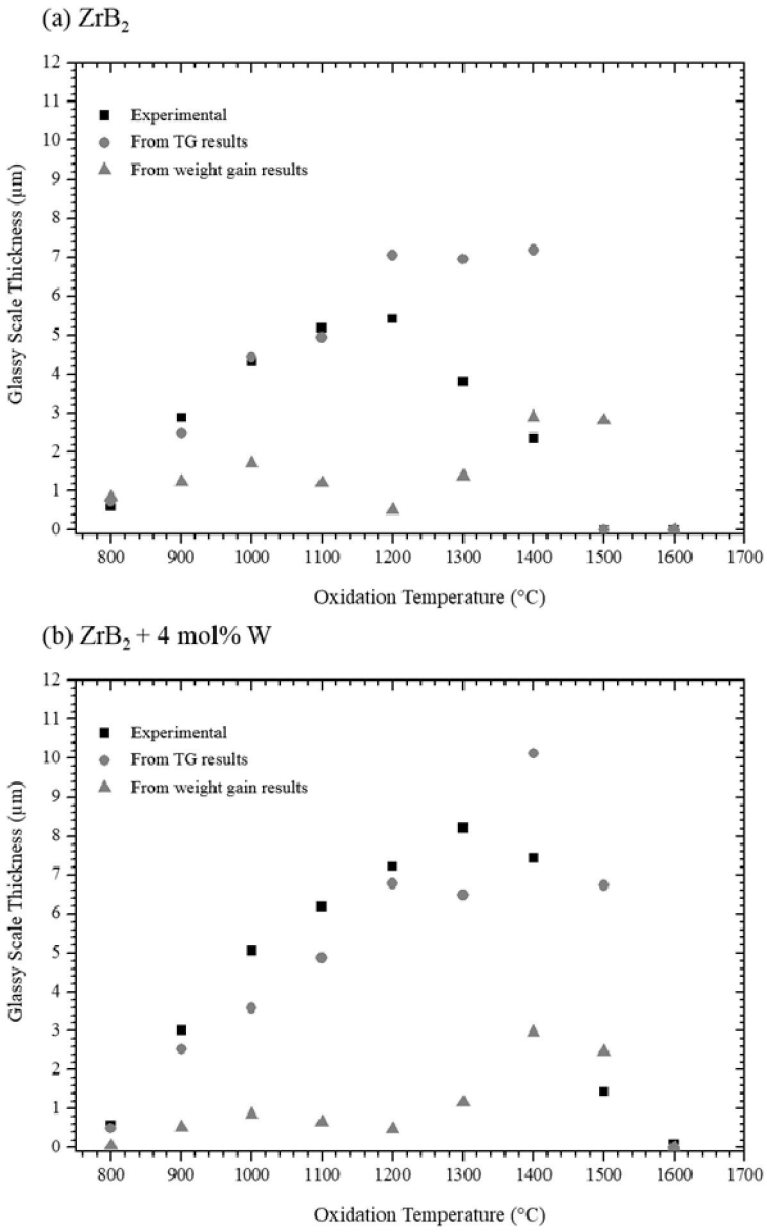

Figure 10. Thicknesses of the glassy scales calculated from weight gains and TG results for ZrB_2 and ZrB_2+4mol%W after oxidation for 0 hours.

2.4. Conclusion

The oxidation behavior of nominally pure ZrB_2 and $(Zr,W)B_2$ ceramics with 4, 6, or 8 mol% W was studied at temperatures ranging from 800 to 1600 °C. Oxidation in this temperature range resulted in the formation of a two-layer scale: (1) an outer glassy layer

containing B_2O_3 with dissolved W for $(Zr,W)B_2$ compositions; and (2) a porous layer composed of oxide particles containing Zr and W for $(Zr,W)B_2$ compositions. Based on scale thickness and weight gain measurements, two regimes of oxidation behavior were observed. The first stage was below 1100 °C for nominally pure ZrB_2 and 1300 °C for $(Zr,W)B_2$ specimens. No significant differences were measured for weight loss or scale thickness between nominally pure ZrB_2 and $(Zr,W)B_2$ compositions at temperatures between 800 and 1000 °C. However, the glassy layer thicknesses and weight gains were higher for $(Zr,W)B_2$ specimens after oxidation from 1100 to 1300 °C. It was concluded that dissolution of W into the B_2O_3 liquid phase increased the stability of the protective liquid layer by reducing the volatility of B_2O_3 from the liquid phase, resulting in a shift in the onset of the second oxidation regime toward higher temperatures for $(Zr,W)B_2$ specimens. This assumption was confirmed by TGA analysis of B_2O_3 and B_2O_3-WO_3 glasses. Above 1500 °C, the outer glassy layer was removed from the surface of nominally pure ZrB_2 by evaporation, while a thin (up to ~3μm) glassy layer was still covering the $(Zr,W)B_2$ specimens. Further, the $(Zr,W)B_2$ compositions showed lower weight gains and had thinner oxidation scales compared to nominally pure ZrB_2 at 1600 °C. The addition of W into B_2O_3 increased the stability of the protective liquid/glassy layer and resulted in higher oxidation resistance for $(Zr,W)B_2$ compared to nominally pure ZrB_2.

Acknowledgment

This work was supported as part of the National Hypersonic Science Center for Materials and Structures (Grant FA9550-09-1-0477) with Dr. Ali Sayir (AFOSR) and Dr. Anthony Calomino (NASA) as program managers. The authors wish to thank project

principal investigator Dr. David Marshall of Teledyne Scientific and Imaging for his support and guidance.

References

1. S. Q. Guo, "Densification of ZrB_2-Based Composites and Their Mechanical and Physical Properties: A Review," *Journal of the European Ceramic Society,* 29[6] 995-1011 (2009).
2. L. Zhang, D. A. Pejaković, J. Marschall, and M. Gasch, "Thermal and Electrical Transport Properties of Spark Plasma-Sintered HfB_2 and ZrB_2 Ceramics," *Journal of the American Ceramic Society,* 94[8] 2562-70 (2011).
3. F. Monteverde, R. Savino, M. D. S. Fumo, and A. Di Maso, "Plasma Wind Tunnel Testing of Ultra-High Temperature ZrB_2–SiC Composites under Hypersonic Re-entry Conditions," *Journal of the European Ceramic Society,* 30[11] 2313-21 (2010).
4. A. Rezaie, W. G. Fahrenholtz, and G. E. Hilmas, "Evolution of Structure during the Oxidation of Zirconium Diboride-Silicon Carbide in Air up to 1500°C," *Journal of the European Ceramic Society,* 27[6] 2495-501 (2007).
5. W. Fahrenholtz, G. Hilmas, G. Talmy, and J. Zaykoski, "Refractory Diborides of Zirconium and Hafnium," *Journal of the American Ceramic Society,* 90[5] 1347-64 (2007).
6. A. K. Kuriakose and J. L. Margrave, "The Oxidation Kinetics of Zirconium Diboride and Zirconium Carbide at High Temperatures," *Journal of The Electrochemical Society,* 111[7] 827-31 (1964).
7. F. Monteverde and A. Bellosi, "Oxidation of ZrB_2-based Ceramics in Dry Air," *Journal of The Electrochemical Society,* 150[11] B552-B59 (2003).
8. J. B. Berkowitz-Mattuck, "High-Temperature Oxidation III. Zirconium and Hafnium Diborides," *Journal of The Electrochemical Society,* 113[9] 908-14 (1966).
9. W. C. Tripp and H. C. Graham, "Thermogravimetric Study of the Oxidation of ZrB_2 in the Temperature Range of 800° to 1500°C," *Journal of The Electrochemical Society,* 118[7] 1195-99 (1971).
10. R. J. Irving and I. G. Worsley, "The Oxidation of Titanium Diboride and Zirconium Diboride at High Temperatures," *Journal of the Less Common Metals,* 16[2] 103-12 (1968).
11. S. C. Zhang, G. E. Hilmas, and W. G. Fahrenholtz, "Improved Oxidation Resistance of Zirconium Diboride by Tungsten Carbide Additions," *Journal of the American Ceramic Society,* 91[11] 3530-35 (2008).
12. T. A. Parthasarathy, R. A. Rapp, M. Opeka, and R. J. Kerans, "A Model for the Oxidation of ZrB_2, HfB_2 and TiB_2," *Acta Materialia,* 55[17] 5999-6010 (2007).
13. T. A. Parthasarathy, R. A. Rapp, M. Opeka, and R. J. Kerans, "A Model for Transitions in Oxidation Regimes of ZrB_2," pp. 823-32. in*,* Vol. 595-598 PART 2. *7th International Symposium on High Temperature Corrosion and Protection of Materials.* Les Embiez, 2008.
14. A. Rezaie, W. G. Fahrenholtz, and G. E. Hilmas, "Oxidation of Zirconium Diboride-Silicon Carbide at 1500°C in a Low Partial Pressure of Oxygen," *Journal of the American Ceramic Society,* 89[10] 3240-45 (2006).

15. C. M. Carney, P. Mogilvesky, and T. A. Parthasarathy, "Oxidation Behavior of Zirconium Diboride Silicon Carbide Produced by the Spark Plasma Sintering Method," *Journal of the American Ceramic Society,* 92[9] 2046-52 (2009).
16. W. M. Guo and G. J. Zhang, "Oxidation Resistance and Strength Retention of ZrB_2-SiC Ceramics," *Journal of the European Ceramic Society,* 30[11] 2387-95 (2010).
17. F. Monteverde, R. Savino, and M. D. S. Fumo, "Dynamic Oxidation of Ultra-high Temperature ZrB_2-SiC under High Enthalpy Supersonic Flows," *Corrosion Science,* 53[3] 922-29 (2011).
18. X. Zhang, L. Xu, S. Du, W. Han, and J. Han, "Preoxidation and Crack-Healing Behavior of ZrB_2-SiC Ceramic Composite," *Journal of the American Ceramic Society,* 91[12] 4068-73 (2008).
19. S. N. Karlsdottir, J. W. Halloran, and C. E. Henderson, "Convection Patterns in Liquid Oxide Films on ZrB_2-SiC Composites Oxidized at a High Temperature," *Journal of the American Ceramic Society,* 90[9] 2863-67 (2007).
20. I. Akin, F. Cinar Sahin, O. Yucel, and G. Goller, "Oxidation Behavior of Zirconium Diboride-Silicon Carbide Composites," pp. 105-11. in 34th International Conference on Advanced Ceramics and Composites*,* Vol. 31. Daytona Beach, FL, 2010.
21. S. N. Karlsdottir and J. W. Halloran, "Oxidation of ZrB_2-SiC: Influence of SiC Content on Solid and Liquid Oxide Phase Formation," *Journal of the American Ceramic Society,* 92[2] 481-86 (2009).
22. M. Mallik, K. K. Ray, and R. Mitra, "Oxidation Behavior of Hot Pressed ZrB_2-SiC and HfB_2-SiC Composites," *Journal of the European Ceramic Society,* 31[1-2] 199-215 (2011).
23. E. J. Opila and M. C. Halbig, "Oxidation of ZrB_2-SiC,*″* pp. 221-28 in 25th Annual Conference on Composites, Advanced Ceramics, Materials and Structures. Vol. 22. (2001).
24. S. Guo, T. Mizuguchi, M. Ikegami, and Y. Kagawa, "Oxidation Behavior of ZrB_2-$MoSi_2$-SiC Composites in Air at 1500°C," *Ceramics International,* 37[2] 585-91 (2011).
25. A. L. Chamberlain, W. G. Fahrenholtz, G. E. Hilmas, and D. T. Ellerby, "Characterization of Zirconium Diboride for Thermal Protection Systems," pp. 493-96. in 8th Conference and Exhibition of the European Ceramic Society*,* Vol. 264-268. Istanbul, Turkey, 2004.
26. D. Sciti, M. Brach, and A. Bellosi, "Oxidation Behavior of a Pressureless Sintered ZrB_2–$MoSi_2$ Ceramic Composite," *Journal of Materials Research,* 20[4] 922-30 (2005).
27. I. G. Talmy, J. A. Zaykoski, and M. M. Opeka, "High-Temperature Chemistry and Oxidation of ZrB_2 Ceramics Containing SiC, Si_3N_4, Ta_5Si_3, and $TaSi_2$," *Journal of the American Ceramic Society,* 91[7] 2250-57 (2008).
28. D. Sciti, V. Medri, and L. Silvestroni, "Oxidation Behaviour of HfB_2-15 vol.% $TaSi_2$ at Low, Intermediate and High Temperatures," *Scripta Materialia,* 63[6] 601-04 (2010).
29. M. M. Opeka, I. G. Talmy, and J. A. Zaykoski, "Oxidation-Based Materials Selection for 2000°C + Hypersonic Aerosurfaces: Theoretical Considerations and Historical Experience," *Journal of Materials Science,* 39[19] 5887-904 (2004).

30. E. J. Opila and M. C. Halbig, "Oxidation of ZrB_2-Based Ultra-High Temperature Ceramics," *Ceramic Engineering and Science Proceedings,* 22[3] 221-28 (2001).
31. S. R. Levine and E. J. Opila, "Tantalum Addition to Zirconium Diboride for Improved Oxidation Resistance." in. NASA/TM-2003-212483, 2003.
32. F. Peng, Y. Berta, and R. F. Speyer, "Effect of SiC, TaB_2 and $TaSi_2$ Additives on the Isothermal Oxidation Resistance of Fully Dense Zirconium Diboride," *Journal of Materials Science,* 24 [5] 1855-67. (2009).
33. I. G. Talmy, J. A. Zaykoski, M. M. Opeka, and S. Dallek, "Oxidation of ZrB_2 Ceramics Modified with SiC and Group IV-VI Transition Metal Diborides," *Electrochemical Society Proceedings,* 12 144-58 (2001).
34. P. Hu, X. H. Zhang, J. C. Han, X. G. Luo, and S. Y. Du, "Effect of Various Additives on the Oxidation Behavior of ZrB_2-Based Ultra-High-Temperature Ceramics at 1800°C," *Journal of the American Ceramic Society,* 93[2] 345-49 (2010).
35. X. H. Zhang, P. Hu, J. C. Han, L. Xu, and S. H. Meng, "The Addition of Lanthanum Hexaboride to Zirconium Diboride for Improved Oxidation Resistance," *Scripta Materialia,* 57[11] 1036-39 (2007).
36. S. C. Zhang, G. E. Hilmas, and W. G. Fahrenholtz, "Oxidation of Zirconium Diboride with Tungsten Carbide Additions," *Journal of the American Ceramic Society,* 94[4] 1198-205 (2011).
37. L. L. Y. Chang, M. G. Scroger, and B. Phillips, "Condensed Phase Relations in the Systems ZrO_2-WO_2-WO_3 and HfO_2-WO_2-WO_3," *Journal of the American Ceramic Society,* 50[4] 211-15 (1967).
38. S. N. Karlsdottir, J. W. Halloran, and A. N. Grundy, "Zirconia Transport by Liquid Convection during Oxidation of Zirconium Diboride-Silicon Carbide," *Journal of the American Ceramic Society,* 91[1] 272-77 (2008).
39. E. M. Levin, "The System WO_3-B_2O_3," *Journal of the American Ceramic Society,* 48[9] 491-92 (1965).
40. G. Pal Singh and D. P. Singh, "Structural and Optical Properties of WO_3-PbO-B_2O_3 Glass-Ceramic," *Journal of Physics and Chemistry of Solids,* 73[4] 540-44 (2012).
41. W. Vogel, "Glass Chemistry," 2nd ed. Springer-Verlag: New York, (1994).

3. Effect of Transition Metal Oxide Additions on the Structure of B_2O_3 Glasses

M. Kazemzadeh Dehdashti, A. Mohammadkhah, W.G. Fahrenholtz, G.E. Hilmas

Department of Materials Science and Engineering, Missouri University of Science and Technology, Rolla, MO 65401, United States

Abstract

The effects of transition metal (TM) oxides such as WO_3, Nb_2O_5, or ZrO_2 on weight loss and structure of B_2O_3 glasses was investigated. According to thermogravimetric analysis performed on (TM-oxide)-B_2O_3 glasses, TM-oxide additions reduced the evaporation of B_2O_3. Raman spectroscopy and ^{11}B high resolution nuclear magnetic resonance spectroscopy were used to study the effect of the TM-oxides on the structure of B_2O_3 glasses. Since no change in the structure of the glasses was detected, the increased stability of (TM-oxide)-B_2O_3 glasses compared to pure B_2O_3 is due to the lower activity of B_2O_3 in (TM-oxide)-B_2O_3 glasses.

Key Words: Borate glasses; tungsten oxide; niobium oxide; zirconium oxide; high-temperature Raman spectroscopy.

3.1. Introduction

Zirconium diboride is a candidate for hypersonic flight vehicle applications due to its high melting point (~3250°C) combined with thermal conductivity as high as ~110 W/m•K at room temperature.[1, 2] However, oxidation behavior has restricted the development of ZrB_2 for aero-propulsion and hypersonic flight applications.[3] Assuming stoichiometric oxidation, exposure of ZrB_2 to air at elevated temperatures results in the formation of liquid B_2O_3 layer (melting point ~450°C) and crystalline ZrO_2 (Reaction 1).[4] The glass forming ability of B_2O_3 results in retention of a glassy structure in the B_2O_3 scale formed by oxidation of ZrB_2 even when slowly cooled to room temperature. Formation of a liquid/glassy B_2O_3 layer on the surface provides passive oxidation protection and results in parabolic kinetics of oxidation. Evaporation of B_2O_3 is significant at temperatures above ~1100°C and results in loss of protection.[5]

$$ZrB_{2\,(s)} + 5/2\ O_{2\,(g)} \rightarrow ZrO_{2\,(s)} + B_2O_{3\,(l)} \qquad (1)$$

The most common method for improving the oxidation resistance of diboride-based ceramics above 1100°C is the addition of silicon-containing compounds such as SiC[4, 6-16], $TaSi_2$ [17, 18], or $MoSi_2$ [19-21]. The borosilicate liquid/glassy layer that forms on Si-containing ZrB_2 is more stable than the borate layer that forms on the surface of the nominally pure ZrB_2. As a result, ZrB_2 containing SiC, $TaSi_2$, or $MoSi_2$ has improved oxidation resistance as demonstrated by parabolic oxidation kinetics due to the presence of a protective glassy layer at temperatures up to at least 1600°C.[4, 16] However, the presence of Si-containing additives causes problems such as formation of a SiC-depleted

layer and rupture of the protective glassy layer due to formation of $SiO_{(g)}$,[22] which result in the loss of protection at temperatures above 1600°C. [23, 24] Several studies have shown the effectiveness of transition metal (TM) additives (e.g., borides of Nb, V, Cr, Ti, Ta, etc.) on improving the oxidation resistance of ZrB_2 ceramics.[24-28] Zhang *et al.*[29, 30] reported that tungsten carbide (WC) additives improved the oxidation resistance of ZrB_2 ceramics by formation of WO_3 in the oxide scale, which decreased the oxygen permeability of the ZrO_2 scale by promoting liquid phase sintering at the oxidation temperature. Previous studies have also indicated that addition of W or Nb to ZrB_2 increased the stability of the protective liquid/glassy B_2O_3 scale, and, consequently, increased the oxidation resistance of ZrB_2.[5, 31] Thermal gravimetric analysis (TGA) studies of the oxidation of nominally pure ZrB_2 and ZrB_2 with 4 at% W additions indicated that addition of W resulted in a higher temperature for the onset of evaporation of B_2O_3 during oxidation at ~1300°C, compared to ~900°C for nominally pure ZrB_2.[5]

Boron oxide is a glass network former, which compared to SiO_2 (the most common glass network forming oxide), has more intermediate-range order structure in the range of 0.5-2 nm.[32] In pure vitreous B_2O_3, each boron is bonded to three bridging oxygen atoms, forming planar $BØ_3$ groups (Ø=bridging oxygen atom).[33] About 70 to 80% of planar $BØ_3$ units in a vitreous B_2O_3 network form boroxol rings (each consist of 3 $BØ_3$ units), which are connected to each other through the remaining 20 to 30% of the $BØ_3$ units.[32, 34, 35] At ambient pressures, crystallization of pure, anhydrous B_2O_3 on cooling is inhibited by the presence of the boroxol rings.[36] The crystalline form of B_2O_3 does not contain boroxol groups, meaning that crystallization of vitreous B_2O_3 requires breaking relatively stable boroxol ring bonds.[33]

Alkali additions modify the structure and properties of B_2O_3. For example, adding 10 or 20 mol% K_2O to B_2O_3 glass results in transformation of some of the boroxol rings into pentaborate groups that consist of $BØ_4$ tetrahedra and $BØ_3$ units.[15] The addition of more than 30 mol% K_2O changes the structure of the borate species from $BØ_4$ tetrahedral units to $BØ_2O^-$ triangular units with one non-bridging oxygen.[37] Heating this high alkali composition above the glass transition temperature gradually reduces the fraction of four-coordinated boron atoms, which converged to a constant value above 1120°C. As more $BØ_2O^-$ units were generated at higher temperatures, the structure of the borate melt becomes less stable and evaporation increases.[37] Doping B_2O_3 glass with modest amounts of transition metal oxides might also transform some of the three-coordinate boron structural units to four-coordinated structures.[37-44] Existence of four-coordinate boron atoms means that more bonds would have to break for evaporation, which translates to higher stability of the B_2O_3 structure. However, the addition of excess TM oxide could lead to formation of non-bridging oxygen atoms, which would decrease stability and increase evaporation.

Whereas previous studies have hypothesized that TM additions improve the oxidation resistance of ZrB_2 by altering the structure of the porous ZrO_2 scale, TM additions may also improve the oxidation resistance of ZrB_2 by altering the structure and properties of the resulting B_2O_3 scale. The purpose of the present paper was to investigate the effect of TM oxides such as WO_3 and Nb_2O_5 on weight loss and structure of B_2O_3 glasses similar to those that form as the result of oxidation of ZrB_2.

3.2. Experimental procedure

To investigate the effect of W, Nb, and Zr on the structure of B_2O_3 glasses, $(WO_3)_x(B_2O_3)_{100-x}$, $(Nb_2O_5)_x(B_2O_3)_{100-x}$, and $(ZrO_2)_x(B_2O_3)_{100-x}$ glasses (with $1 \leq x \leq 10$) were prepared. High purity (≥99.5%) boric acid powder ($B_2O_3 \cdot 3H_2O$, ACS reagent, Sigma-Aldrich, Saint Louis, MO) was used along with WO_3 (99.99%, metal basis, Alfa Aesar, Ward Hill, MA), Nb_2O_5 (99.99%, metal basis, Alfa Aesar, Ward Hill, MA) or ZrO_2 (99%, metal basis, Alfa Aesar, Ward Hill, MA) to prepare 15 g batches of borate glasses. Batches were mixed by dry ball milling followed by grinding with a mortar and pestle. The mixtures were dehydrated at 500 °C in a platinum crucible until no bubbling (water evaporation) was observed. The glasses were then melted at temperatures between 900 and 1400°C, depending on the composition, for 1 hour followed by quenching using a high cooling rate twin-roller quencher.[45] Mass losses were monitored during dehydration and melting. In all cases, mass losses were consistent with decomposition of boric acid and evaporation of H_2O. Excess mass losses, due to evaporation of B_2O_3 and/or the TM-oxide during melting, were always less than 2 wt%. After cooling, glasses were kept in a desiccator under vacuum to keep them dry due to their hygroscopic nature.

The composition of the glasses were characterized using inductively coupled plasma-optical emission spectrometry (ICP-OES) (2000D, Perkin Elmer, USA) after dissolving glasses in 1 vol% nitric acid. Thermal gravimetric analysis (TGA; Netzsch Simultaneous TGA/DTA, Selb, Germany) was performed on ~100 mg of glass particles that were ground to <177μm. Powders of the different compositions were examined in a flowing nitrogen atmosphere. Each sample was heated to 170˚C with a rate of 10˚C/min and held for 1 hour to eliminate the possible water adsorbed on the glass particle surfaces during preparation or storage, followed by heating to 1500˚C at 10˚C/min. X-ray

diffraction (XRD; Philips X-Pert Pro diffractometer, Westborough, MA) was used to examine glasses for possible crystalline phases. A LabRAM HR800 Raman microscope (Horiba, Japan) with a 532 nm Verdi V2 DPSS green laser as the probing light source was used to perform *in situ* high temperature light scattering.[46] The NMR experiments were performed at room temperature using Avance II 600 solids (Bruker, USA). ^{11}B single pulse magic angle spinning (MAS) measurements were performed at 192.50 MHz using a 14.1 T magnet at spinning frequencies of 12.0 KHz, while the pulse lengths were 0.5 μs (20° flip angle) and the recycle delays were 5 s. A $CDCl_3$ solution of BF_3•OEt_2 was used as a reference for chemical shifts. The MestReNova LITE software was used for deconvolution of the NMR spectra. Results obtained by Raman spectroscopy and NMR were normalized for ease of comparison.

3.3. Results

The measured glass compositions were typically ±1 at% of the nominal batch compositions (Table 1). A few compositions were within 2 at% of the nominal batch composition (8W, 4 Nb, 8Nb, and 4 Zr), while only the composition of 8Zr was more than 2 at% from the nominal batch composition. As shown in Figure 1, no crystalline peaks were identified in XRD spectra for additions of up to 8 at% WO_3, 4 at% Nb_2O_5, or 2 at% ZrO_2; however, crystalline peaks were detected for borate glasses containing at least 10 at% WO_3, 8 at% Nb_2O_5, or 4 at% ZrO_2.

Table 1. Nominal batch and measured compositions for the glasses.

Designation	B_2O_3 (at%)	WO_3 (at%)	Nb_2O_5 (at%)	ZrO_2 (at%)	Metal oxide concentration
Pure	100				
1W	99	1			1.7±0.2
2W	98	2			2.7±0.4
3W	97	3			1.8±0.1
4W	96	4			3.3±0.4
5W	95	5			4.3±0.3
6W	94	6			3.9±0.4
7W	93	7			6.8±1.1
8W	92	8			6.1±0.2
9W	91	9			9.0±1.9
10W	90	10			9.2±2.0
2Nb	98		2		1.7±0.2
4Nb	96		4		2.8±0.2
8Nb	92		8		6.7±0.2
2Zr	98			2	2.1±0.1
4Zr	96			4	2.9±0.6
8Zr	92			8	3.1±0.5

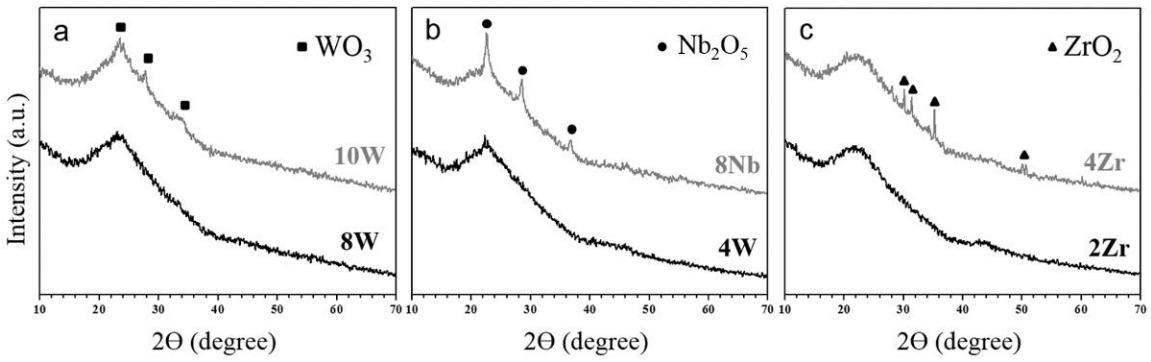

Figure 1. X-ray diffraction analysis of (a): WO_3-B_2O_3, (b): Nb_2O_5-B_2O_3, and (c): ZrO_2-B_2O_3 compositions showing crystalline phases in 10W, 8Nb, and 4Zr, while lower amounts of additives resulted in amorphous solids.

The evaporation behavior of B_2O_3 glasses with WO_3, Nb_2O_5, or ZrO_2 additions was studied by TGA. Nominally pure B_2O_3 and B_2O_3 glasses containing 2, 4, or 8 at% WO_3, Nb_2O_5, or ZrO_2 were tested at temperatures ranging from 25 to 1500°C. Figure 2 shows the total weight loss curves as a function of temperature for pure B_2O_3 and B_2O_3 containing 2 at% of TM-oxides as representative of the (TM-oxide)-B_2O_3 glasses. Even with careful storage and handling, boric acid formation was unavoidable due to the high sensitivity of B_2O_3 to humidity. Decomposition of boric acid initiated at about 170°C and was completed by about 430°C.[47] Therefore, all of the weight loss curves were normalized to the weight at 500°C to minimize the influence of different levels of hydration among the different compositions. The normalization temperature is above the decomposition temperature for boric acid, but below the temperature at which significant evaporation of B_2O_3 begins. The weight loss for pure B_2O_3 was not significant (less than about 0.5%) between 500 and 1000 °C, but increased linearly from ~0.5% at 1000°C to

~5% at 1400°C. Weight loss from B_2O_3 increased sharply above 1400°C. In comparison, all of the compositions containing TM-oxides had weight losses of less than 0.6% up to 1300°C and showed a sharp increase in weight loss at temperatures above 1400°C. Hence, the presence of TM-oxides in the borate glasses reduced the volatility of B_2O_3 at temperatures below 1300°C. The evaporation was linear above 1400 °C for all of the borate glasses.

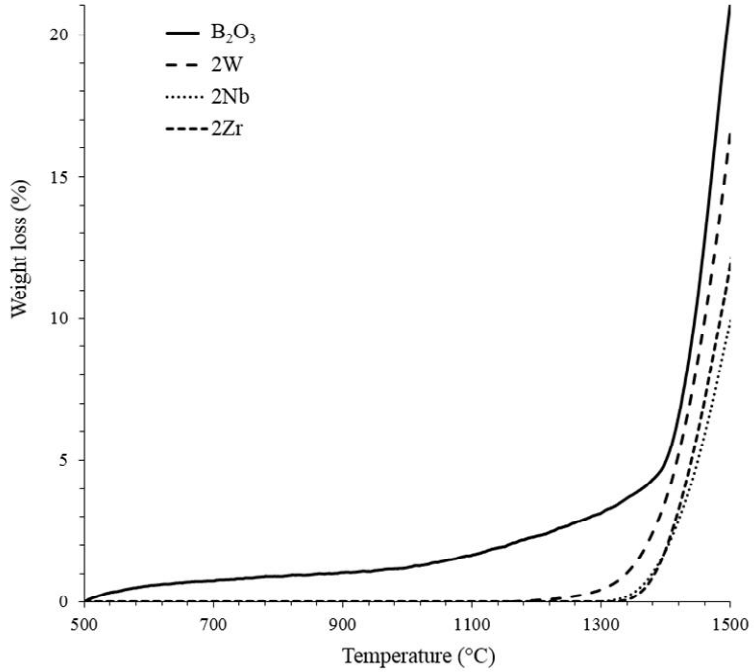

Figure 2. Weight loss as a function of temperature for pure B_2O_3, 2W, 2Nb, and 2Zr glasses at temperatures between 500 and 1500°C.

Figure 3 shows the evaporation rates above 1400 °C for pure B_2O_3 and B_2O_3 glasses containing 2, 4, or 8 at% WO_3, Nb_2O_5, or ZrO_2 that were calculated from the TGA results. Pure B_2O_3 had the highest evaporation rate (~0.2 wt%/°C) compared with

B_2O_3 glasses containing TM-oxide additives. Among the B_2O_3 glasses containing 2 at% TM-oxides, 2W had the highest evaporation rate (~0.15 wt%/°C), followed by 2Zr (~0.10 wt%/°C), and 2Nb (~0.08 wt%/°C). The lowest evaporation rate was for 8Nb (~0.06 wt%/°C), which was about 4 times lower than pure B_2O_3.

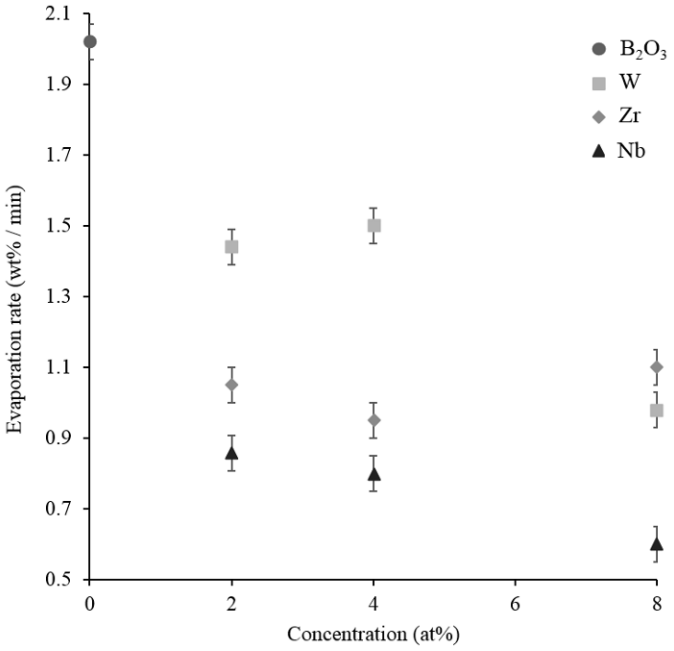

Figure 3. Evaporation rate for pure B_2O_3 and B_2O_3 glasses containing 2, 4, or 8 at% WO_3, Nb_2O_5, or ZrO_2 at temperatures above 1400°C.

For more clarity, Figure 4 shows the weight losses for pure B_2O_3 and B_2O_3 glasses containing 2, 4, or 8 at% WO_3, Nb_2O_5, or ZrO_2 glasses at 1500 °C. Again, B_2O_3 had the highest weight loss (~20%) compared with B_2O_3 glasses with TM-oxide additions. The same trends were observed for the total weight losses that had been observed for evaporation rates; the addition of Nb results in lower weight loss compared

to W and Zr, and higher amounts of additives result in lower overall weight losses. For total weight loss, the differences among 2 Nb, 4Zr, 4Nb, and 8Nb were not significant and they all had lower weight losses than the other B_2O_3 glasses (~9%), which was about half of the amount measured for pure B_2O_3.

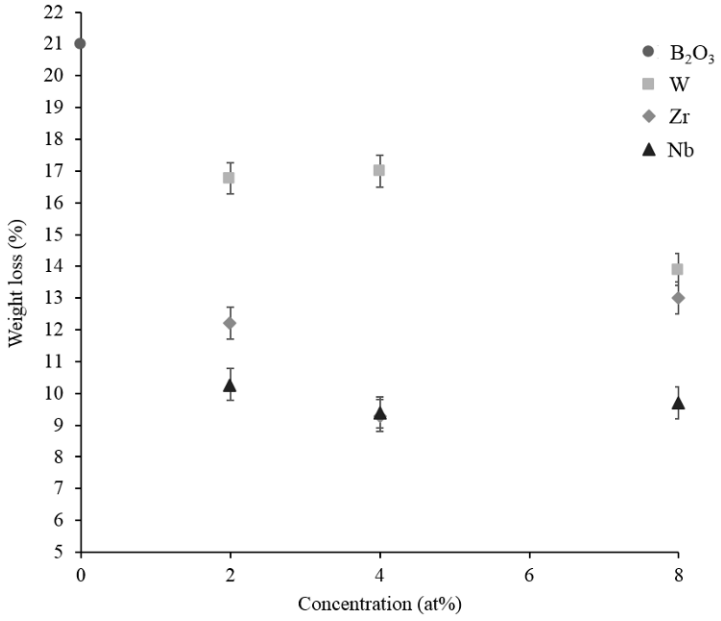

Figure 4. Total weight loss at 1500°C for pure B_2O_3 and B_2O_3 glasses containing 2, 4, or 8 at% WO_3, Nb_2O_5, or ZrO_2.

Raman spectroscopy and ^{11}B HR-NMR were used to characterize the effects of TM oxide additions on the structure of B_2O_3 glasses. Figure 5 shows the Raman spectra at room temperature for B_2O_3 glasses containing 2, 4, or 8 at% of WO_3, Nb_2O_5, or ZrO_2. The peak at 808 cm^{-1} has been assigned to the symmetric breathing vibration of the boroxol ring.[34, 48] No significant differences in the shape or position of this peak were

observed between the borate glasses with different amounts or types of TM-oxide additions. If $BØ_4$ units had formed, a peak would be expected to appear at about 770 cm^{-1} due to symmetric breathing vibrations of the six-membered rings with one or two $BØ_3$ units replaced with $BØ_4$ units.[42, 49, 50] As can be seen in Figure 5, no peaks were observed at 770 cm^{-1} for any of the compositions at room temperature.

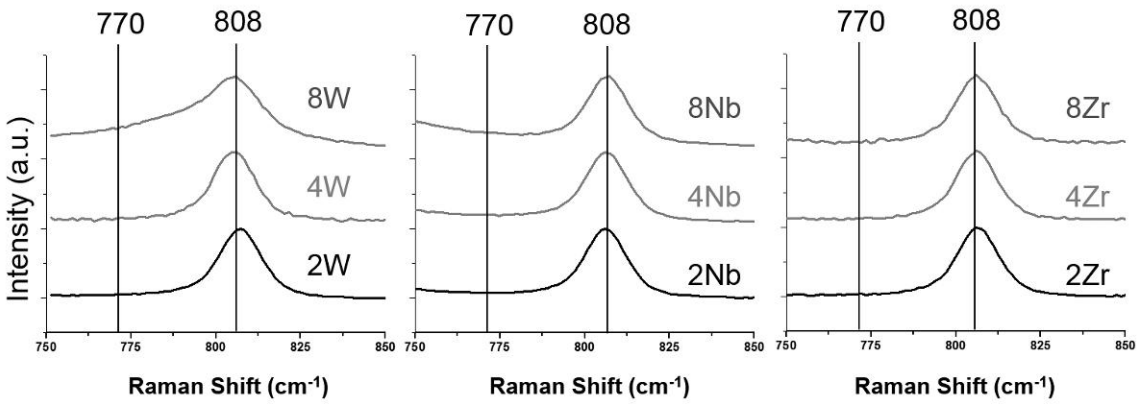

Figure 5. Room temperature Raman spectra for B_2O_3 glasses containing 2, 4, or 8 at% WO_3, Nb_2O_5, or ZrO_2.

To investigate the effect of temperature on the structure of WO_3-B_2O_3 glasses, Raman spectra were obtained from 8W while heating from room temperature to 800°C with 50°C intervals. Measurements were taken after the temperature inside the heating stage had stabilized for 5 min (Figure 6). The only change that was observed between the spectra obtained at room temperature and 350°C was the disappearance of a small peak at 877 cm^{-1} that is assigned to $B(OH)_3$ units.[51] A peak was also observed at 980 cm^{-1} that is assigned to the $BØ_3$ units in the $B_3O_3(OH)_4^-$ or $B_3O_3(OH)_5^{2-}$ structural units.[51] The

intensity of this peak decreased as temperature increased until it disappeared at about 500°C when the melt was completely dehydrated. The peak assigned to the symmetric breathing of the boroxol rings shifted from 808 cm^{-1} at room temperature to 798 cm^{-1} at 800°C, similar to the observations of Hassan *et al.*[36] and Walrafen *et al.*[34] The full width at half maximum (FWHM) of the 808 cm^{-1} peak increased with increasing temperature as a result of thermal excitation.[34] Several other broad bands were observed at room temperature, including those at ~260, ~330, and ~711 cm^{-1} that correspond to bending of O-W-O and the stretching of W-O bonds.[52, 53] The relative intensity of these peaks increased with increasing temperature and they appeared as sharp peaks from 500°C to 600°C. As shown in Figure 7, these peaks are similar to the Raman spectra collected for the WO_3 powder that was used for preparation of the glasses. Broadening of the WO_3 peaks at 800°C is due to thermal distortion of the WO_3 structure. The peak corresponding to the asymmetric stretching of W-O-W at 810 cm^{-1} for WO_3 increased the width of the right side of the 808 cm^{-1} peak for W-containing glasses. The crystalline WO_3 peaks remained after cooling the 8W glass from 800°C to room temperature. Also, XRD analysis performed on the 8W specimen after Raman spectroscopy at 800°C showed sharp WO_3 peaks (not shown). The small peak observed at room temperature at 1260 cm^{-1} is assigned to the bridging of the boroxol rings with one or more planar $BØ_3$ triangles.[36] The intensity of this peak decreases with increasing temperature as the boroxol rings open and the connectivity of the $BØ_3$ units change.[36] Figure 8 shows that after cooling back to lower temperatures, the WO_3 peaks are similar to the peaks appeared by heating. Also, the XRD analysis (not included) performed on the 8W specimen after Raman spectroscopy at 800°C showed sharp peaks of WO_3.

Raman spectroscopy performed on other W and Nb glasses with different amounts of WO_3 and Nb_2O_5 (not included) showed the same results as mentioned above, while the intensity of the TM-oxide peaks formed at elevated temperatures depended on the amount of the TM-oxide in the glass.

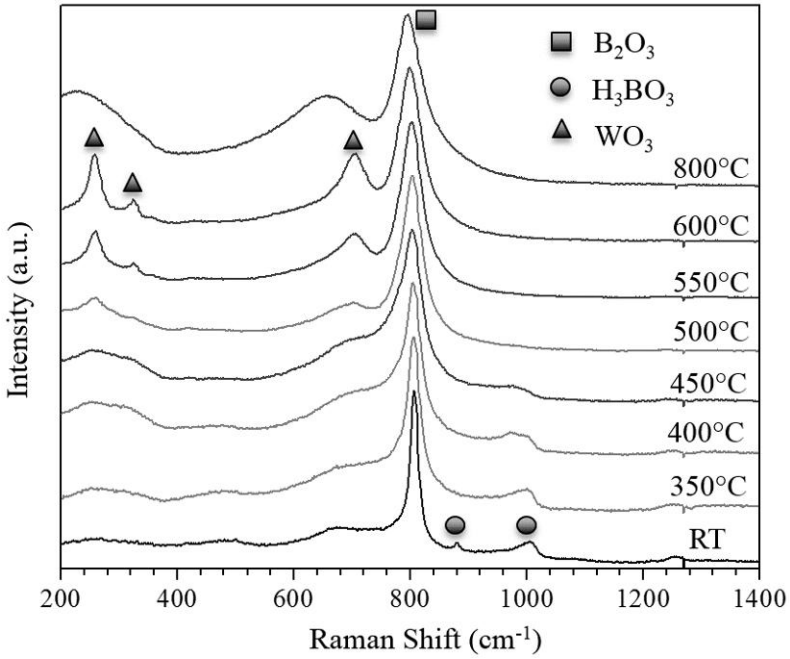

Figure 6. Elevated temperature Raman spectra for 8W at temperatures between room temperature and 800°C.

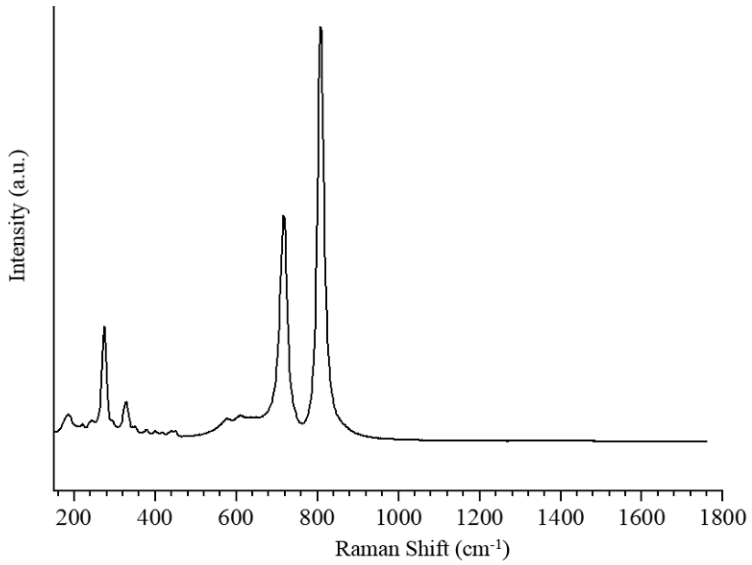

Figure 7. Room temperature Raman spectrum for WO_3 powder.

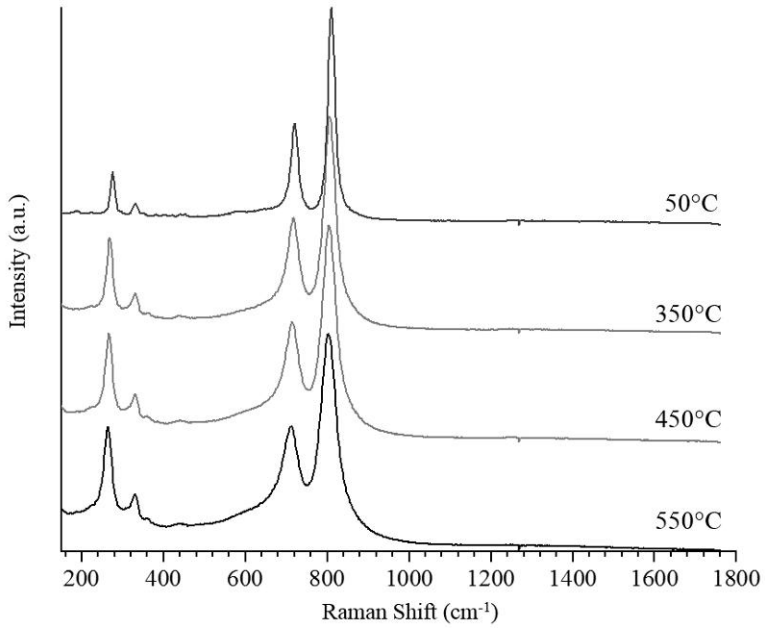

Figure 8. Raman spectra of 8W obtained during cooling at temperatures between 550 and 50°C.

Figure 9 shows ^{11}B NMR for B_2O_3 glasses containing 1 to 10 at% WO_3. No differences were observed in the shape or position of the peaks with different amounts of

WO_3. The complex line shape of the peak between 5 and 20 ppm was characteristic of a rigid-lattice second-order quadrupolar line shape due to trigonal boron coordination as was observed in previous ^{11}B NMR studies of B_2O_3 glass.[35, 54, 55] The small peak between 1 and 4 ppm is believed to be due to the contamination on the rotor. Figure 10 shows a magnified view of the peaks at 0 and 20 ppm without any offset in the Y axis to allow direct comparison of the line positions. The intensity of the shoulder on the left side (between 16 and 17 ppm) decreased with increasing WO_3 content in the B_2O_3 glass. In contrast, the intensity of the shoulder on the right side of the peak (between 8 and 10 ppm) increased with increasing WO_3 content. The line shape between 5 and 20 ppm is a result of the combination of two saddle-like components attributed to the boron in $BØ_3$ ring sites on the left and $BØ_3$ in non-ring sites on the right.[38] The decrease in the intensity of the left shoulder and increase in the intensity of the right shoulder with increasing WO_3 content in Figure 10 is due to a decrease in the number of boroxol rings and increase in the $BØ_3$ non-ring units with increasing WO_3 content, although the change is not substantial.

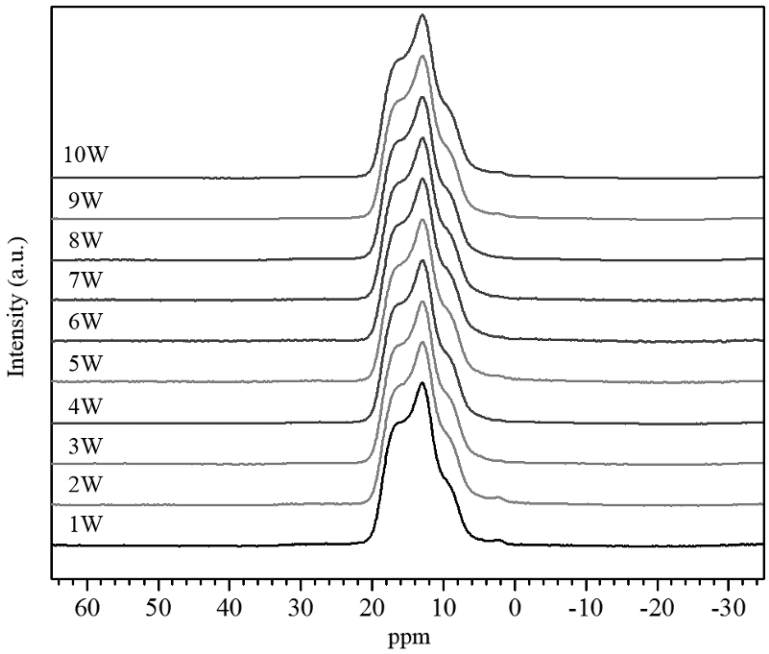

Figure 9. ^{11}B NMR spectra for B_2O_3 glasses containing 1 to 10 at% WO_3 additions.

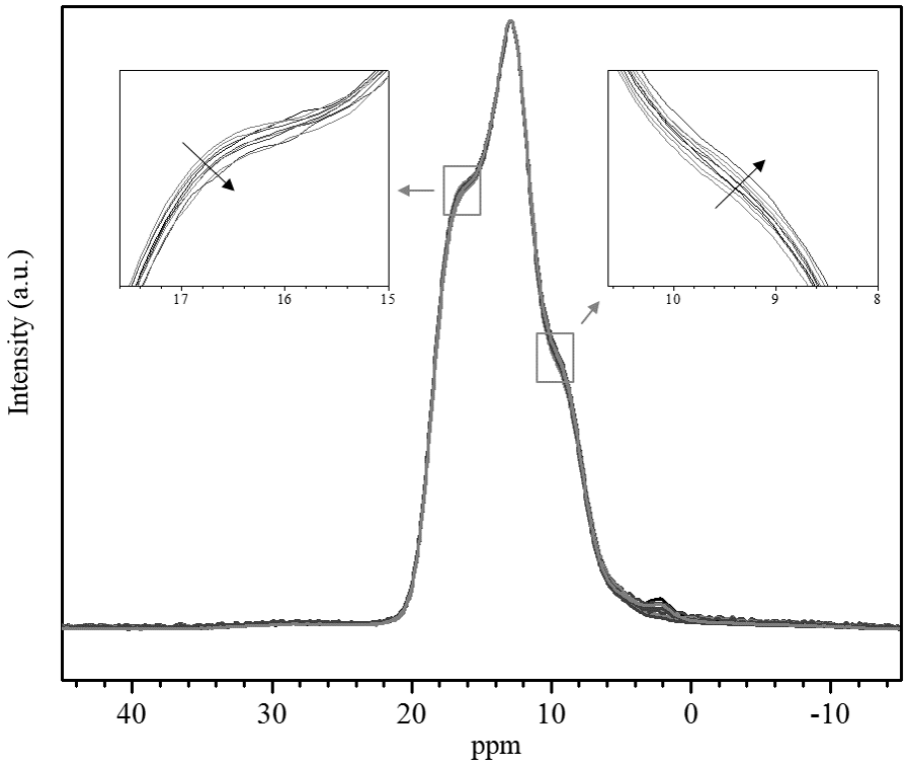

Figure 10. ^{11}B NMR spectra for B_2O_3 glasses containing 1 to 10 at% WO_3. The arrows in the inset images show the direction of change with increasing WO_3 content.

3.4. Discussion

Weight loss measurements from borate glasses containing TM-oxide additives showed that evaporation from nominally pure B_2O_3 initiated at about 900°C, while evaporation from TM-containing compositions was negligible below 1300°C. The effectiveness of the TM-oxide additions on reducing evaporation from borate melts was in the order of $WO_3<ZrO_2<Nb_2O_5$. The effect of ZrO_2 on reducing the evaporation of B_2O_3 results in higher stability of the B_2O_3 scale that is formed on the surface of pure ZrB_2 during oxidation, compared to the stability that would be expected from pure B_2O_3. The higher effectiveness of Nb_2O_5 on reducing the weight loss of B_2O_3 compared with WO_3, should result in formation of a more stable protective borate liquid scale on the surface and improve the oxidation resistance of $(Zr,Nb)B_2$ compared with $(Zr,W)B_2$.

XRD analysis did not reveal any peaks for crystalline phases in WO_3-B_2O_3, Nb_2O_5-B_2O_3, or ZrO_2-B_2O_3 compositions for concentrations of WO_3 of less than 8 at%, Nb_2O_5 of less than 4 at%, or ZrO_2 of less than 2 at%. Larger TM-oxide additions resulted in formation of crystalline phases that were detected by XRD analysis in the glasses. This indicates that the glasses with higher concentrations of TM-oxides contain crystalline phases corresponding to the TM-oxide that was added. However, the analysis does not preclude the presence of crystalline TM-oxides in the glasses with lower level additions as the amount of TM-oxide could be below the detection limit or the TM-oxides could be nano-sized, which would produce broad, low intensity peaks that might not be distinguished from the background. In addition, the TM oxides could be present in an amorphous phase. Because XRD analysis of glasses after high temperature Raman analysis showed sharp peaks for TM-oxide phases, it seems likely that the TM oxides were in an amorphous phase or as nano-sized TM-oxide crystallites inside the glass.

Hence, up to the aforementioned limits of TM-oxide additions of 8 at% WO_3, 4 at% Nb_2O_5, and 2 at% ZrO_2, the TM-oxide was amorphous or nano-sized, while higher TM-oxide additions resulted in formation of crystalline phases at room temperature, even after quenching with the very high cooling rates achieved in the roller quencher.

Other additives, such as alkalis, change the B_2O_3 network structure by converting some $BØ_3$ units to $BØ_4$ units, which produces a peak at about 770 cm^{-1} in Raman spectra.[37-44] However, the Raman spectra obtained at room temperature for B_2O_3 containing TM-oxide additions did not have a noticeable peak at 770 cm^{-1}. Hence, no $BØ_4$ units were detected in the roller-quenched glasses. Therefore, the presence of TM-oxides did not alter the borate glass network structure at room temperature. Broad WO_3 peaks were observed in the room temperature Raman spectra for W-containing compositions, which could indicate the presence of amorphous WO_3 along with the B_2O_3 glass.[56-59] Heating the glasses to temperatures up to 800°C resulted in the appearance of sharp peaks for WO_3 in the 8W glass. Increasing the temperature and/or holding time increased the intensities of the WO_3 peaks. XRD analysis obtained from the 8W glass after high temperature Raman analysis at 800°C showed sharp peaks for WO_3. Although Nb_2O_5 peaks were observed in the Raman spectrum for 8Nb at room temperature, the intensity of the peaks increased relative to the 808 cm^{-1} peak of B_2O_3 during annealing, indicating growth of the Nb_2O_5 crystallites at elevated temperatures. As with the W-containing glasses, no $BØ_4$ units were observed for Nb-containing compositions at any temperature. The formation of crystalline WO_3 at elevated temperatures, coupled with the lack of peaks associated with $BØ_4$ units at any temperature, indicated that the WO_3 must

have initially been in an amorphous phase, but crystallized during heating. However, 8Nb had some crystalline Nb_2O_5 in the as-quenched state.

NMR spectra for B_2O_3 glasses containing WO_3 additions ranging from 1 to 10 at% showed a complex line shape associated with trigonal boron. No significant differences were observed for different amounts of WO_3 added. No peak could be observed between -5 and 5 ppm as would be expected if $BØ_4$ units had formed.[54, 60] Hence, NMR results confirm the results from Raman spectroscopy that no $BØ_4$ units exist at room temperature in the glasses. With increasing WO_3 concentration, decrease in the shoulder on the left side of the peak and the corresponding increase in the shoulder on the right side of the peak was observed. The changes in the peak might indicate a decrease in the number of $BØ_3$ ring units and a corresponding increase in the $BØ_3$ non-ring units with increasing WO_3 content, which could be due to higher amounts of amorphous WO_3 in B_2O_3 glasses with higher WO_3 contents.

The WO_3-B_2O_3 phase diagram[61] shows simple eutectic behavior with an S-shaped liquidus covering the diagram between the eutectic point (close to the melting points of pure B_2O_3 at ~450°C) and the melting point of pure WO_3 (~1435°C). The system shows that no compounds form nor does it indicate any solution formation in the solid phases or immiscibility in the liquid phase. Since no $BØ_4$ units were detected in the W glasses, WO_3 is not soluble in B_2O_3 glass, and according to the characterization results, the WO_3-B_2O_3 glasses should consist of mixtures of amorphous B_2O_3 and WO_3.

The Nb_2O_5-B_2O_3 system[62] is characterized by a binary compound $3Nb_2O_5$-B_2O_3 that melts incongruently at 1150°C, about 200°C below a monotectic. A large liquid immiscibility region exists at 1352°C between 10 and 65.7 at% Nb_2O_5. It was reported

that the liquids devitrified on quenching and homogeneous glasses were never obtained for any composition.[62] The solubility of Nb_2O_5 in B_2O_3 is lower than WO_3, as only 5 at% Nb_2O_5 (10 at% Nb_2O_5) dissolved in B_2O_3 above 1300°C to form a homogeneous liquid phase.

The ZrO_2-B_2O_3 phase diagram[63] is also a eutectic type and does not show any compound or solid solution formation. However, a small region of phase separation was observed between 600°C and 1000°C for compositions ranging from 2 at% to 32 at% ZrO_2. The solubility of ZrO_2 in B_2O_3 is lower than either WO_3 or Nb_2O_5. For example, at 10 at% ZrO_2 a homogeneous liquid phase only forms above ~1500°C.

No $BØ_4$ units were observed in the TM-oxide-B_2O_3 glasses at any temperature. Hence, a change in the structure does not appear to be a reason for the increased stability of B_2O_3 with TM-oxide additions. However, dissolution of TM-oxides into the liquid phase, even without a change in the B_2O_3 network structure, should decrease the activity of B_2O_3 in the liquid phase and reduce both the vapor pressure and evaporation rate of B_2O_3. The compositions containing TM-oxide additions were less hydroscopic during handling, which could be a sign of lower B_2O_3 activity with TM-oxide additions. If that was the only effect, the amount of TM-oxide should play a more important role than the kind of TM-oxide. However, addition of Nb resulted in lower weight loss of B_2O_3. For the systems with binary compounds between the TM-oxide and B_2O_3, e.g. Nb_2O_5-B_2O_3, addition of TM-oxide to B_2O_3 could result in greater decrease in the activity of B_2O_3.

According to the phase diagrams, several oxides form high melting temperature compounds with B_2O_3, such as In_2O_3, La_2O_3, and Sc_2O_3. However, only additives with equal or higher valences than Zr should be used as additives to ZrB_2 to prevent an

increase in oxidation rate due to the formation of oxygen vacancies in stabilized ZrO_2. Hence, according to the available phase diagrams, Nb_2O_5 and Ta_2O_5 may be the best additives for improving the stability of the protective B_2O_3 liquid/glassy layer during oxidation of ZrB_2 ceramics.

3.5. Conclusions

The evaporation behavior of B_2O_3 with TM oxide additions was analyzed. Additions of tungsten, niobium, and zirconium oxides decreased the evaporation rate and increased the onset temperature for evaporation in B_2O_3-based glasses in the order of $WO_3<ZrO_2<Nb_2O_5$. High temperature Raman spectroscopy showed that WO_3 in the B_2O_3 glass was initially amorphous, but crystallized at elevated temperatures. In addition, the intensity of Nb_2O_5 peaks in the glass increased as a result of crystallization. No signs of formation of $BØ_4$ units was observed in the borate glasses by Raman spectroscopy or NMR. It was concluded that additions of WO_3, Nb_2O_5, or ZrO_2 to B_2O_3 did not change the structure of B_2O_3. Hence, the higher oxidation resistance of $(Zr,TM)B_2$ ceramics and lower evaporation rate of (TM-oxide)-B_2O_3 glasses may be due to the fact that the dissolution of TM-oxide in B_2O_3 decreases the activity of B_2O_3 and, consequently, decreases the vapor pressure and evaporation rate of B_2O_3. Also, formation of $3Nb_2O_5$-B_2O_3 compound with high melting temperature could be the reason of lower evaporation rate of Nb_2O_5-B_2O_3 glasses compared to other (TM-oxide)-B_2O_3 glasses.

Acknowledgment

This work was supported as part of the National Hypersonic Science Center for Materials and Structures (Grant FA9550-09-1-0477) with Dr. Ali Sayir (AFOSR) and Dr. Anthony Calomino (NASA) as program managers. The authors wish to thank project principal investigator Dr. David Marshall of Teledyne Scientific and Imaging for his support and guidance. The authors are also thankful to Prof. Richard Brow, Kathryn Goetschius and Charmayne Smith for discussions about glass structure and assistance with preparation of glasses. Special thanks to Dr. Mario Affatigato from Coe College for giving us the opportunity to use the high cooling rate twin-roller quencher. The authors also thank Dr. Steve Martin from Iowa State University for support and use of the nuclear magnetic resonance instrument. In addition, the authors would like to express deepest appreciation to Dr. Liping Huang from Rensselaer Polytechnic Institute for providing access to high-temperature Raman spectroscopy.

References

1. S. Q. Guo, "Densification of ZrB_2-Based Composites and Their Mechanical and Physical Properties: A Review," *Journal of the European Ceramic Society,* 29[6] 995-1011 (2009).
2. L. Zhang, D. A. Pejaković, J. Marschall, and M. Gasch, "Thermal and Electrical Transport Properties of Spark Plasma-Sintered HfB_2 and ZrB_2 Ceramics," *Journal of the American Ceramic Society,* 94[8] 2562-70 (2011).
3. A. Bongiorno, C. J. Först, R. K. Kalia, J. Li, J. Marschall, A. Nakano, M. M. Opeka, I. G. Talmy, P. Vashishta, and S. Yip, "A Perspective on Modeling Materials in Extreme Environments: Oxidation of Ultrahigh-Temperature Ceramics," *MRS Bulletin,* 31[05] 410-18 (2006).
4. A. Rezaie, W. G. Fahrenholtz, and G. E. Hilmas, "Evolution of Structure during the Oxidation of Zirconium Diboride-Silicon Carbide in Air up to 1500°C," *Journal of the European Ceramic Society,* 27[6] 2495-501 (2007).
5. M. Kazemzadeh Dehdashti, W. G. Fahrenholtz, and G. E. Hilmas, "Effects of Temperature and the Incorporation of W on the Oxidation of ZrB_2 Ceramics," *Corrosion Science,* 80 221-28 (2014).
6. A. Rezaie, W. G. Fahrenholtz, and G. E. Hilmas, "Oxidation of Zirconium Diboride-Silicon Carbide at 1500°C in a Low Partial Pressure of Oxygen," *Journal of the American Ceramic Society,* 89[10] 3240-45 (2006).
7. C. M. Carney, P. Mogilvesky, and T. A. Parthasarathy, "Oxidation Behavior of Zirconium Diboride Silicon Carbide Produced by the Spark Plasma Sintering Method," *Journal of the American Ceramic Society,* 92[9] 2046-52 (2009).
8. W. M. Guo and G. J. Zhang, "Oxidation Resistance and Strength Retention of ZrB_2-SiC Ceramics," *Journal of the European Ceramic Society,* 30[11] 2387-95 (2010).
9. F. Monteverde, R. Savino, and M. D. S. Fumo, "Dynamic Oxidation of Ultra-high Temperature ZrB_2-SiC under High Enthalpy Supersonic Flows," *Corrosion Science,* 53[3] 922-29 (2011).
10. X. Zhang, L. Xu, S. Du, W. Han, and J. Han, "Preoxidation and Crack-Healing Behavior of ZrB_2-SiC Ceramic Composite," *Journal of the American Ceramic Society,* 91[12] 4068-73 (2008).
11. S. N. Karlsdottir, J. W. Halloran, and C. E. Henderson, "Convection Patterns in Liquid Oxide Films on ZrB_2-SiC Composites Oxidized at a High Temperature," *Journal of the American Ceramic Society,* 90[9] 2863-67 (2007).
12. I. Akin, F. Cinar Sahin, O. Yucel, and G. Goller, "Oxidation Behavior of Zirconium Diboride-Silicon Carbide Composites," pp. 105-11. in 34th International Conference on Advanced Ceramics and Composites*,* Vol. 31. Daytona Beach, FL, 2010.
13. S. N. Karlsdottir and J. W. Halloran, "Oxidation of ZrB_2-SiC: Influence of SiC Content on Solid and Liquid Oxide Phase Formation," *Journal of the American Ceramic Society,* 92[2] 481-86 (2009).
14. F. Monteverde, R. Savino, M. D. S. Fumo, and A. Di Maso, "Plasma Wind Tunnel Testing of Ultra-High Temperature ZrB_2–SiC Composites under Hypersonic Re-

entry Conditions," *Journal of the European Ceramic Society,* 30[11] 2313-21 (2010).
15. M. Mallik, K. K. Ray, and R. Mitra, "Oxidation Behavior of Hot Pressed ZrB_2-SiC and HfB_2-SiC Composites," *Journal of the European Ceramic Society,* 31[1-2] 199-215 (2011).
16. E. J. Opila and M. C. Halbig, "Oxidation of ZrB_2-SiC,″ pp. 221-28 in 25th Annual Conference on Composites, Advanced Ceramics, Materials and Structures. Vol. 22. (2001).
17. I. G. Talmy, J. A. Zaykoski, and M. M. Opeka, "High-Temperature Chemistry and Oxidation of ZrB_2 Ceramics Containing SiC, Si_3N_4, Ta_5Si_3, and $TaSi_2$," *Journal of the American Ceramic Society,* 91[7] 2250-57 (2008).
18. D. Sciti, V. Medri, and L. Silvestroni, "Oxidation Behaviour of HfB_2-15 vol.% $TaSi_2$ at Low, Intermediate and High Temperatures," *Scripta Materialia,* 63[6] 601-04 (2010).
19. S. Guo, T. Mizuguchi, M. Ikegami, and Y. Kagawa, "Oxidation Behavior of ZrB_2-$MoSi_2$-SiC Composites in Air at 1500°C," *Ceramics International,* 37[2] 585-91 (2011).
20. A. L. Chamberlain, W. G. Fahrenholtz, G. E. Hilmas, and D. T. Ellerby, "Characterization of Zirconium Diboride for Thermal Protection Systems," pp. 493-96. in 8th Conference and Exhibition of the European Ceramic Society*,* Vol. 264-268. Istanbul, Turkey, 2004.
21. D. Sciti, M. Brach, and A. Bellosi, "Oxidation Behavior of a Pressureless Sintered ZrB_2–$MoSi_2$ Ceramic Composite," *Journal of Materials Research,* 20[4] 922-30 (2005).
22. M. M. Opeka, I. G. Talmy, and J. A. Zaykoski, "Oxidation-Based Materials Selection for 2000°C + Hypersonic Aerosurfaces: Theoretical Considerations and Historical Experience," *Journal of Materials Science,* 39[19] 5887-904 (2004).
23. E. J. Opila and M. C. Halbig, "Oxidation of ZrB_2-Based Ultra-High Temperature Ceramics," *Ceramic Engineering and Science Proceedings,* 22[3] 221-28 (2001).
24. S. R. Levine and E. J. Opila, "Tantalum Addition to Zirconium Diboride for Improved Oxidation Resistance." in. NASA/TM-2003-212483, 2003.
25. F. Peng, Y. Berta, and R. F. Speyer, "Effect of SiC, TaB_2 and $TaSi_2$ Additives on the Isothermal Oxidation Resistance of Fully Dense Zirconium Diboride," *Journal of Materials Science,* 24 [5] 1855-67. (2009).
26. I. G. Talmy, J. A. Zaykoski, M. M. Opeka, and S. Dallek, "Oxidation of ZrB_2 Ceramics Modified with SiC and Group IV-VI Transition Metal Diborides," *Electrochemical Society Proceedings,* 12 144-58 (2001).
27. P. Hu, X. H. Zhang, J. C. Han, X. G. Luo, and S. Y. Du, "Effect of Various Additives on the Oxidation Behavior of ZrB_2-Based Ultra-High-Temperature Ceramics at 1800°C," *Journal of the American Ceramic Society,* 93[2] 345-49 (2010).
28. X. H. Zhang, P. Hu, J. C. Han, L. Xu, and S. H. Meng, "The Addition of Lanthanum Hexaboride to Zirconium Diboride for Improved Oxidation Resistance," *Scripta Materialia,* 57[11] 1036-39 (2007).
29. S. C. Zhang, G. E. Hilmas, and W. G. Fahrenholtz, "Oxidation of Zirconium Diboride with Tungsten Carbide Additions," *Journal of the American Ceramic Society,* 94[4] 1198-205 (2011).

30. S. C. Zhang, G. E. Hilmas, and W. G. Fahrenholtz, "Improved Oxidation Resistance of Zirconium Diboride by Tungsten Carbide Additions," *Journal of the American Ceramic Society,* 91[11] 3530-35 (2008).
31. M. Kazemzadeh Dehdashti, W. G. Fahrenholtz, and G. E. Hilmas, "Oxidation of Zirconium Diboride with Niobium Additions," *Journal of the European Ceramic Society,* 33[10] 1591-98 (2013).
32. R. E. Youngman, S. T. Haubrich, J. W. Zwanziger, M. T. Janicke, and B. F. Chmelka, "Short- and Intermediate-range Structural Ordering in Glassy Boron Oxide," *Science,* 269[5229] 1416 (1995).
33. A. C. Wright, "Borate Structures: Crystalline and Vitreous," *Physics and Chemistry of Glasses-European Journal of Glass Science and Technology Part B,* 51[1] 1-39 (2010).
34. G. E. Walrafen, S. Samanta, and P. Krishnan, "Raman Investigation of Vitreous and Molten Boric Oxide," *The Journal of Chemical Physics,* 72 113 (1980).
35. A. H. Silver and P. J. Bray, "Nuclear Magnetic Resonance Absorption in Glass. I. Nuclear Quadrupole Effects in Boron Oxide, Soda-Boric Oxide, and Borosilicate Glasses," *The Journal of Chemical Physics,* 29[5] 984-90 (1958).
36. A. Hassan, L. Torell, L. Börjesson, and H. Doweidar, "Structural Changes of B_2O_3 Through the Liquid-glass Transition Range: A Raman-scattering Study," *Physical Review B,* 45[22] 12797 (1992).
37. R. Akagi, N. Ohtori, and N. Umesaki, "Raman Spectra of K_2O–B_2O_3 Glasses and Melts," *Journal of non-crystalline solids,* 293 471-76 (2001).
38. L.-S. Du and J. F. Stebbins, "Nature of Silicon−Boron Mixing in Sodium Borosilicate Glasses: A High-Resolution ^{11}B and ^{17}O NMR Study," *The Journal of Physical Chemistry B,* 107[37] 10063-76 (2003).
39. P. Hudon and D. R. Baker, "The Nature of Phase Separation in Binary Oxide Melts and Glasses. III. Borate and Germanate Systems," *Journal of non-crystalline solids,* 303[3] 354-71 (2002).
40. H. A. A. Sidek, H. B. Senin, M. K. Halimah, W. M. Daud, A. M. Khamirul, and A. S. Halim, "Glass Formation and Elastic Behavior of Bismuth Borate Glass System," *AIP Conference Proceedings,* 1017[1] 321-25 (2008).
41. R. C. Lucacel, C. Marcus, V. Timar, and I. Ardelean, "FT-IR and Raman Spectroscopic Studies on B_2O_3–PbO–Ag_2O Glasses Dopped with Manganese Ions," *Solid State Sciences,* 9[9] 850-54 (2007).
42. D. Maniu, T. Iliescu, I. Ardelean, S. Cinta-Pinzaru, N. Tarcea, and W. Kiefer, "Raman Study on B_2O_3–CaO Glasses," *Journal of Molecular Structure,* 651 485-88 (2003).
43. D. Maniu, T. Iliescu, I. Ardelean, R. Ciceo-Lucacel, M. Bolboaca, and W. Kiefer, "Raman Study of B_2O_3–SrO–CuO Glasses," *Vibrational spectroscopy,* 29[1] 241-44 (2002).
44. T. Iliescu, I. Ardelean, V. Simon, and D. Maniu, "Raman Study of B_2O_3-PbO-Nd_2O_3 Glasses," *Journal of Materials Science Letters,* 14[6] 393-95 (1995).
45. A. Havel, S. Feller, M. Affatigato, and M. Karns, "Design and Operation of a New Roller Quencher for Rapidly Cooling Melts into Glasses," *Glass Technology-European Journal of Glass Science and Technology Part A,* 50[4] 227-29 (2009).

46. M. Guerette and L. Huang, "A Simple and Convenient Set-up for High-temperature Brillouin Light Scattering," *Journal of Physics D: Applied Physics,* 45[27] 275302 (2012).
47. F. Sevim, F. Demir, M. Bilen, and H. Okur, "Kinetic Analysis of Thermal Decomposition of Boric Acid from Thermogravimetric Data," *Korean J. Chem. Eng.,* 23[5] 736-40 (2006).
48. F. L. Galeener, G. Lucovsky, and J. Mikkelsen Jr, "Vibrational Spectra and the Structure of Pure Vitreous B_2O_3," *Physical Review B,* 22[8] 3983 (1980).
49. K. Fukumi, K. Ogawa, and J. Hayakawa, "Intensities of Raman Bands in Borate Glasses," *Journal of non-crystalline solids,* 151[3] 217-21 (1992).
50. B. Dwivedi, M. Rahman, Y. Kumar, and B. Khanna, "Raman Scattering Study of Lithium Borate Glasses," *Journal of Physics and Chemistry of Solids,* 54[5] 621-28 (1993).
51. L. Xiaoping, G. Shiyang, and X. Shuping, "Investigations of Kinetics and Mechanism of Chloropinnoite in Boric Acid Aqueous Solution at 303 K by Raman Spectroscopy," *Spectrochimica Acta Part A: Molecular and Biomolecular Spectroscopy,* 60[12] 2725-28 (2004).
52. R. F. Garcia-Sanchez, T. Ahmido, D. Casimir, S. Baliga, and P. Misra, "Thermal Effects Associated with the Raman Spectroscopy of WO_3 Gas-Sensor Materials," *The Journal of Physical Chemistry A* (2013).
53. M. Daniel, B. Desbat, J. Lassegues, B. Gerand, and M. Figlarz, "Infrared and Raman Study of WO_3 Tungsten Trioxides and WO_3,xH_2O Tungsten Trioxide Hydrates," *Journal of solid state chemistry,* 67[2] 235-47 (1987).
54. H. Maekawa, Y. Inagaki, S. Shimokawa, and T. Yokokawa, "Dynamics of a Glass-forming System: ^{11}B NMR of B_2O_3," *The Journal of chemical physics,* 103 371 (1995).
55. M. M. Smedskjaer, J. C. Mauro, R. E. Youngman, C. L. Hogue, M. Potuzak, and Y. Yue, "Topological Principles of Borosilicate Glass Chemistry," *The Journal of Physical Chemistry B,* 115[44] 12930-46 (2011).
56. H. Habazaki, Y. Hayashi, and H. Konno, "Characterization of Electrodeposited WO_3 Films and its Application to Electrochemical Wastewater Treatment," *Electrochimica Acta,* 47[26] 4181-88 (2002).
57. C. Santato, M. Odziemkowski, M. Ulmann, and J. Augustynski, "Crystallographically Oriented Mesoporous WO3 Films: Synthesis, Characterization, and Applications," *Journal of the American Chemical Society,* 123[43] 10639-49 (2001).
58. M. Deepa, M. Kar, and S. A. Agnihotry, "Electrodeposited Tungsten Oxide Films: Annealing Effects on Structure and Electrochromic Performance," *Thin Solid Films,* 468[1–2] 32-42 (2004).
59. S. Khamseh, "A Study of the Oxidation Behavior of Multilayered Tungsten Nitride/Amorphous Tungsten Oxide Film Prepared in a Planar Magnetron Sputtering System," *Ceramics International,* 40[1, Part A] 465-70 (2014).
60. D. Larink, H. Eckert, M. Reichert, and S. W. Martin, "Mixed Network Former Effect in Ion-Conducting Alkali Borophosphate Glasses: Structure/Property Correlations in the System $[M_2O]_{1/3}[(B_2O_3)_x(P_2O_5)_{1-x}]_{2/3}$ (M= Li, K, Cs)," *The Journal of Physical Chemistry C,* 116[50] 26162-76 (2012).

61. E. M. Levin, "The System WO_3-B_2O_3," *Journal of the American Ceramic Society,* 48[9] 491-92 (1965).
62. E. M. Levin, "Phase Equilibria in the System Niobium Pentoxide-Boric Acid," *Journal of Research of the National Bureau of Standards,* 70A[1] 11-16 (1966).
63. S. N. Karlsdottir, J. W. Halloran, and A. N. Grundy, "Zirconia Transport by Liquid Convection during Oxidation of Zirconium Diboride-Silicon Carbide," *Journal of the American Ceramic Society,* 91[1] 272-77 (2008).

4. Effects of Transition Metals on the Oxidation Behavior of ZrB_2 Ceramics

M. Kazemzadeh Dehdashti, W.G. Fahrenholtz, G.E. Hilmas

Department of Materials Science and Engineering, Missouri University of Science and Technology, Rolla, MO 65401, United States

Abstract

The effects of transition metal (TM) additives, specifically W, Mo, or Nb, on oxidation behavior of ZrB_2 ceramics at 1600°C were investigated. Oxide scale thicknesses were measured from fractured surfaces after isothermal oxidation. The stability of the B_2O_3 layers on different samples of $(Zr,TM)B_2$ ceramics were compared and the consequent effect on the oxide scale thicknesses is discussed. Addition of TM additives improved the oxidation resistance of ZrB_2 ceramics even after the protective B_2O_3 layer was removed. The oxide layer composed of two sub-layers, an outer layer that was porous and appeared light in optical microscopy and an inner layer that was dense and appeared dark. The effects of TM additives on the thicknesses and morphology of the light and dark zirconia layers were also investigated. Additions of Mo or Nb were found to be more effective than W on improving the oxidation resistance of ZrB_2 at 1600°C.

4.1. Introduction

Ultra high temperature ceramics (UHTCs) are a class of materials that includes diborides (i.e. ZrB_2, HfB_2), carbides (i.e. ZrC, HfC), and nitrides (i.e. ZrN, HfN). UHTCs have melting temperatures in excess of 3000°C and the ability to withstand extreme heating environments. Diboride-based UHTCs have performance advantages compared to the carbides and nitrides due to their high oxidation resistance and the capability to transfer and redistribute heat (thermal conductivity >100 W/m•K) at elevated temperatures. These characteristics make them good candidates for sharp leading edges for hypersonic aerospace vehicles, which must not only be capable of operating in oxidizing atmospheres at high temperatures and high flow rates, but also have high thermal conductivity to transfer heat away from the hottest areas and redistribute it to cooler areas.[1, 2]

Zirconium diboride has advantages over other UHTCs for aerospace applications due to its high melting point (~3250°C), low theoretical density (6.09 g/cm^3), and a thermal conductivity of over 100 W/m•K at room temperature.[3, 4] However, oxidation at temperatures above 800°C has limited the development of ZrB_2 ceramics for aero-propulsion and hypersonic flight applications.[5] Oxidation of ZrB_2 is usually assumed to be stoichiometric and results in measurable mass gain due to formation of B_2O_3 and ZrO_2 according to the following reaction.[6]

$$ZrB_{2\,(s)} + 5/2\ O_{2\,(g)} \rightarrow ZrO_{2\,(s)} + B_2O_{3\,(l)} \qquad (1)$$

Previous studies have recognized three different temperature stages for oxidation of ZrB_2.[7] The low temperature stage occurs below about 1100°C, at which a continuous crystalline ZrO_2 layer and a liquid/glassy B_2O_3 layer form on the surface of unoxidized ZrB_2 matrix, providing passive oxidation protection. Based on mass gain and increasing oxide scale thickness, the kinetics of oxidation is parabolic in the first stage.[8-12] The second oxidation stage is between ~1100 and ~1400°C. At these temperatures, the weight change represents a combination of mass gain due to formation of ZrO_2 and B_2O_3, and mass loss from evaporation of B_2O_3.[9, 12, 13] Kinetics in this stage are para-linear due to the combination of the protective nature of the B_2O_3 layer (parabolic component) and the mass loss due to B_2O_3 evaporation (linear component). The third oxidation stage is above ~1500°C. At these temperatures, the evaporation rate of B_2O_3 is more significant. As a result, nearly all of the B_2O_3 is lost by evaporation and a porous ZrO_2 scale covers the surface. In this stage, the mass gain kinetics are linear, indicating that the oxide layers do not act as a barrier to oxygen transport.[8]

Several studies have shown that addition of transition metals such as Mo-, Nb-, V-, Cr-, Ti-, and Ta-borides or silicates can improve the oxidation resistance of ZrB_2 and ZrB_2-SiC ceramics.[14-19] However, very few studies have examined the effects of transition metal additives on oxidation behavior of silicon-free ZrB_2 ceramics. Zhang *et al.*[13, 20] reported that the additions of tungsten carbide (WC) improved the oxidation resistance of ZrB_2 ceramics by formation of WO_3 in the oxide scale. The WO_3 reacted with ZrO_2 to form a liquid phase, which acted as a sintering aid for ZrO_2 scale and, consequently, increased the relative density of the scale. Subsequent studies have shown

that the addition of W and Nb to nominally pure ZrB_2 improved its oxidation resistance by increasing the stability of the protective liquid/glassy B_2O_3 scale.[7, 21]

The purpose of the present study was to investigate the effects of different transition metal additives such as W, Mo, and Nb on the oxidation behavior of ZrB_2 ceramics at 1600°C, to find the most effective TM for improving the oxidation resistance of ZrB_2 ceramics at elevated temperatures.

4.2. Experimental procedure

High purity (>99%) ZrB_2 powder (~2 μm, Grade B, H.C. Starck, Newton, MA) was used to prepare the ZrB_2 specimens for this study. Also, 2 wt% B_4C (~0.8 μm, Grade HS, H.C Starck) was added to all batches to remove the oxide impurities from the surface of ZrB_2 powder particles and enhance densification.[22] For some batches, 4 mol% tungsten, molybdenum, or niobium was added in form of W (~3 μm, Alfa Aesar, Ward Hill, MA), Mo (~3 μm, Alfa Aesar), and Nb (~1 μm, Alfa Aesar) all with reported purities of >99.9%. Hereafter, ZrB_2 ceramics with only B_4C additions are referred to as "nominally pure ZrB_2", while ZrB_2 with B_4C and W, Mo, or Nb additions are referred to as $(Zr,W)B_2$, $(Zr,Mo)B_2$, and $(Zr,Nb)B_2$, respectively.

Ball milling in methyl ethyl ketone with ZrO_2 media for 24 hr was used to mix the powders. Measurement of the mass of zirconia media before and after ball milling showed that the amount of ZrO_2 contamination added to the powder mixtures was less than 1 wt% based on the mass of ZrB_2 powder. After drying and sieving (-80 mesh), the powders were densified by hot pressing (Model HP-3060, Thermal Technology, Santa Rosa, CA) at 2100 °C for 45 min at a pressure of 32 MPa. Bars with dimensions of 10 mm by 4 mm by 4 mm were cut from the hot pressed billets and finished by polishing on

all sides with a final polishing step using a 15 μm diamond slurry. The bulk density of the hot pressed billets was measured by using the Archimedes technique, with water as the immersing medium. X-ray diffraction (XRD; Philips X-Pert Pro diffractometer, Westborough, MA) was used to identify major crystalline phases present in the pre-oxidized composites.

A $MoSi_2$ resistance-heated horizontal tube furnace (Model 0000543, CM Inc., Bloomfield, NJ) with a high-purity alumina tube with a diameter of 6.35 cm was used for oxidation studies. Specimens were heated to desired temperatures with a heating rate of ~5 °C/min and an air flow rate of 0.2 cm/s (linear flow rate was calculated from the volumetric flow rate and the diameter of the tube). Specimens were removed from the furnace after the desired oxidation time and air quenched to room temperature to minimize changes such as further oxidation or evaporation of B_2O_3 that may occur during cooling. Specimens that were quenched immediately after reaching the desired temperature were said to be oxidized for "0 hours" while other specimens were oxidized up to 6 hours before quenching. To study the microstructure and calculate the thicknesses of the oxide layers, fracture surfaces were observed using secondary electron scanning electron microscopy (SEM; S-4700, Hitachi, Japan) and optical microscopy (Hirox KH-8700, Hackensack, NJ). The thickness of the oxide layers were measured using image analysis software (ImageJ, U. S. National Institutes of Health, Bethesda, MD) and averaging of 20 measurements. Chemical compositions of the oxide scales were studied using energy dispersive spectroscopy (EDS; EDAX, Mahwah, NJ).

4.3. Results and Discussion

4.3.1. Scale thickness and morphology

All of the ZrB_2 specimens reached relative densities of >95%. Archimedes' density measurements indicated that open porosity was not significant in any of the specimens. Hence, porosity was not considered to have a significant effect on the oxidation behavior. In addition, XRD analysis indicated that all of the TM additives dissolved into the ZrB_2, forming $(Zr,TM)B_2$ solid solutions.

Assuming that oxidation proceeds stoichiometrically, oxidation of $(Zr,TM)B_2$ should produce a combination of molten B_2O_3 (melting temperature ~450°C), solid ZrO_2 (monoclinic below 1170°C and tetragonal above), and solid TM-oxide. As reported in previous studies,[7, 21] two distinct layers covered the surface of the ZrB_2 and $(Zr,TM)B_2$ ceramics after oxidation at temperatures between 800 and 1600°C: (1) an outer glassy layer mainly consisting of B_2O_3, and (2) an inner layer mainly consisting of porous zirconia with the pores filled with B_2O_3. Due to low sensitivity of EDS to light elements, quantification of the boron content in the glassy phase was not possible. However, results obtained by EDS indicated that the glassy phase contained O and TM along with a small amount of Zr. According to the ZrO_2-B_2O_3 [23], WO_3-B_2O_3 [24], and Nb_2O_5-B_2O_3 [25] phase diagrams, the solubility of ZrO_2 and Nb_2O_5 in pure liquid B_2O_3 at 800 °C is negligible, while approximately 10 mol% WO_3 can dissolve into B_2O_3 at that temperature. No phase diagram was found for B_2O_3-Mo oxide systems. The formation of two-layer scales is due to immiscibility of ZrO_2 and B_2O_3 combined with the large volume expansion (~300% based on density calculations) associated with oxidation of ZrB_2 to ZrO_2 and B_2O_3.[6] The addition of TM to ZrB_2 does not affect the formation of the two layer structure, but

varying amounts of the TMs are incorporated into the B_2O_3, depending on the solubility of the particular TM.

Figure 1 shows the SEM images obtained from the surfaces of nominally pure ZrB_2 and ZrB_2 containing 4 mol% W, Mo, or Nb after oxidation at 1600°C for 0 hours. The majority of the areas of the surfaces of the specimens had light contrast, but some areas were darker. The light-colored areas contained Zr and TM oxides, while the darker areas had a glassy appearance and was composed of B_2O_3 containing small amounts of Zr and TM. The amount of the dark phase observed on the surfaces of ceramics oxidized at 1600°C for 0 hours increased from ~5% of the surface covered for nominally pure ZrB_2 to ~10% for $(Zr,W)B_2$, ~20% for $(Zr,Mo)B_2$, and ~15% for $(Zr,Nb)B_2$. At 1600°C, the dissolution of ZrO_2 into B_2O_3 increases to 24 mol%,[23] while both WO_3 and Nb_2O_5 are completely miscible with B_2O_3 due to the lower melting points of the TM oxides (1435°C[24] for WO_3 and 1485°C[25] for Nb_2O_5) compared to the melting point of ZrO_2 (2715°C). Since MoO_3 melts at 795°C, it is also expected to be completely miscible with B_2O_3 at 1600°C.

The higher coverage of the glassy phase on $(Zr,Nb)B_2$ compared to $(Zr,W)B_2$ is consistent with evaporation data obtained by thermogravimetric analysis that showed lower weight loss from B_2O_3 containing Nb_2O_5 compared to B_2O_3 containing WO_3.[26] One possible reason for the lower stability of the WO_3-B_2O_3 glass is the evaporation rate of WO_3, which is high at temperatures above 1300°C.[27, 28]

After oxidation at 1600°C for 0 hours, the thickness of the porous scale for nominally pure ZrB_2 was ~85 μm compared to ~30 μm for $(Zr,W)B_2$, and ~40 μm for $(Zr,Mo)B_2$ and $(Zr,Nb)B_2$ (Table 1). The lower thickness of the scales on $(Zr,TM)B_2$

ceramics is an indication of the effectiveness of W, Mo and Nb additions on improving the oxidation resistance of ZrB_2. Since the liquid/glassy B_2O_3 scale is the diffusion barrier that protects unoxidized ZrB_2 from oxygen in the external atmosphere, retention of the glassy phase on $(Zr,TM)B_2$ specimens should improve the oxidation resistance of these ceramics compared to nominally pure ZrB_2. Interestingly, $(Zr,W)B_2$ had a lower porous scale thickness compared to $(Zr,Mo)B_2$ and $(Zr,Nb)B_2$, despite higher stability of the glassy phases on ZrB_2 with Mo or Nb additions. The improved oxidation protection of the W-containing ceramic could be due to the effect of WO_3, which alters the microstructure of the porous ZrO_2 layer by liquid phase sintering.[13, 20] The higher relative density of the ZrO_2 scale on $(Zr,W)B_2$ ceramics apparently resulted in lower oxygen permeability and, therefore, lower oxide scale thickness at this condition.

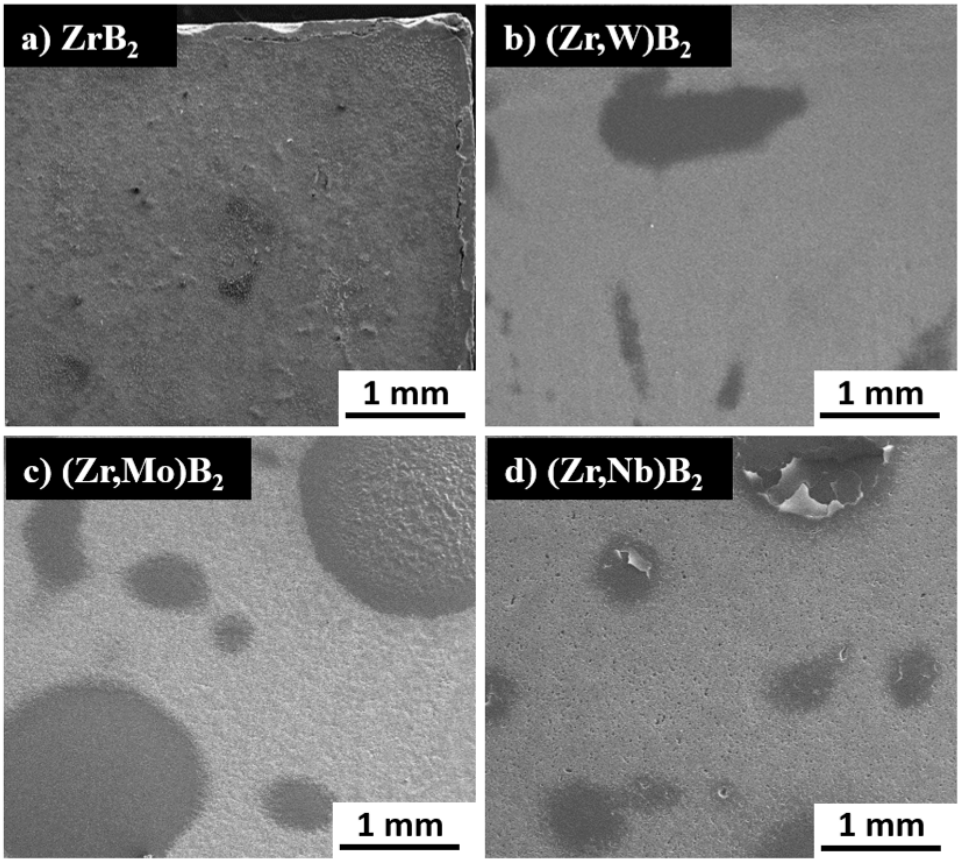

Figure 1. Surfaces of (a) nominally pure ZrB_2, (b) $(Zr,W)B_2$, (c) $(Zr,Mo)B_2$, and (d) $(Zr,Nb)B_2$ after oxidation at 1600°C for 0 hours.

After oxidation at 1600°C for 3 hours, the scales formed on all of the specimens consisted of a porous oxide layer. Some residual glassy phase was observed between the oxide particles in the $(Zr,TM)B_2$ ceramics, but the glassy phase was not continuous. Although no continuous glassy layer covers the top surface, the glassy phase between the oxide particles would reduce permeability of the pore channels and reduce oxidation rate.[29] The thickness of the porous oxide layer was highest for nominally pure ZrB_2 (~570 μm), while it was about 0.7 as thick for $(Zr,W)B_2$ (~380 μm), $(Zr,Mo)B_2$ (~390 μm), and

$(Zr,Nb)B_2$ (~300 μm) (Table 1). Hence, even after most of the glassy phase has evaporated, the transition metals have some beneficial effect on scale thickness.

Table 1. Thickness of porous oxide scales of nominally pure ZrB_2 and ZrB_2 with 4 mol% W, Mo, or Nb after oxidation at 1600°C for 0 or 3 hours.

Material	Oxide scale thickness (μm)	
	0 hours	3 hours
ZrB_2	85 ± 6	570 ± 19
$(Zr,W)B_2$	30 ± 3	376 ± 16
$(Zr,Mo)B_2$	40 ± 2	386 ± 17
$(Zr,Nb)B_2$	41 ± 2	294 ± 13

Figure 2 shows the surfaces of nominally pure ZrB_2 and $(Zr,TM)B_2$ specimens after oxidation at 1600°C for 3 hours. The surfaces of nominally pure ZrB_2 and $(Zr,W)B_2$ were rough. As shown in the image insets in Figure 2a and Figure 2b, raised areas about 10 μm in diameter were observed on the surfaces. Charging around the highest points of the raised areas produced the contrast observed in the images. There were some gaps between the grain boundaries and more severely on the triple points between the oxide grains on the surfaces of ZrB_2 and $(Zr,W)B_2$. The similarity of the morphology of the oxide scales for nominally pure ZrB_2 and $(Zr,W)B_2$ at 1600°C may be due to the volatility of the respective liquid oxides. Both B_2O_3 and WO_3 are volatile at 1600°C. The

complete evaporation of these oxides from the surface, along with the accompanying precipitation of ZrO_2 from the evaporating liquid, may be a contributing factor to the morphology of the surface of the scale.

The surfaces of $(Zr,Mo)B_2$ and $(Zr,Nb)B_2$ were different than nominally pure ZrB_2 and $(Zr,W)B_2$ after oxidation at 1600°C for 3 hours. The white dashed lines in Figure 2c and Figure 2d correspond to the last areas of the surfaces that were covered by pools of liquid oxide. Bubbles and ruptured bubbles were observed in some of the areas between the glassy pools as shown by black dashed lines. The effect was more pronounced for $(Zr,Mo)B_2$. As shown in the image insets in Figure 2c and Figure 2d, the areas between the pools on $(Zr,Mo)B_2$ and $(Zr,Nb)B_2$ were continuous and showed no sign of rupture or gaps. The areas between the pools appeared to be nearly fully dense with the porosity of the surrounding oxide layer increasing near the pools.

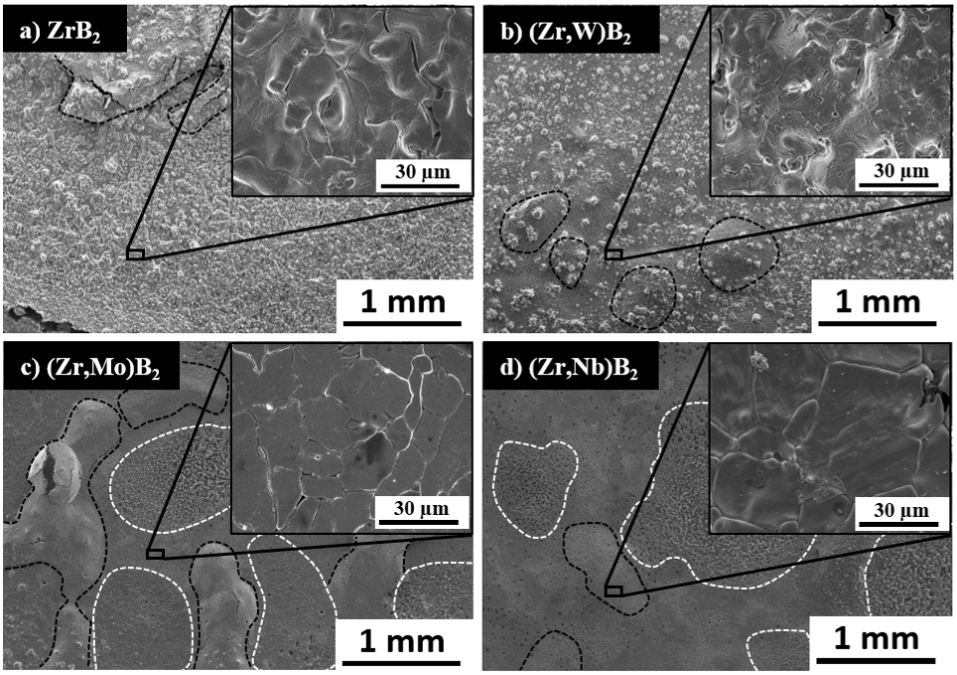

Figure 2. Surfaces of (a) nominally pure ZrB_2, (b) $(Zr,W)B_2$, (c) $(Zr,Mo)B_2$, and (d) $(Zr,Nb)B_2$ after oxidation at 1600°C for 3 hours. The black dashed lines shows the large swellings on the surfaces, while the white dashed lines show the last areas of the surfaces that were covered by the glassy pools.

Figure 3 shows cross sectional SEM images from areas with ruptures or gaps in the scale that form on nominally pure ZrB_2 and $(Zr,Nb)B_2$ after oxidation at 1600°C for 3 hours. The raised area marked with an arrow in Figure 3a is similar to the features that appeared to be the high points of raised areas in Figure 2a. The scale appears to be thicker and the gap in the scale indicates poor adhesion between the outer layer with the layer beneath it. Again, the raised areas are thought to form due to evaporation of B_2O_3. Figure 3b shows a cross section of an area near what appears to be a void in the oxide scale. This area also seems to be where the scale has delaminated. Similar voids are seen in the oxide scale on both $(Zr,Mo)B_2$ and $(Zr,Nb)B_2$. Presumably, the voids are channels to allow release of B_2O_3 vapor, which cannot otherwise escape as the surrounding scale

appears to be dense. The voids may be caused by rupture of the top surface of the oxide layers on $(Zr,Mo)B_2$ and $(Zr,Nb)B_2$. These ruptures appear to be similar to those observed by Karlsdottir et al.[23], which occurred as result of evaporation of $SiO_{(g)}$ formed during oxidation of ZrB_2-SiC ceramics. However, since the scale on nominally pure ZrB_2 and $(Zr,W)B_2$ are composed of crystalline ZrO_2-based grains, rupture appears to occur at grain boundaries, resulting in several small ruptures across the surfaces. As a result, the outer oxide layers on nominally pure ZrB_2 and $(Zr,W)B_2$ are not adhered well to the layers beneath and tend to spall. The top layers on $(Zr,Mo)B_2$ and $(Zr,Nb)B_2$ have better adhesion and less tendency to spall.

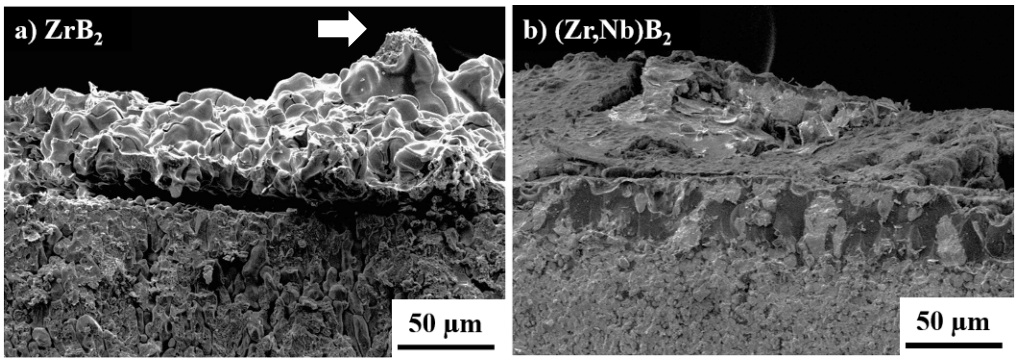

Figure 3. Fracture surfaces of (a) nominally pure ZrB_2, and (b) $(Zr,Nb)B_2$ after oxidation at 1600°C for 3 hours, showing the difference between the raised areas on ZrB_2 and $(Zr,Nb)B_2$.

4.3.2. Dark and light zirconia scale layers

Previously published studies and the analysis presented above present oxide scale thickness as a quantity that can be measured easily. However, examination as part of the present study has revealed several complications that have likely led to inconsistencies

measuring and reporting scale thicknesses. The next several paragraphs describe the presence of two sub-layers within what is described as the "porous ZrO_2" layer above. Specimen size raises additional complications with measurements that are discussed.

Figure 4 shows optical micrographs of fracture surfaces of nominally pure ZrB_2 and (Zr,TM)B_2 specimens after oxidation at 1600°C for 6 hours. Here, specimens were oxidized at 1600°C for 6 hours to thicken both layers and enable better resolution using optical microscopy. The oxide scales consisted of two layers similar to observations of Zhang et al.[20] The outer layer (outside the white line) was lighter in contrast while the inner layer was darker. The dark layer appeared dense with a metallic shine, like the unoxidized matrix. In contrast, the outer layer had a lighter color, was porous, and did not exhibit a metallic appearance. The dark layer appeared to be strongly adhered to the unoxidized matrix with no delamination observed between the dark layer and the matrix. However, adhesion between the light and dark layers was weaker, which often resulted in damage to the interface during polishing. Higher apparent density of the dark layer compared to the light layer should result in lower oxygen transport through the dark layer, which might make it the rate limiting step of oxidation in absence of the liquid/glassy B_2O_3 layer.

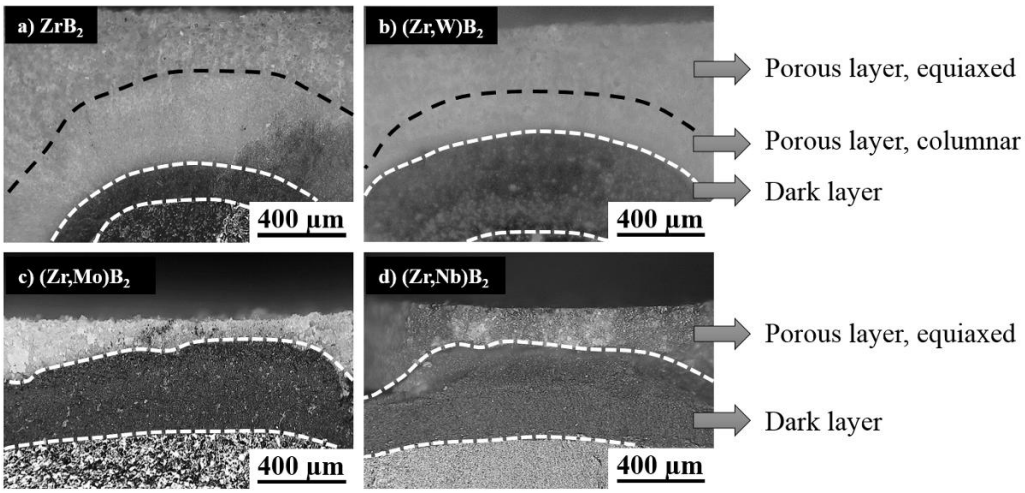

Figure 4. Optical micrographs of fracture surfaces of (a) nominally pure ZrB_2, (b) $(Zr,W)B_2$, (c) $(Zr,Mo)B_2$, and (d) $(Zr,Nb)B_2$ after oxidation at 1600°C for 6 hours.

Figure 5 shows SEM images of a fracture surface and polished cross section of $(Zr,W)B_2$ after oxidation at 1600°C for 6 hours. The dark layer was nearly impossible to distinguish from the unoxidized matrix in SEM images of polished specimens. Hence, the thickness of the dark layer is likely to not be included in scale thickness measurements for studies that utilize polished cross sections and SEM images for analysis of oxidation behavior. Examination of fracture surfaces allowed for more contrast due to topology differences between the dark layer and the unoxidized matrix that are removed by polishing; however, the dark and light layers were not distinguishable from the fracture surface. As a result, the scale thickness might be reported as ~1000 µm from the fracture surface, but ~540 µm from the polished section even though these specimens were oxidized under the same conditions. This discrepancy is only an issue for oxidation conditions at which the glassy scale has retreated beneath the outer surface.

The best ways to characterize scale thicknesses, to capture both the dark and light layers, seems to be optical microscopy combined with SEM of fractured surfaces. Regions of the oxide scale from which the glassy phase has evaporated appear lighter in color (i.e., white and porous) while regions in which the pores are still filled with B_2O_3 appear dark. Studies using SEM analysis of polished sections may not observe the layer that appears darker by optical microscopy and, therefore, underestimate the total oxide layer thickness.

Another complication is that oxide layers can have a curved shape after severe oxidation as shown in Figures 4 and 5. The curvature is an artifact of specimen size. In this case, the oxide-matrix interface curves (i.e., the oxide layer becomes thicker) near the corners of the original specimen due to oxygen permeation from orthogonal faces. For the present study, all the measurements of oxide scale thicknesses were performed near the middle of the faces of specimens, which had lower curvatures and were assumed to be more representative of the oxidation of an infinite plate.

Considering both layers of the scale, the thickness after oxidation at 1600°C for 6 hours was highest for $(Zr,W)B_2$ at ~910 μm followed by ~860 μm for ZrB_2, ~610 μm for $(Zr,Nb)B_2$, and ~520 μm for $(Zr,Mo)B_2$. The higher apparent density of the dark scale should make it a better barrier to oxidation compared to the lighter scale. Therefore, the vulnerability of specimens to oxidation can be determined from the thickness of the lighter layer. Nominally pure ZrB_2 had the greatest thickness of the light layer (~700 μm), followed by $(Zr,W)B_2$ (~460 μm). The lighter layers were significantly thinner for $(Zr,Nb)B_2$ (~180 μm) and $(Zr,Mo)B_2$ (~120 μm). Likewise, the dark layer was thinnest for nominally pure ZrB_2 (~160 μm) compared to dark layers that were more than twice as

thick for $(Zr,Mo)B_2$ (~400 μm), $(Zr,Nb)B_2$ (~430 μm), and $(Zr,W)B_2$ (~450 μm). The standard deviations for the mentioned thicknesses were between 10 and 20 μm. While W additions may not provide a significant improvement to oxidation resistance at 1600°C, Mo and Nb additions resulted in significantly lower thicknesses for the light oxide layers. As mentioned above, the light layer forms as B_2O_3 evaporates. The lower thickness of the light layer for $(Zr,Mo)B_2$, $(Zr,Nb)B_2$, and $(Zr,W)B_2$ compared to nominally pure ZrB_2 indicate higher stability of the glassy phases in these materials.

As discussed in a previous article,[21] the outer surface of the porous oxide scale is initially composed of equiaxed particles when it is still covered by a layer of liquid/glassy B_2O_3. The particles form as the result of dissolution of ZrO_2 and TM oxides into the B_2O_3 melt followed by reprecipitation. As B_2O_3 evaporates, the solution-precipitation mechanism is no longer possible due to loss of liquid B_2O_3 at the outer surface, but ZrO_2 will continue to precipitate as the B_2O_3 scale evaporates. As the B_2O_3 surface recedes into the porous oxide, ZrO_2 takes a columnar morphology. The black dashed lines in Figure 4 indicates the border between equiaxed ZrO_2 and ZrO_2 with the columnar morphology for the scale on nominally pure ZrB_2 and $(Zr,W)B_2$. Under the same oxidation conditions, the light layer on $(Zr,Mo)B_2$ and $(Zr,Nb)B_2$ specimens was composed of only equiaxed particles. Liquid phases with higher stability at lower oxidation temperatures resulted in thicker primary precipitated oxide layers on $(Zr,Mo)B_2$ and $(Zr,Nb)B_2$. In turn, the thicker primary oxide layers may lead to improved oxidation resistance due to the more uniform morphology. In addition, the equiaxed oxide may be less prone to spallation than the columnar oxide on ZrB_2.

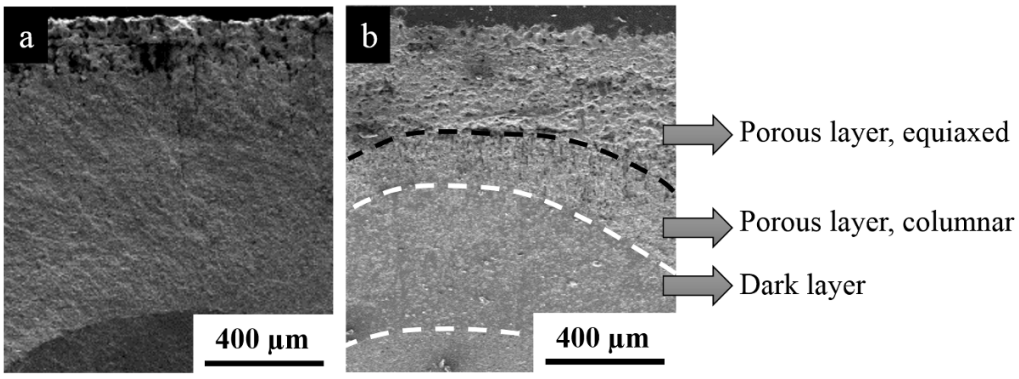

Figure 5. SEM images of (a) a fracture surface, and (b) a polished cross section of $(Zr,W)B_2$ after oxidation at 1600°C for 6 hours.

4.3.3. Model of oxidation of ZrB_2 ceramics at 1600°C

Figure 6 is a schematic that describes the evolution of the structure of the oxide layer that forms during oxidation of ZrB_2 ceramics at 1600°C. In the early stages of oxidation (left panel), a liquid B_2O_3 layer is present along with ZrO_2 particles. At this stage, liquid B_2O_3 fills all of the pores of the ZrO_2 and this oxide scale has an iridescent appearance, similar to observations for oxidation of zirconium and zirconium alloys.[30-32] Similar to the oxide scale at this stage, the dark oxide layer on zirconium is dense, adherent, and protective against oxidation, resulting in parabolic oxidation kinetics.[31] Parabolic oxidation kinetics indicate that the oxide layer acts as a barrier to inward transport (presumably diffusion) of oxygen. For Zr and its alloys, a process called "transition" or "breakaway" converts part of the dark layer (presumably oxygen-deficient ZrO_2) to a lighter layer that is porous and tends to spall. Once this transformation occurs, linear oxidation kinetics are observed, indicating that the oxide layer is no longer protective. The mechanism of breakaway is still controversial.[31, 33] The formation of a

similar dark scale has been reported for ZrB_2 ceramics,[20, 34, 35] but has not been discussed in detail in any publication.

In the initial stages of oxidation, equiaxed oxide particles form beneath the liquid B_2O_3 layer. The particles form by solution-precipitation as has been discussed elsewhere.[21] With increasing oxidation temperature or time, evaporation of B_2O_3 increases and some parts of the porous layer are exposed, and, consequently, become the layer that appears lighter in optical micrographs. Evaporation of B_2O_3 is more severe at higher temperatures, resulting in recession of the liquid into the porous layer (second panel in the schematic), and, eventually, nearly complete loss of B_2O_3 (final panel in the schematic). When the liquid recedes from the outer surface, ZrO_2 particles can no longer form at the outer surface due to lack of the liquid phase to transport dissolved ZrO_2. Continued growth of ZrO_2 presumably occurs mainly from the receding front, which is now beneath the outer surface of the specimen. Hence, the columnar morphology may develop as the originally equiaxed particles act as growth sites for ZrO_2 precipitating from the receding B_2O_3.

At temperatures at which the (TM-oxide)-B_2O_3 layer formed on (Zr,TM)B_2 also evaporates (i.e. above about 1400°C) the differences between the TMs were more obvious. The higher volatility of WO_3 and the resulting WO_3-B_2O_3 mixtures, compared to Nb_2O_5-B_2O_3, resulted in lower coverage of the surface of (Zr,W)B_2 by the glassy phase compared to (Zr,Nb)B_2 after oxidation at 1600°C for 0 hours. The thicker porous zirconia layer for (Zr,Nb)B_2 compared to (Zr,W)B_2 was presumably due to liquid phase sintering of ZrO_2 in the presence of WO_3. However, increasing the oxidation time to 3 hours at 1600°C resulted in more WO_3 evaporation making the surface of (Zr,W)B_2 appear similar

to nominally pure ZrB_2 rather than $(Zr,Nb)B_2$. Earlier evaporation of the protective glassy layer from $(Zr,W)B_2$ resulted in a thicker zirconia layer for $(Zr,W)B_2$ compared to $(Zr,Nb)B_2$. Although no phase diagrams were available for the MoO_3-B_2O_3 and ZrO_2-MoO_3 systems, the oxidation behavior of $(Zr,Mo)B_2$ was very similar to $(Zr,Nb)B_2$, meaning that the MoO_3-B_2O_3 and MoO_3-ZrO_2 systems likely resemble their Nb analogues.

After oxidation at 1600°C for 6 hours, the porous (light) oxide layer was thicker for $(Zr,W)B_2$ compared to $(Zr,Mo)B_2$ or $(Zr,Nb)B_2$, which indicates a resistance to oxygen transport from the surface to the dark layer. However, the thicknesses of the dark oxide layers were almost the same for all of the $(Zr,TM)B_2$ ceramics and higher than for nominally pure ZrB_2. It can be speculated that all of the TM additions have about the same effect on the transport rate of oxygen from the interface between the light and dark layers to the unoxidized matrix.

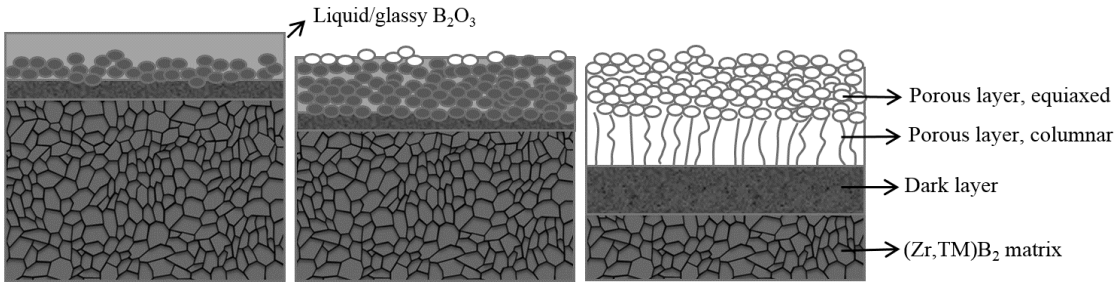

Figure 6. Model of the evolution of the oxide structure of ZrB_2 ceramics.

4.4. Conclusion

The effects of additions of W, Mo, or Nb on oxidation behavior of ZrB_2 were investigated. After oxidation at 1600°C for 0 hour, the higher stability of Nb_2O_5-B_2O_3 resulted in lower oxide scale thicknesses for $(Zr,Nb)B_2$ compared to nominally pure ZrB_2 and other $(Zr,TM)B_2$ specimens. Two distinct sub-layers were observed in the porous oxide layer after oxidation at 1600°C for 6 hours, an outer layer that was lighter in color and an inner layer that was darker. The thickness of the light layer for nominally pure ZrB_2 was almost 1.5 times greater than for $(Zr,W)B_2$ and 4 times higher than $(Zr,Mo)B_2$ and $(Zr,Nb)B_2$. Lower scale thicknesses of the light layer for $(Zr,Mo)B_2$ and $(Zr,Nb)B_2$ indicated that Mo and Nb were more effective in reducing oxygen transport from the external atmosphere toward the interface between the light and dark layers. However, the thicknesses of the dark layers were almost the same for all of the $(Zr,TM)B_2$ specimens and almost twice as thick as the dark layer for nominally pure ZrB_2, showing the same effect of TM additions on lowering oxygen diffusion through the dark layer toward the unoxidized matrix. Additions of Mo or Nb were most effective in improving the oxidation resistance of ZrB_2 by increasing the stability of the protective liquid/glassy B_2O_3 layer and reducing oxygen transport through the light layer.

Acknowledgment

This work was supported as part of the National Hypersonic Science Center for Materials and Structures (Grant FA9550-09-1-0477) with Dr. Ali Sayir (AFOSR) and Dr. Anthony Calomino (NASA) as program managers. The authors wish to thank project principal investigator Dr. David Marshall of Teledyne Scientific and Imaging for his support and guidance.

References

1. K. Upadhya, J. M. Yang, and W. P. Hoffman, "Materials for Ultrahigh Temperature Structural Applications," *American Ceramic Society Bulletin,* 76[12] 51-56 (1997).
2. D. M. Van Wie, D. G. Drewry Jr, D. E. King, and C. M. Hudson, "The hypersonic environment: Required operating conditions and design challenges," *Journal of Materials Science,* 39[19] 5915-24 (2004).
3. S. Q. Guo, "Densification of ZrB_2-Based Composites and Their Mechanical and Physical Properties: A Review," *Journal of the European Ceramic Society,* 29[6] 995-1011 (2009).
4. L. Zhang, D. A. Pejaković, J. Marschall, and M. Gasch, "Thermal and Electrical Transport Properties of Spark Plasma-Sintered HfB_2 and ZrB_2 Ceramics," *Journal of the American Ceramic Society,* 94[8] 2562-70 (2011).
5. A. Bongiorno, C. J. Först, R. K. Kalia, J. Li, J. Marschall, A. Nakano, M. M. Opeka, I. G. Talmy, P. Vashishta, and S. Yip, "A Perspective on Modeling Materials in Extreme Environments: Oxidation of Ultrahigh-Temperature Ceramics," *MRS Bulletin,* 31[05] 410-18 (2006).
6. A. Rezaie, W. G. Fahrenholtz, and G. E. Hilmas, "Evolution of Structure during the Oxidation of Zirconium Diboride-Silicon Carbide in Air up to 1500°C," *Journal of the European Ceramic Society,* 27[6] 2495-501 (2007).
7. M. Kazemzadeh Dehdashti, W. G. Fahrenholtz, and G. E. Hilmas, "Effects of Temperature and the Incorporation of W on the Oxidation of ZrB_2 Ceramics," *Corrosion Science,* 80 221-28 (2014).
8. W. C. Tripp and H. C. Graham, "Thermogravimetric Study of the Oxidation of ZrB_2 in the Temperature Range of 800° to 1500°C," *Journal of The Electrochemical Society,* 118[7] 1195-99 (1971).
9. A. K. Kuriakose and J. L. Margrave, "The Oxidation Kinetics of Zirconium Diboride and Zirconium Carbide at High Temperatures," *Journal of The Electrochemical Society,* 111[7] 827-31 (1964).
10. F. Monteverde and A. Bellosi, "Oxidation of ZrB_2-based Ceramics in Dry Air," *Journal of The Electrochemical Society,* 150[11] B552-B59 (2003).
11. J. B. Berkowitz-Mattuck, "High-Temperature Oxidation III. Zirconium and Hafnium Diborides," *Journal of The Electrochemical Society,* 113[9] 908-14 (1966).
12. R. J. Irving and I. G. Worsley, "The Oxidation of Titanium Diboride and Zirconium Diboride at High Temperatures," *Journal of the Less Common Metals,* 16[2] 103-12 (1968).
13. S. C. Zhang, G. E. Hilmas, and W. G. Fahrenholtz, "Improved Oxidation Resistance of Zirconium Diboride by Tungsten Carbide Additions," *Journal of the American Ceramic Society,* 91[11] 3530-35 (2008).
14. F. Peng, Y. Berta, and R. F. Speyer, "Effect of SiC, TaB_2 and $TaSi_2$ Additives on the Isothermal Oxidation Resistance of Fully Dense Zirconium Diboride," *Journal of Materials Science,* 24 [5] 1855-67. (2009).

15. I. G. Talmy, J. A. Zaykoski, M. M. Opeka, and S. Dallek, "Oxidation of ZrB_2 Ceramics Modified with SiC and Group IV-VI Transition Metal Diborides," *Electrochemical Society Proceedings,* 12 144-58 (2001).
16. P. Hu, X. H. Zhang, J. C. Han, X. G. Luo, and S. Y. Du, "Effect of Various Additives on the Oxidation Behavior of ZrB_2-Based Ultra-High-Temperature Ceramics at 1800°C," *Journal of the American Ceramic Society,* 93[2] 345-49 (2010).
17. X. H. Zhang, P. Hu, J. C. Han, L. Xu, and S. H. Meng, "The Addition of Lanthanum Hexaboride to Zirconium Diboride for Improved Oxidation Resistance," *Scripta Materialia,* 57[11] 1036-39 (2007).
18. S. R. Levine and E. J. Opila, "Tantalum Addition to Zirconium Diboride for Improved Oxidation Resistance." in. NASA/TM-2003-212483, 2003.
19. D. Sciti, M. Brach, and A. Bellosi, "Oxidation Behavior of a Pressureless Sintered ZrB_2–$MoSi_2$ Ceramic Composite," *Journal of Materials Research,* 20[4] 922-30 (2005).
20. S. C. Zhang, G. E. Hilmas, and W. G. Fahrenholtz, "Oxidation of Zirconium Diboride with Tungsten Carbide Additions," *Journal of the American Ceramic Society,* 94[4] 1198-205 (2011).
21. M. Kazemzadeh Dehdashti, W. G. Fahrenholtz, and G. E. Hilmas, "Oxidation of Zirconium Diboride with Niobium Additions," *Journal of the European Ceramic Society,* 33[10] 1591-98 (2013).
22. G. J. K. Harrington, G. E. Hilmas, and W. G. Fahrenholtz, "Effect of Carbon and Oxygen on the Densification and Microstructure of Hot Pressed Zirconium Diboride," *Journal of the American Ceramic Society,* 96[11] 3622-30 (2013).
23. S. N. Karlsdottir, J. W. Halloran, and A. N. Grundy, "Zirconia Transport by Liquid Convection during Oxidation of Zirconium Diboride-Silicon Carbide," *Journal of the American Ceramic Society,* 91[1] 272-77 (2008).
24. E. M. Levin, "The System WO_3-B_2O_3," *Journal of the American Ceramic Society,* 48[9] 491-92 (1965).
25. E. M. Levin, "Phase Equilibria in the System Niobium Pentoxide-Boric Acid," *Journal of Research of the National Bureau of Standards,* 70A[1] 11-16 (1966).
26. M. K. Dehdashti, W. G. Fahrenholtz, and G. E. Hilmas, "Effect of Transition Metal Oxide Additions on the Structure of B_2O_3 Glasses."
27. J. Batty and R. Stickney, "Quasiequilibrium Treatment of Gas-solid Reactions. III. Rate of Volatilization of Tungsten by High-temperature Oxidation," *Oxidation of Metals,* 3[4] 331-55 (1971).
28. A. P. Richard and D. D. Edwards, "Subsolidus Phase Relations and Crystal Structures of the Mixed-oxide Phases in the In_2O_3–WO_3 System," *Journal of Solid State Chemistry,* 177[8] 2740-48 (2004).
29. T. A. Parthasarathy, R. A. Rapp, M. Opeka, and R. J. Kerans, "A Model for the Oxidation of ZrB_2, HfB_2 and TiB_2," *Acta Materialia,* 55[17] 5999-6010 (2007).
30. N. Ni, D. Hudson, J. Wei, P. Wang, S. Lozano-Perez, G. D. W. Smith, J. M. Sykes, S. S. Yardley, K. L. Moore, S. Lyon, R. Cottis, M. Preuss, and C. R. M. Grovenor, "How the Crystallography and Nanoscale Chemistry of the Metal/oxide Interface Develops during the Aqueous Oxidation of Zirconium Cladding Alloys," *Acta Materialia,* 60[20] 7132-49 (2012).

31. T. Ahmed and L. H. Keys, "The Breakaway Oxidation of Zirconium and its Alloys: A Review," *Journal of the Less Common Metals,* 39[1] 99-107 (1975).
32. J. Lin, H. Li, J. Szpunar, R. Bordoni, A. Olmedo, M. Villegas, and A. Maroto, "Analysis of Zirconium Oxide Formed during Oxidation at 623 K on Zr–2.5 Nb and Zircaloy-4," *Materials Science and Engineering: A,* 381[1] 104-12 (2004).
33. M. Tupin, M. Pijolat, F. Valdivieso, and M. Soustelle, "Oxidation Kinetics of ZrNbO in Steam: Differences between the Pre- and Post-Transition Stages," *Journal of Nuclear Materials,* 342[1–3] 108-18 (2005).
34. S. Zhou, W. Li, P. Hu, C. Hong, and L. Weng, "Ablation Behavior of ZrB_2-SiC-ZrO_2 Ceramic Composites by Means of the Oxyacetylene Torch," *Corrosion Science,* 51[9] 2071-79 (2009).
35. I. Akin, F. Cinar Sahin, O. Yucel, and G. Goller, "Oxidation Behavior of Zirconium Diboride-Silicon Carbide Composites," pp. 105-11. in 34th International Conference on Advanced Ceramics and Composites*,* Vol. 31. Daytona Beach, FL, 2010.

SECTION

3. SUMMARY AND CONCLUSIONS

The purpose of this dissertation was to investigate the effect of transition metals (TMs) on the oxidation behavior of ZrB_2 ceramics. Previous studies had shown that the addition of TMs improved the oxidation resistance of ZrB_2-SiC and ZrB_2 ceramics. However, the fundamental mechanisms of the oxidation behavior of nominally pure ZrB_2 with various TM additions were not investigated. This section provides a summary of the research followed by several conclusions that were reached from the overall project.

3.1. SUMMARY

This section summarizes the research related to the four questions stated in the introduction. Each question served as the focus for one of the main chapters of the dissertation.

1. How do the TM additives affect the oxide scale growth on ZrB_2?

The oxidation behavior of $(Zr,Nb)B_2$ ceramics was studied to determine the effect of Nb on the thickness and morphology of the oxide scales on ZrB_2. At 1500 °C, exposure to air resulted in the formation of a two-layer oxide scale structure on $(Zr,Nb)B_2$. The two layers were: (1) an outer layer of a glassy phase containing B_2O_3 with Nb and Zr dissolved in it; and (2) a porous oxide layer composed of oxide particles containing Zr and Nb. Small spherical particles, presumably a ZrO_2 containing dissolved Nb, grew in the glassy phase with increasing exposure time. Some of the particles were spherical while others were elongated. As the B_2O_3 evaporated, the particles became

concentrated and were eventually incorporated into the newly exposed porous oxide layer, which contained both ZrO_2 and $Nb_2Zr_6O_{17}$. As the glass receded, the small precipitated particles joined the porous oxide layer that was present under the glassy layer. Because of high melting point of $Nb_2Zr_6O_{17}$ that was formed in the porous oxide layer, liquid phase sintering was not active as has been reported for W-containing ZrB_2. However, dissolution of Nb into the B_2O_3 liquid phase increased the stability of the protective liquid layer by reducing the volatility of B_2O_3 from the liquid phase. Hence, $(Zr,Nb)B_2$ showed improved oxidation resistance compared to pure ZrB_2.

2. *What are the effects of W additives on the thickness of the porous oxide scale and the protective B_2O_3 layer in different regimes of oxidation behavior?*

The oxidation behavior of nominally pure ZrB_2 and $(Zr,W)B_2$ ceramics with 4, 6, or 8 mol% W was studied at temperatures ranging from 800 to 1600°C. Oxidation in this temperature range resulted in the formation of a two-layer scale: (1) an outer glassy layer containing B_2O_3 with dissolved W; and (2) a porous layer composed of oxide particles containing Zr and W. Based on scale thickness and weight gain measurements, two regimes of oxidation behavior were observed. The first stage was below 1100°C for nominally pure ZrB_2 and 1300°C for $(Zr,W)B_2$ specimens. No significant differences were measured for weight loss or scale thickness between nominally pure ZrB_2 and $(Zr,W)B_2$ compositions at temperatures between 800 and 1000°C. However, the glassy layer thicknesses and weight gains were higher for $(Zr,W)B_2$ specimens after oxidation from 1100 to 1300°C. It was concluded that dissolution of W into the B_2O_3 liquid phase increased the stability of the protective liquid layer by reducing the volatility of B_2O_3

from the liquid phase, resulting in a shift in the onset of the second oxidation regime toward higher temperatures for $(Zr,W)B_2$ specimens. This assumption was confirmed by TGA analysis of B_2O_3 and B_2O_3-WO_3 glasses. Above 1500°C, the outer glassy layer was removed from the surface of nominally pure ZrB_2 by evaporation, while a thin (up to ~3μm) glassy layer was still covering the $(Zr,W)B_2$ specimens. Further, the $(Zr,W)B_2$ compositions showed lower weight gains and had thinner oxidation scales compared to nominally pure ZrB_2 at 1600°C. The addition of W into B_2O_3 increased the stability of the protective liquid/glassy layer and resulted in higher oxidation resistance for $(Zr,W)B_2$ compared to nominally pure ZrB_2.

3. *How do the TM additives affect the evaporation and structural properties of B_2O_3 glass?*

The evaporation behavior of B_2O_3 with TM oxide additions was analyzed. Additions of tungsten, niobium, and zirconium oxides decreased the evaporation rate and increased the onset temperature for evaporation in B_2O_3-based glasses in the order of $WO_3<ZrO_2<Nb_2O_5$. High temperature Raman spectroscopy showed that WO_3 in the B_2O_3 glass was initially amorphous, but crystallized at temperatures above 500°C. In addition, the intensity of Nb_2O_5 peaks in the glass increased as a result of crystallization. No signs of formation of $BØ_4$ units was observed in the borate glasses by Raman spectroscopy or NMR. It was concluded that additions of WO_3, Nb_2O_5, or ZrO_2 to B_2O_3 did not change the structure of B_2O_3. Hence, the higher oxidation resistance of $(Zr,TM)B_2$ ceramics and lower evaporation rate of (TM-oxide)-B_2O_3 glasses should be due to the fact that the

dissolution of TM-oxide in B_2O_3 decreases the activity of B_2O_3 and, consequently, decreases the vapor pressure and evaporation rate of B_2O_3.

4. *What are the differences between the effects of different TM additives such as W, Mo, or Nb on oxidation of ZrB_2?*

The effects of additions of W, Mo, or Nb on oxidation behavior of ZrB_2 were investigated. After oxidation at 1600°C for 0 hours, the higher stability of Nb_2O_5-B_2O_3 resulted in lower oxide scale thicknesses for $(Zr,Nb)B_2$ compared to nominally pure ZrB_2 and other $(Zr,TM)B_2$ specimens. Two distinct sub-layers were observed in the porous oxide layer after oxidation at 1600°C for 6 hours, an outer layer that was lighter in color and an inner layer that was darker. The thickness of the light layer for nominally pure ZrB_2 was almost 1.5 times greater than for $(Zr,W)B_2$ and 4 times higher than $(Zr,Mo)B_2$ and $(Zr,Nb)B_2$. Lower scale thicknesses of the light layer for $(Zr,Mo)B_2$ and $(Zr,Nb)B_2$ indicated that Mo and Nb were more effective in reducing oxygen transport from the external atmosphere toward the interface between the light and dark layers. However, the thicknesses of the dark layers were almost the same for all of the $(Zr,TM)B_2$ specimens and almost twice as thick as the dark layer for nominally pure ZrB_2, showing the same effect of TM additions on lowering the oxygen diffusion through the dark layer toward the unoxidized matrix. Additions of Mo or Nb were most effective in improving the oxidation resistance of ZrB_2 by increasing the stability of the protective liquid/glassy B_2O_3 layer and reducing the oxygen transport through the light layer.

3.2. CONCLUSIONS

The addition of transition metals to ZrB_2 improved the oxidation resistance of ZrB_2 as a result of the following effects:

1. Addition of TMs to B_2O_3 decreased the evaporation rate of the B_2O_3 glasses in the order of $WO_3<ZrO_2<Nb_2O_5$, due to the lower activity of B_2O_3 in (TM-oxide)-B_2O_3 glasses. The increase in the stability of the liquid/glassy B_2O_3 resulted in an increase in the onset temperature of the transition in oxidation, followed by lower oxide scale thickness for the (Zr,TM)B_2 specimens compared to nominally pure ZrB_2.

2. Higher solubility of the TM-oxides in liquid B_2O_3 compared to ZrO_2, promoted the solution and reprecipitation of the oxides in B_2O_3 and resulted in higher thickness of the oxide layer with equiaxed grain. The equiaxed structure of the oxide layer should result in lower oxygen transport rate compared to the oxide layer with columnar grains formed on nominally pure ZrB_2.

3. At 1600°C, the protective B_2O_3 layer was removed from the outer surface of ZrB_2 by evaporation, leaving an oxide layer that was composed of two sub-layers, an outer layer that was porous and appeared light in optical microscopy and an inner layer that was dense and appeared dark. The addition of TMs resulted in a decrease in the thickness of the light oxide layer and an increase in the thickness of the dark oxide layer. The thicker dark layer, which had a higher apparent density compared to the light layer, resulted in lower oxygen transport from the outer layers toward the unoxidized matrix, and, consequently, improved the oxidation resistance of ZrB_2.

4. SUGGESTIONS FOR FUTURE WORK

Research presented in this dissertation discussed some effects of transition metals on oxidation behavior of ZrB_2 ceramics. However, finding the answers to the following questions might increase knowledge of the oxidation behavior of (Zr,TM)B_2 ceramics, and help design ZrB_2 ceramic parts with improved oxidation resistance.

1. *Which TM additives have the most effect on reducing the evaporation of B_2O_3?*

Since formation of binary compounds in the (TM-oxide)-B_2O_3 system is a probable reason for the reduction in the evaporation rate of B_2O_3, TM-oxides forming a binary compound with B_2O_3 should be studied. However, the TM oxide or oxides that are chosen should have greater valence(s) than Zr^{4+} to avoid increasing the oxygen vacancy concentration in the zirconia oxide layer, which would increase oxygen diffusivity through the oxide scale.

2. *What are the basic differences between the light and dark oxide layers?*

Due to the higher apparent density of the dark layer, it is believed to have a lower oxygen transport rate compared to the light layer. However, the basic differences between the light and dark layers are not well known yet. Gaining knowledge about the dark layer could help us find some method to improve its stability and improve the oxidation resistance of ZrB_2 ceramics.

3. *Which TM additives promote formation and stability of the dark oxide layer?*

As mentioned above, a thicker dark layer should increase the oxidation resistance of ZrB_2. The fact that the dark layer can affect the oxidation behavior above the temperatures at which the protective B_2O_3 layer is removed, emphasizes the importance of this study for increasing oxidation resistance at ultra-high temperatures.

4. *What is the effect of the TM additives on oxidation behavior of ZrB_2 in extreme environment?*

Since the liquid/glassy B_2O_3 layer is less stable in extreme environments, e.g. high air flow rates, the effect of TM additives on improving the oxidation resistance might not be as much as their effect on oxidation in a furnace studies. However, TM additives are expected to still improve the oxidation resistance due to their effects on densification of the oxide scale and the thickness of the dark layer.

Testing $(Zr,TM)B_2$ specimens in extreme environments, such as arc heaters or similar facilities, would provide useful information about the response of response of $(Zr,TM)B_2$ ceramics in environments that simulate hypersonic flight and/or atmospheric re-entry.

VITA

Maryam Kazemzadeh Dehdashti was born on January 5, 1982 in Tehran, Iran. Spending her middle and high school years in Farzanegan School as part of the Iranian National Organization for Development of Exceptional Talents. In October 2000, she started the college education at Tehran Polytechnic University, the second best engineering school in Iran. After receiving her Bachelor's degree in Metallurgical Engineering, Maryam continued her graduate study in the field of Ceramic Engineering at Tarbiat Modares University, where she obtained her Master's degree in July 2009. Since August 2009, Maryam has been working on her Ph.D. under the supervision of Dr. Bill Fahrenholtz, and with additional guidance from Dr. Greg Hilmas.

Her Ph.D. research focused on the development and characterization of ultra-high temperature ceramics for use in hypersonic aviation. She presented her work at seven conferences and published two manuscripts with four more pending. She successfully defended her doctorate degree in January 2014 and received her Ph.D. degree in August 2014.